Bed Modeling of a Biomass Grate-Firing Furnace:

A Numerical Study

By

Zahra Taban

A Thesis submitted to the Faculty of Graduate Studies of

The University of Manitoba

In partial fulfillment of the requirements for the degree of

Master of Science

Department of Mechanical Engineering

University of Manitoba

Winnipeg

ABSTRACT

Biomass is a renewable source of energy that can play a vital role in achieving a more sustainable energy supply. It can also substitute fossil fuels in many applications such as heating. Biomass combustion in grate firing furnaces is a conventional approach to convert biomass fuel into heat and electricity. However, this technology is associated with some challenges such as low efficiency and pollutant emissions. Most of published studies on biomass combustion are focused on gaining a better understanding of thermal conversions occurring in the bed section and subsequent chemical reactions taking place in the freeboard. Nevertheless, the conversion of solid biomass in the bed section of furnace is a very complex phenomenon; and still requires further research. In this thesis, a numerical study is performed to describe the conversion of solid fuel in the bed section. Four different bed models are introduced and tested. For each model, a separate MATLAB code containing physical equations and chemical sub models is developed to predict species mass fraction and temperature over the bed surface.

To test the performance of these models, and due to the lack of experimental data, the bed models outlets are applied as boundary conditions to the freeboard simulation modeled by eddy dissipation concept (EDC). Then, the freeboard numerical results are compared with the experimental measurements at furnace outlet. The results show that the predicted released mass fraction and temperature from furnace with application of 1-D three-zone bed model are in better agreement with experiments. The results also, indicate that the temperature distribution in the freeboard strongly depends on the adopted bed model.

ACKNOWLEDGMENTS

This thesis would not have been possible without the guidance, support, and cooperation of several individuals whom in different ways contributed and extended their valuable assistance in the preparation and completion of this work.

First and foremost my utter gratitude to my adviser, Professor Madjid Birouk, whose inspirational guidance, great patience, and cheerful encouragements, supported me through this process and propelled me to finish this study.

I would also like to express my appreciation to my committee members, Prof. Behzad Kordi and Prof. Vijay Chatoorgoon for their efforts put into reviewing the thesis, and their invaluable comments and suggestions.

A lot of gratitude goes to the Biovalco Inc., University of Manitoba, Province of Manitoba and the National Science and Engineering Research Council of Canada, (NSERC), for providing financial support on this work.

Thanks to my colleague Mohammadreza Farokhi, for sharing his experience and knowledge.

I also am deeply in debt to my parents, my father Ali Taban and my mother Nahid Saneie, whose unconditional love and support give me the possibility of pursuing my dreams and education.

Finally, I indeed am grateful for having my husband, Saeed Shahabi whose endless love and support made this path more comfortable for me; I would like to sincerely thank him for sharing these moments of life, with me.

TABLE OF CONTENTS

LIST OF FIGURES

LIST OF TABLES

LIST OF ABBREVIATION

Nomenclature

HHV	High heating value [KJ/kg]
LHV	Low heating value [KJ/kg]
H_h	High heat value [KJ/kg]
W	Water percentage
V	Velocity [m/s]
$S_\emptyset$	Source terms
T_{fl}	Freeboard flame temperature [K]
T_s	Solid temperature [K]
Z	The height of the fuel bed [m]
Z_0	The initial height of fuel bed [m]
d_p	Equilibrium diameter of particles [mm]
T	Temperature [K]
K	Conduction coefficient
Y_i	Mass fraction of species
C_{ps}	Specific heat capacity [KJ/kg.K]
h_s	Enthalpy of solid [KJ/K]
v_g	Gas velocity [m/s]
D	Mass dispersion tensor
S	The surface area of fuel bed per unit volume
P_0	Atmospheric pressure
R_g	Universal gas constant

$\overline{M}$	Average molar mass
$\dot{m_{total}}$	Entire mass flow rate toward furnace bed
$\dot{m_{moisture}}$	The mass flow rate of existing moisture
$\dot{m_{fuel}}$	The mass flow rate of fuel toward furnace bed
$\dot{m_{PA}}$	The mass flow rate of primary air
Y_{ash}	Ash concentration in the fuel
Y_{if}	species concentration in the fuel
h_{PA}	Enthalpy of primary air
$q_{radiation}$	Radiation heat flux
h_{daf}	Enthalpy of dry ash free fuel
$h_{combustion}$	Heat released from the hot gases reactions in the freeboard
h_i	Inlet energy
h_o	Outlet energy
m_i	Inlet mass
m_o	Outlet mass
r_{char}	Kinetic rate of char oxidization reactions
r_{pyr}	Kinetic rate of pyrolysis reactions
r_{drying}	Kinetic rate of drying reaction

Greek Symbols

ε	Porosity [-]
ρ	Density [Kg/m^3]
Γ	Diffusion coefficient for heat transfer

α	Bed permeability [m^2]
ε_g	Gas porosity [-]
ε_s	Solid fuel porosity [-]
σ	Stephan-Boltzmann constant [$wm^{-2}K^{-1}$]
$\lambda_{radiation}$	Conduction coefficient caused by radiation
ρ_g	Gas density [Kg/m^3]
ω_{is}^{gs}	Heterogeneous source of mass for species
ω_{is}^{s}	Homogenous source of mass for species
Λ_s	Heat dispersion tensor
ω_h^{gs}	Source term for enthalpy
α_T	Exchange coefficient

Acronyms

CFD	Computational fluid dynamic
Si	Silicon
Al	Aluminum
Fe	Ferrous
Ca	Calcium
S	Sulfur
Ti	Titanium
Mg	Magnesium
Na	Sodium
P	Phosphor
K	Potassium

0-D	Zero dimensional
1-D	One dimensional
PA	Primary air
daf	Dry ash free fuel
UDF	User defined function

CHAPTER 1: INTRODUCTION & BACKGROUND

1. Introduction and Background

1.1 Introduction:

There is a general understanding that fossil fuels will be exhausted, or at least become excessively costly to produce [1, 2, 3]. Petroleum products meet around 80% of the world energy demand and only 15% originates from renewable energies including biomass, hydro, solar energy and wind [1, 4]. The limited resources of conventional fossil fuels combined with global warming have fueled considerable interest in developing nuclear power and renewable energy based systems using wind, wave, solar, hydroelectric and biomass, which are more evenly distributed around the world than the other resources [4]. Also, renewable energies have a significant positive impact on controlling global warming, which is one of the most significant concerns of governments around the world, by reducing greenhouse gas emissions.

The results presented in this thesis are a contribution towards the optimization of biomass combustion in grate firing furnaces via developing a comprehensive bed model. This chapter starts with a discussion of the social and economic background of the work described in this thesis. A brief introduction then follows it into grate furnace conversion technology in which the principle of grate firing furnace combustion and conversion of solid biomass are described. Finally, the outline of this thesis is presented.

1.2 Introduction to Biomass:

Biomass is a natural material derived mostly from living or recently living organisms. Biomass can be utilized as a source of inexhaustible and renewable energy and is generally sourced from

plants which are not needed as sustenance. Therefore, the origin of all biomass materials is from the photosynthesis process [5]. Biomass matter is mostly based on the elemental composition of carbon, hydrogen, and oxygen.

Advantages of biomass compared to coal reside in its high potential of volatile gases and low amount of ash. For instance, its volatile amount is around 80%-90% (dry-base ash free) for woody biomass type [5]. The water content can also be up to 60% of the total mass for freshly cut trees; however, this number fluctuates between 12%-20% for air-dried woody biomass. This highly variable moisture content can change the heating value of the biomass fuel between 5MJ/kg and 20 MJ/kg which is comparable to coal that has a heating value between 22 MJ/kg and 34 MJ/kg [5].

Biomass fuel covers a vast scope of various living species, so it is classified into multiple groups depending on its origin. Biomass, depending on feedstocks, can be utilized immediately as a fuel or changed into another type of energy which is accessible on a sustainable basis [6]. Typical biomass feedstocks include dedicated energy crops, crops, agricultural residues, forests residues, plants, municipal waste (MSW), and animal waste. According to the literature, the average percentages of biomass energy production sources are classified as shown in the following chart [7].

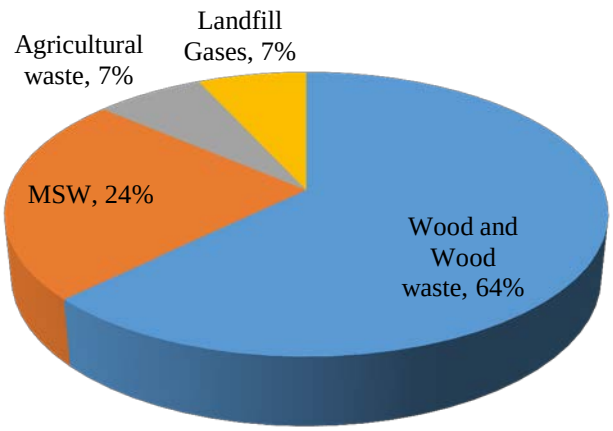

Figure 1.1. Distribution of biomass species **[7]**

1.2.1 Biomass resources in Canada:

Canada is a nation with a tremendous amount of natural materials, from wood to waste, and could be at the front line of this old-yet new energy source. With its expansive landmass and dynamic forests and farming lands, Canada provides extensive biomass resources [8]. Currently, bioenergy is the second most critical type of sustainable power source in Canada which accounts for approximately 4.4% of Canada's essential energy resources [8]. A significant portion of the biomass limit is found in areas with critical foresters' exercises British Columbia, Ontario, Quebec, Alberta and New Brunswick [8]. The contribution of forest land biomass to Canada's energy amounted was between 5% and 6% in 2013, and Manitoba is the leading Canadian region in biomass creation [8]. Therefore, Canada's forests represent an abundant source of biomass, and the following picture illustrates the expansion of forests in Canada [9].

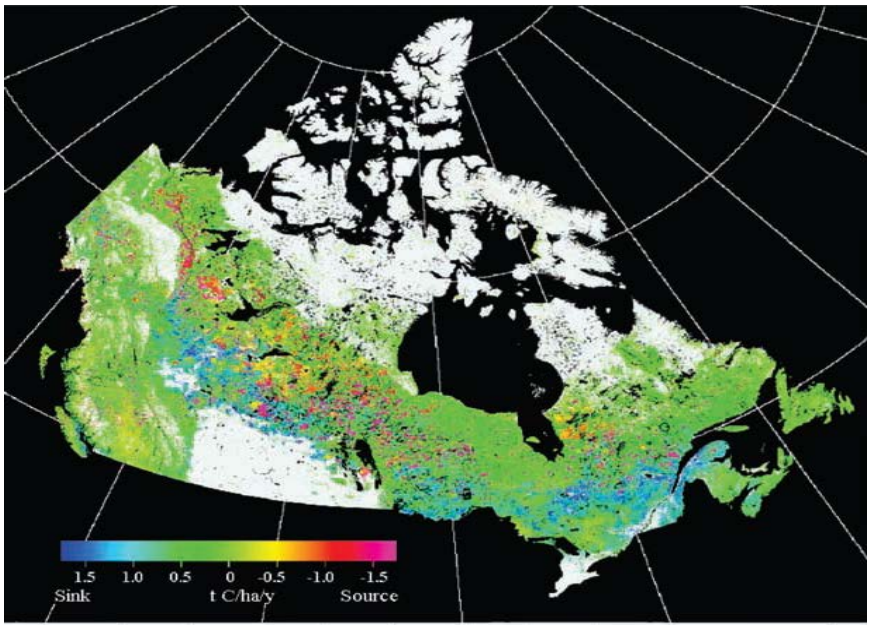

Figure 1.2. Biomass resources distribution in Canada **[9]**

1.2.2 Biomass fuel characteristics:

The characteristics of chemical and phase composition of solid fuel biomass are both the initial and most essential step in the investigation and analysis of the applications of such fuel. Biomass composition is unique and helps in determining the properties, quality, potential use and emissions related to any fuel. Many studies were carried out on solid fuels such as chemical and mineralogical studies [10]. This include proximate analysis (Fixed Carbon, volatile matter, ash yield, and moisture); ultimate analysis: (C, O, H, S, N); ash analysis (*Si, Al, Fe, Ca, S, Mg, K, Ti, Na, P*), petrographic analysis: (Organic and inorganic analysis); separation procedures: (different fraction); and other analysis of fuel like the temperature of ash etc. [10].

1.2.2.1 Biomass general contents

The general properties for the various types of biomass are discussed in the following section.

Moisture: Moisture content is crucial for determining the net energy content of biomass material. Dry biomass has a higher heating value or net energy potential as it uses a small amount of its energy to evaporate the water through the solid fuel [11].

Ash: The noncombustible parts and elements of biomass are referred to as ash. High ash content in solid fuels results in fouling problems, especially if ash is high in metal elements like potassium. Biomass fuels, especially the agriculture residues and crops, have high amounts of ash which are also high in potassium. This tends to cause the ash to melt in low temperatures and result in clinkers, which could jam furnace elements. The amount of ash in biomass fuels varies. For instance, wood has less than 1% ash, while bark can have up to 3% ash. Crops have a higher ash content of 3% or more top [11].

Carbon: The content of Carbon in biomass fuels varies by the types of biomass, but an average of 45% is found in most of biomass fuel [11]. The amount of Carbon content affects the magnitude of the heating value.

Hydrogen: The amount of Hydrogen in biomass usually is about 6%. High values of hydrogen will result in high heating values [11].

Nitrogen: The standard amount of nitrogen is between 0.2% and 1%. Fuel-bound Nitrogen is responsible for most NO_x emissions produced from biomass combustion [11].

Sulphur: Most biomass fuels have a sulfur content of less than 2%. Sulfur oxides are produced during biomass combustion and will contribute to pollution and acid rain [11].

Chloride: Combustion of biomass fuels with high Chloride values can result in ash fouling. Also, it's high amount of Chlorides will produce acid in boilers tubes, which can cause corrosion [11].

1.2.2.2 Biomass physical and chemical properties:

Physical properties

- Biomass size and density:

The size and density of biomass fuel particles are also important. They alter the burning characteristics of the fuel by affecting the rate of heating and drying during the combustion process. Improper size of biomass undermines the efficiency of the combustion process and may also result in system damage. Smaller sized fuels are more common for commercial-scale furnaces because smaller scale fuel is easier to use in an automatic feed system, and they also allow for more delicate control of the burn rate [11].

- Mass reduction:

Biomass mass and volume reduce during the conversion processes on the grate. Gaur and Reed [12] developed some diagrams to display the effect of the heat rate of biomass combustion on size change. These effects depend on the amount of heat transferred from particles to the surrounding gas.

Biomass chemical analysis

- Proximate analysis:

Biomass characterization is required to predict its behavior as a reliable fuel. When considering biomass thermal conversion, the proximate analysis is one of the essential characterization methods. This technique determines moisture, ash, volatile matter and fixed carbon contents of the raw biofuel. These values affect both plant design and combustion behavior. In this way, high

moisture values decrease the combustion yield while highly volatile matter/fixed carbon ratio is related to carbons reactivity [13].

- Ultimate analysis:

For engineering estimations, ultimate data and heating value are critical for proper design and operation of conversion facilities. Conventional laboratory measurements of biomass compositions as mentioned above are tedious and time-consuming. Modern technologies use Near Infrared Spectroscopy (NIRS), which is a spectroscopic method that utilizes the near region electromagnetic waves, to detect the number of different species of the biomass such as *C, H, N, O, Cl, S…etc.* [14].

- Heating value:

The heat value or amount of heat/energy available per unit mass, (kJ/kg), is one of the most critical characteristics of biomass fuel because it indicates the total amount of energy that is available in the fuel. The heat value of a given fuel is mostly a function of the fuels chemical composition. The heat value is expressed as: Higher Heating Value (HHV) or the Lower Heating Value (LHV) depending on the water phase. The HHV is the total amount of heat energy that is available in the fuel including the latent energy contained in the water vapor in the exhaust gases. In contrast, the LHV does not include the energy embodied in the water vapor. Generally the HHV is the appropriate value to use for the biomass combustors.

Some species of biomass tend to have more energy per unit mass than others. The heat content of a particular fuel can vary significantly depending on the climate and the soil in which biomass fuel is grown, as well as other conditions. The caloric value of biomass fuels is approximated using experimental equations and correlations based on elemental compositions of biomass

particle which is known via ultimate analysis. Dulong [5] developed a formulation which has been largely used to calculate the heat value of coal and wood in stockers and furnaces [12].

$$H_h = 81.C + 342.5.\left(H - \frac{1}{8}.O\right) + 22.5S - 6.(9.H + W) \quad (1.1)$$

Where H_h is the higher heating value, C is the carbon fraction (%), H is the hydrogen fraction (%), S is the sulfur fraction (%), O is the oxygen fraction (%) and W is the water or moisture percentage.

1.3 Technologies for biomass energy conversion:

There exist two major technologies to convert and burn biomass into useful energy resources; namely biochemical and thermochemical. Both of these technologies turn biomass into either direct heat or an energy carrier [5]. The biochemical conversion method uses bacteria to change biomass into an energy carrier. In this method, bacteria dissolves organic matters and make high-methane content gases, which also consist of methanol and ethanol [5]. On the other hand, the thermochemical method uses heat to extract energy carriers out of biomass residues or directly convert it to energy via combustion [5].

1.3.1 Pyrolysis:

Pyrolysis is the base of all thermochemical processes since all the chemical changes are encompassed [15]. Thus, interest is progressively moving toward pyrolysis because this procedure is streamlined to deliver energy-rich oils, chars, and gases [16]. Pyrolysis is thermal decomposition of wood structure without an oxidizing operator. The outputs of biomass pyrolysis are water, chars (fixed carbon), oils or tars (light hydrocarbon), gases including methane, hydrogen, carbon monoxide and carbon dioxide. The origin of biomass conversion in

the pyrolysis process is the final temperature which is applied to the fuel [15]. Charcoal has been the most significant industrial output of biomass pyrolysis for quite a while and is the most abundant single biofuel delivered today. Table 1.1, presents some examples of the amount of released pyrolysis products in different temperature ranges.

Table 1.1. Percentage of released pyrolysis products at different temperature ranges **[17]** .

Temp (K)	***Char (%)***	***Oil (%)***	***Water (%)***
673	44	24	13
773	28	32	17
973	21	26	13

1.3.2 Gasification:

Gasification of biomass is the second method in thermochemical technology. It can offer a potential approach to manage the expanding demand of the bioenergy and meet the objectives set for CO_2 reduction. Biomass gasification is viewed as a standout amongst the most encouraging methods of syngas production cycles [18]. In the case of gasification, which is an augmentation of pyrolysis, the heat is boosted to give the most elevated yield of carbon and energy in the gas state, rather than making liquid and char. The majority of commercial gasifiers are fractional oxidation reactors; in which adequate air or oxygen is acquainted which consumes some portion of the biomass to inject the heat into pyrolysis and gasification [15]. The overall reaction of biomass in gasification can be presented as follows:

$$CH_xO_y + O_2 + H_2O = CH_4 + CO + CO_2 + H_2 + H_2O + C + tar \quad (1.2)$$

1.3.3 Combustion:

Combustion is a series of highly exothermic synthetic responses between a fuel and an oxidizer accompanied by the transformation of compound species. Straight combustion of biomass fuel is one of the simplest ways of converting biomass into energy. Industrial furnaces are the proper and suitable devices capable of facilitating direct biomass combustion [5].

1.4 Types of biomass combustion furnaces:

The design of commercial furnaces varies depending on several factors such as fuel type, ash properties, moisture content, and heating value [5]. The two most common types of furnaces for biomass burning are fixed and fluidized bed combustors, both of which have excellent fuel adaptability and can be entirely fueled by biomass or even co-fired with coal [19]. There is another industrial furnace for combusting biomass fuel, known as the suspension furnace, which is less common compared to the other two furnaces [19]. These furnaces are usually used for burning biomass pellets or raw biomass which is pulverized with coal. The problem with suspension furnaces is that they are highly sensitive toward any changes in fuel content which can affect their efficiency visibly [19].

Fluidized Bed (FB) systems only use a few percentages of fuel and treat the rest as inert materials like ashes, sands, and sorbents. The bed itself is located on a stationary air merchant grind through which air is propelled at high speed. Moreover, the low ignition temperature (800-950°C) in fluidized bed systems is a result of the vast amount of inactive material inside the heater [5].

Fixed bed furnace has a fuel bed located on a grate which can either be fixed, moving, rotate or vibrating. Pit fire is one the most basic types of fixed bed systems [5, 20]. Industrial systems are

generally much more complicated. Stockers and pellet burners are examples of fixed bed industrial systems. These systems are manufactured to have drying, de-volatilization and char oxidization occur on the bed surface [5]. Fixed bed systems, which are also known as grate firing, are one of the technologies which are popular in the production of heat and electrical energy [19]. The most notable benefits of grate firing furnaces over the other types of biomass conversion systems is that these furnaces can burn any biomass fuel containing various amounts of moisture and ash [5, 19]. Low cost and fuel availability are other advantages of grate firing or fixed bed biomass boilers [19]. Table 1.2 compares grate firing biomass combustion with other biomass combustion technologies.

Table 1.2. Main combustion technologies and their application comparison to biomass firing [21]

	Suspension or PF firing	**FBC**	**Grate-firing**
Fuel flexibility	Poor	Very good	Very good
3T(temperature, turbulence, time)	High temperature-very good mixing- very short residence time	The low temperature-very good mixing-long residence time	Intermediate temperature- Poor mixing-very long residence time
Excess O_2	Typically 4%-6%	3%-4%	5%-8%
Efficiency	High	High	Low
Environmental impacts	Low NO_x emissions with efficient air	Low NO_x emissions due to low temperature; Easy capture of Sulphur	Low NO_x emissions need special technology in old units and can be achieved in modern units via advanced secondary air
Economics	Highest capital cost; Highest operation cost	High capital and operation costs	Low capital and operation costs
Use in existing biomass-fired CHP plants	About 50% are equipped with PF boilers; mainly co-firing woody biomass at low thermal shares	Nearly 40% are based on FBC; can fire pure biomass	About 10% are using grate-firing; often pure fire biomass of all types
The obstacle for use in biomass and waste combustion	1. Low fuel quality; 2.Hard to mill biomass to similar sizes. 3) Low ash melting temperature	1. Potential bed de-fluidization, 2. Hard to meet the directive on waste incineration	No inherent obstacle but grate-firing needs to be advanced for higher efficiency and lower emissions

1.5 Challenges of biomass grate firing furnaces and thesis objectives:

Although grate firing furnaces technology has financial advantages over other biomass technologies, it still suffers from emitting harmful emissions [22, 23]. Therefore, grate firing boilers should be optimized further in order to improve their efficiency and emissions [21].

Several studies have been devoted to understand and hence develop reliable methods to improve biomass furnaces efficiency [4]. Numerous studies in the past two decades focused on grate firing biomass combustion [24]. Although experimental tests are considered the most trusted approaches, they are economically costly, time-consuming, and mostly limited to lab-scale cases [24]. CFD is a cost-effective tool which allows more detailed information on the combustion process occurring inside the furnace. However, the success of the CFD method depends on the accuracy of the sub-models that are employed in the computational framework [25].

The main objective of this thesis is to develop a more comprehensive bed modelling of biomass fuel conversion in grate-firing bed. It is also the goal of this thesis to examine the sensitivity of freeboard combustion process to bed modelling.

1.5.1 Outline of the thesis:

Chapter 1 presents challenges and motivations as well as research objectives of this thesis. Background and literature review on biomass grate-firing furnaces and CFD methods role in grate combustion modeling are presented in Chapter 2. Also, the importance of grate combustion modeling in bed and different classification of packed bed modeling approaches along with an overview of published bed models are reported in Chapter 2. The methodology and numerical solution algorithms for packed bed models are summarized in Chapter 3. The modeling process for biomass conversion in the bed section of the furnace including the mathematical description

of the models, the biomass fuel properties, empirical models of packed bed, together with chemical sub-models are introduced in this chapter. Also, the gas phase combustion modeling along with the physical setup are briefly mentioned in Chapter 3. Chapter 4 documents the results and discussion. Conclusions and some suggestions for future work are outlined in Chapter 5.

CHAPTER 2: LITERATURE REVIEW

2. Literature Review

2.1 Introduction:

In this chapter, a review of existing fixed bed models is reported and the areas that require more research are introduced. This chapter starts with a classification of published bed models including their physical and chemical features. Then, an overview of the mathematical setups for the different models is presented.

2.2 Importance of biomass combustion modeling: Bed section

Computational Fluid Dynamics (CFD) technique is now a common method used for the design and simulation of biomass fuel combustion systems. It is used for an extensive range of furnaces from small-scale to industrial scale, biomass burners and wood stoves [26]. Although current CFD codes are practical and useful in the simulation of combustion systems, their prediction quality still depends on the accuracy of input data, such as sub models of biomass conversion. A typical model for biomass combustion of a grate firing burner consists mainly of biomass conversion in the grate (bed) and the combustion of the released volatile gases in the bed top (freeboard).

One of the critical factors of modeling the bed section of a grate firing burner is the approximation rate of conversion processes within the bed [26]. As combustion proceeds along the fuel layer, different types of gases are released from the bed and enter the freeboard where the species concentrations, temperatures, and mass flow rates are required as boundary and initial conditions for modeling the freeboard (gas-phase) combustion [26]. These boundary conditions

are important in the numerical modeling especially in the case of grate firing furnace in which biomass conversion in the bed section and volatile combustion in the over-bed zones are strongly coupled, and consequently improper treatment of the bed may result in inaccurate predictions of CFD modeling [26]. Figure 2.1, shows a typical grate firing furnace with inlet boundary conditions.

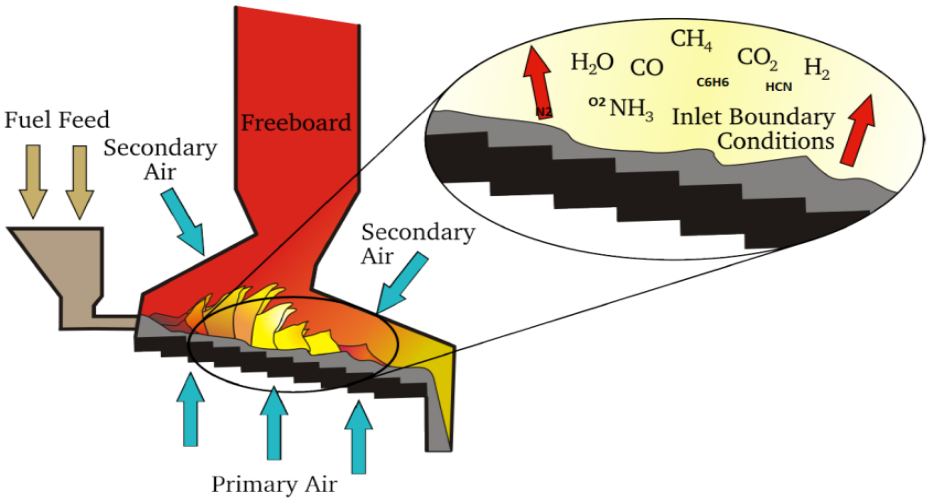

Figure 2.1. Typical grate firing furnace which displays details of the grate boundary conditions [26]

Modeling biomass conversion in a grate firing bed is a very complicated process. This process involves not only chemical reactions but also comes with heat and mass transfer processes between solid particles and surrounding gases, as well as between solid particles themselves. These solid particles consist of various properties which have to be considered in the modeling. As biomass burns, inconsistent thermo-chemical reactions cause uneven gas distribution over the bed and ultimately erosion. Therefore, modeling a full-scale furnace bed needs extensive resources and computational storage which make CFD approach challenging [5]. That's why simple, but inclusive, bed models are required.

2.3 An overview of packed bed modeling approaches:

As reported in [26] numerous packed (fixed) bed models have been developed and presented in literature during the last five decades. These include both very basic models with simple assumptions and highly complicated ones with specific details. According to the literature [26, 27, 28], these models can be classified in different ways. In this section, a straight classification of these models is presented which is also appropriate for the aim of this thesis.

2.3.1 Classification of packed bed models:

This part provides information on typical features of all published bed models along with their classifications. Three major modeling techniques that are extensively discussed in the literature are outlined as follows [26]:

2.3.1.1 Empirical modeling:

The empirical approach is the most common method in bed modeling which is based on experimental measurements from, or very close to, the fuel bed surface [29, 30]. Although the obtained results from the empirical method are more accurate, this approach is not strong enough to predict combustion for design of new boilers. In empirical methods, since mass and energy conservations are applied to the conversion processes in bed, a deviation of the model predictions from reality may occur [26].

2.3.1.2 Porous zone CFD modeling:

CFD commercial codes like ANSYS FLUENT allow their users to define a porous zone through the domain. By establishing a resistance, the porous zone causes a drop in the fluid flow pressure, and therefore this approach is appropriate for gas flow in the fuel layer. In this method,

all heat sources, additional governing equations, solid fuel properties, and chemical reactions equations must be defined within the porous zone so that the combustion process can be thoroughly described. However, solving all of these equations is the CFD code is a challenging task. In this approach, there is no need to apply profiles of variables like species concentrations and mass flux to boundary conditions instead of introducing the properties of primary air and radiation heat absorbed from the freeboard by bed suffices. Compared to the empirical approach, this model [31] is more complicated and time consuming for the simulation of combustion within the bed section, however it predicts more satisfactory results. Typically, porous zone modeling is suitable for situations which require a general view of the furnace operation, and the fuel bed details are not the primary concern [32].

2.3.1.3 Stand-alone approach:

Some researchers (e.g., [27, 33, 34, 35]) developed stand-alone models to predict all the processes occurring inside the bed. This model uses the same assumptions and procedure as those of porous zone modeling. However, the stand-alone method is independent of the CFD code, and no coupling is required. Also, a stand-alone bed model can be extended for different functionalities on the porous zone. Figure 2.2, describes a schematic view of the stand-alone and porous zone approaches.

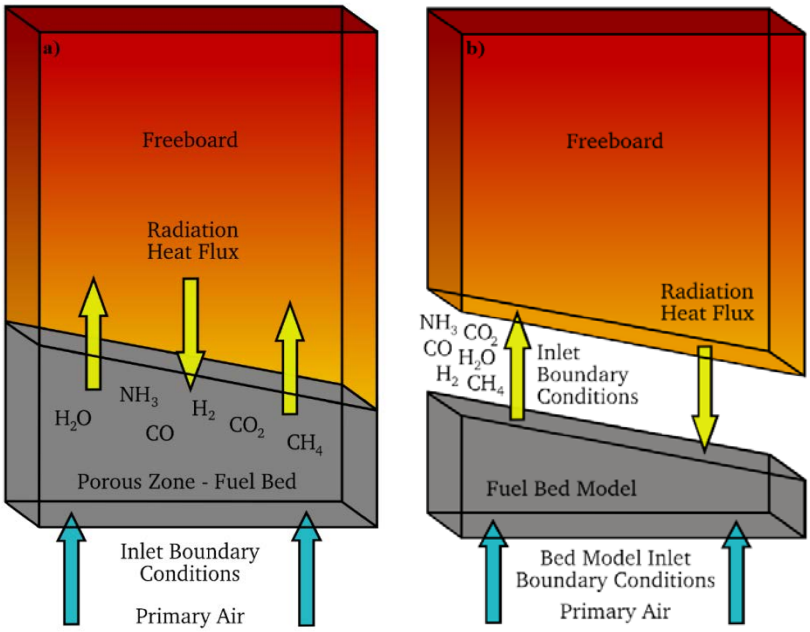

Figure 2.2. Schematic shape of grate firing a) Porous zone and b) Stand-alone model models [5]

2.3.1.4 Mathematical classification of bed models:

To model complicated processes of combustion, various types of models are developed whose diversities are mostly based on their solution method (numerical or analytical), purpose, and application field [27]. One of the defined mathematical classifications for the current bed models is presented below.

- Simple 1-D models:

In this model, a finite number of governing equations are solved analytically. These models are commonly used for bed conversions where oxygen is injected from the top of the fuel layer [36, 37, 38, 39]. This model is usually considered for low air flows and tiny fibers.

- Comprehensive 1-D models:

The second group of models (e.g., [28, 40]) includes numerical solutions of governing equations. These models are more comprehensive and accurate regarding the chemical and physical conversions that happen on a grate and fuel bed. For this type of models, heterogeneous conversion of solid fuel on the bed is described by chemical kinetic rates. Also, these models include source terms [41, 42, 43]. Application of these models is mostly used for wood combustion, but it has also been used for coal gasification as well [30]. 1-D numerical based models provide the best details for applications in a grate-firing furnace. Physics, chemistry, and structure of these models are presented in chapter three of this work.

- Comprehensive multi-dimensional models:

These models apply 2-D and 3-D numerical solutions to fuel bed equations and solve the equations in small grid cells [44, 45]. There exist some other types of classifications for fuel bed conversion modeling. For instance, De Souza Santos [46] presented a noticeable classification for bed models. In his work, the bed models are categorized into two groups. The first group consists of phenomenological models which are based on the solution of mass, energy, and momentum equations and the second group contains, empirical and semi-empirical models that display the basis of the conversion process [46]. In this classification, 0-D simplified models reaching to 3-D complex dynamic ones are considered in phenomenological class.

2.4 Overview of existing packed-bed models:

Fixed bed models still need to be refined in order to improve the simulation of small scale biomass burners [32, 47, 48, 49, 50]. A review of papers published on packed bed modeling revealed a large number of different models for simulating packed bed systems. This section

reviews previous approaches, especially those which are related to fixed-bed modeling in biomass combustion furnaces. Generally, the typical approach for packed bed modeling which is highlighted in the literature, is to separate the simulation of bed and freeboard even though they are strongly coupled. Commercial codes are used to model the freeboard section while for the simulation of the bed, modeling may be carried out by in-house codes and then the results are applied to the freeboard simulations [51]. According to Yin et al. [19], in order to develop a strong and reliable model, it should be confirmed that the model itself obyes conservation principle; for example mass, energy, and species equations are conserved in the bed which ultimately results in accurate quantity of mass and energy carried to the freeboard via flue gas [26].

By reviewing the literature, it is noticeable that many of the studies conducted on bed combustion in the past were focused on coal combustion [5]. Hobbes et al [52] have done comprehensive work on fixed bed modeling for coal combustion. Hobbes et al. [71] have reviewed a considerable number of bed models in their work from which some are zero-dimensional models, most are one dimensional, and only a few of them are two dimensional bed models. However, the recent focus on biomass fixed bed modeling has increased so that one-dimensional model is counted as the most popular for biomass modeling [42, 53]. Giltrap et al. [53] have developed a steady one-dimensional bed model. Their model only considers combustion and gasification of char and volatile on the bed. They assumed the chemical composition of biomass as $H_{3.03}\,O_{1.17}$, and did not consider any tar in their model as only $CO, CH_4, H_2\,O$ are assumed as bed products. Their model reasonably predicted only CO and CO_2 (in agreement with actual data), while it is still capable of giving a reasonable overview for other chemical species [5]. Brunch et al. [42] developed a bed model to cover the entire chemical and

physical conversion process of biomass on the grate. The model assumes that the bed is a structure of a finite number of particles where, within each particle, there is one dimensional heat transfer. Bed shrinkage is only considered in char oxidization zone while drying and de-volatilization do not include any shrinkage factors. This model fits perfectly with biomass combustion process, although there are some problems with its prediction of other conversion procedures. Shin et al. [54] developed a one-dimensional transient concept that has been used across the bed. In this model, it is assumed that each chemical conversion (drying, de-volatilization, char combustion) occurs in a separate section. Thunman et al. [55] developed a one dimensional bed model where they used empirical approach and correlations to determine the species concentration and temperature using mass and energy conservation equations. They considered heat transfer within large bed particles.

One of the most straightforward approaches that exist in the literature for fixed bed modeling can be found in [32] where the inlet conditions are used for fuel bed. This approach can be either a constant function of the total grate or the chemical rate can be a function of the position on the fuel bed [32]. Inlet conditions are calculated from the application of mass and heat equations over the entire bed domain. A more complex method is to build separate sub models that calculate temperature, species concentrations, and mass flow rates on the top of the bed and couple it with the radiation heat absorbed from the freeboard combustion similar to the work presented by Chaney et al. [32].

Another method which is not typical is to define a subroutine user-defined function (UDF) in the CFD code to describe the characteristics of the solid fuel and its chemical conversion rates. This is similar to the approach used by Chaney et al. [32]. There are some other models in the literature which are capable of predicting solid fuel conversion on grate firing bed. For example,

Ford et al. [56] developed a model in which the combustion procedure is completely monitored by boundary condition diffusion and did not consider the fuel flow in the bed. To predict the flow rate and velocity of the gases leaving the bed, Fatehi et al. [42] developed a model by applying equilibrium equations through the whole bed [42]. Hartne [5] developed a heterogeneous transient model through the one-dimensional discretization of mathematical equations for the conversion of solid fuel [42]. Some researchers (e.g., [57]) developed a model for fixed bed biomass combustion in which they separated the bed surface of the furnace to multiple zones so that each zone is described by a different reaction happening within it [57]. Kuo et al. [5] utilized a different approach where empirical correlations are obtained from lab-scale furnaces experiments to determine the combustion rates on the bed. Some studies presented simple biomass bed models in their work which are also capable of covering the whole conversion process. For instance, Bauer et al. [22] built an elementary mathematical model for grate firing boilers, but their model is not complete in terms of the influence of primary air zones and multiple velocities of the grate. Zhou et al. [58] developed a model for straw (one specific type of biomass) in a fixed bed system with an emphasis on *NO* precursor's formation. Costa et al. [46] developed a set of packed bed models with different simple mathematical and chemical assumptions where one of the models was a 0-D steady state, and the other one was a 1-D semi-empirical model. For these models, they used numerical methods to solve the mass balance and energy conservation equations [46].

2.5 A summary and contribution of the thesis:

Despite the extensive use of CFD method in modeling, bed modeling still requires an approach to confirm the heterogeneity of solid biomass gasification [12]. All previous studies on bed modeling, as mentioned above, can be divided into two major categories: empirical and

theoretical models. Empirical approaches are mostly used for practical goals like approximating initial or boundary conditions; including bed surface temperature and released gas concentrations. Empirical models are simple, efficient, and also known as industry-friendly models [12] since they do not require colossal computer resources and lengthy calculations.

Theoretical models are usually used for academic research purposes including the development of new theories and validating them with experimental results and measurements. These models are complex and require substantial computer resources they investigate bed systems in more details than empirical approaches. The only issue that exists with these theoretical models is that they do not describe the heterogeneity of solid biomass fuel which results in their inability to provide a compatible simulation of bed with freeboard [12]. For instance, Peters et al. [12] applied the Discrete Element Method (DEM) solution to predict particle behavior in fuel bed conversion while using only one specific type of biomass particle with particular features, and the model is therefore not capable of predicting the behavior of various biomass particles. Empirical bed models existing in the literature consist of simple chemistry sub-models for describing solid biomass conversion like the model developed by Shins et al. [12] which does not define the interaction between different sections of the bed [12]. Furthermore, the current bed models are not capable of predicting all effects of fuel conversion on the bed such as the variation of solid flow, transient feature, and mixing phenomena of particles.

The principal contribution of this thesis is the development of comprehensive bed models for biomass fuel thermal conversion in grate firing furnace. For instance, while the majority of existing bed models in the literature considered only a specific section of the conversion process, the developed bed models in this thesis cover the entire conversion process of solid biomass fuel in grate firing furnace. Existing bed models are also optimized and improved in terms of

chemical and thermal conversion of sub models. Also, the developed 1-D semi empirical bed model includes detailed chemistry, which makes it adequate for predicting chemical and thermal conversion length of grate firing biomass furnace.

CHAPTER 3: METHODOLOGY & NUMERICAL SIMULATION

3. Methodology and numerical simulation

3.1 Introduction:

In this chapter, four biomass combustion bed models are developed and the processes for these bed models are explained briefly. First, the governing equations are introduced in general form, and then for each bed model, the equations are presented with specific simplifications to match the model assumptions. The mathematical setups and the detailed chemical sub models are presented for each model. Also, the solution methods and algorithms for these models are displayed.

3.2 Biomass conversion in grate firing bed: The modeling process

Mathematically, two types of fixed bed models are configured in this work, namely 0-D and 1-D steady models. Different types of physical and chemical conversion sub models are also applied to these two bed models which results in the development of four separate bed models. However, transport equations are the basis of each model [26].

3.2.1 Properties of fixed bed numerical modeling:

The features of these models are discussed in details here. The physics, chemistry, and model configuration are described below [27].

3.2.1.1 Physics:

The physics of bed model includes the governing equations to describe the transport of mass, element, species, and energy along with the expression of coefficients for these equations. Drying and radiation are physical phenomena.

- Transport equations:

Overall bed models consist of mass, momentum, and energy conservation laws. Heat, mass and dispersion coefficients are included in these equations for the simulation of the fuel bed. Heat and mass exchange coefficients define the transfer of heat through reactants, products, and boundaries in the fuel bed [27], while the dispersion coefficients simulate heat and mass transport along the flow direction. Generally, fixed bed models utilize the terms and expressions which were summarized by Wakao [59] for determining the coefficients as:

- Drying:

Drying is the initial process for solid biomass conversion in the bed which occurs promptly after the fuel is fed into the system. Fuel heats up by absorbing the surroundings gases and furnace walls heat. Heat is transferred through convection and radiation from the surroundings and conduction from the next particles. When the inner side of the biomass fuel reaches 100 degree Celsius, the fuel moisture dries up and reduces the temperature of the burning device. It is not possible to combust fuel with a moisture amount of 60% or more since the energy needed to vaporize the moisture is more than the energy that the fuel produces [5]. There are several approaches in the literature to describe drying. Thunman [30] used a single step reaction with Arrhenius expression to model vaporization in which the moisture is released at its boiling point. Wurzenberger [42] applied an equilibrium model that includes a balance between the water liquid inside fuel particles and gas species. Yang [60] used two expressions for drying rate, one for the temperature below 373 [K] and the other one for temperature above 373 [K].

- Radiation:

To model the radiation flux, which is the result of combusting the gas species in freeboard and is

directed and absorbed by solid fuel bed, the following equation is used [61]:

$$Q^{'''}(z) = \alpha\sigma\left(\varepsilon_g T_{fl}^4 - \varepsilon_s T_s^4\right)e^{-\alpha(z_0 - z)} \quad (3.1)$$

where z is the height of fuel bed [m], ε_g and ε_s are the gas and solid porosity [-], respectively, α is bed permeability [m^2], σ is Stephan-Boltzmann constant [$W\,m^{-2}\,K^{-1}$], $T_{fl}\ and\ T_s$ are freeboard flame temperature and solid bed temperature [K], respectively. Based on experiments [62], z_0 is estimated as 12 [mm], which equals two layers of solid biomass fuel, distributed evenly on the grate surface.

- Diffusion modeling:

Radiation heat from freeboard combustion causes thermal conductivity between particles in each zone and ultimately, between the zones themselves as well. Through the voids, K (conduction coefficient) is modeled as follows [62]:

$$K = \lambda_{radiarion} = \frac{\varepsilon_g}{(1 - \varepsilon_g)}\, 4\sigma d_p\, T^3 \quad (3.2)$$

where ε_g [-] is the gas porosity, σ [$W\,m^{-2}\,K^{-1}$] is Stephan-Boltzmann constant, d_p is the equilibrium diameter of particles, and T [K] is the temperature on the bed surface caused by radiation [62].

3.2.1.2 Chemistry assumptions:

The chemistry in bed models consists of released species, de-volatilization, gas phase reactions, char oxidization and NO-chemistry.

- Species:

The species of the solid biomass fuel are volatiles moisture, char, and ash. The species that are

assumed in the gas phase are $N_2, H_2, CO_2, CO\ and\ H_2O$ in addition to tar. Tar contains light and heavy hydrocarbons and is represented by $C_iH_j\ and\ C_iH_jO$. In this work, tar contains $CH_4\ and\ C_6H_6$. In some published models, several species are considered for tar while in others only one single species is used to represent tar [40, 41]

- De-volatilization:

De-volatilization section includes both pyrolysis and gasification in which volatiles form. Through pores in the fuel bed surface, the volatile gases leave the fuel and then burn when reacting with air in diffusion flame mode [5]. The heat releases from the combustion of volatiles supports both drying and de-volatilization processes. Usually, the temperature range in the de-volatilization zone is between 200 and 500 degree Celsius [5]. After the release of volatiles from the fuel, only char and ash are left. Therefore, the higher the de-volatilization temperature and rates are, the more char will be left off the fuel bed. Mostly, it is believed that de-volatilization is complete if the bed temperature is above 500 Celsius. For the devolatilization process, simple models from single step to multiple steps can be used. Thunman and Johansson [63] used a single step approach based on the three-step mechanism method of Chan [40], and used a single conversion rate which is the summation of the rate used by Chan [53]. Yang [60] used a single step model to test the various experimental rates existing in the literature.

- Char combustion:

In the de-volatilization area, due to the flow of released gases from the bed, it is not easy for oxygen to contact the particles surface and react with the remained solid carbon in the particles. However, after de-volatilization, it is feasible for the oxygen to react with char particles on the fuel bed surface. The density of char largely depends on the final temperature and heating rates.

According to [64], slow heat rates increase char concentration as more time is available for char to be produced from chemical bounds conversions. Char burning is a diffusion monitored procedure for which its combusting rate mostly depends on the exposed surface, available oxygen, and surrounding temperature. Significant outlets of char burning are CO and CO_2 gases. [5]. Multiple approaches exist in the literature to model char oxidization. Thuman and Johansson [40, 63] used a four-step mechanism which consists of oxidization, gasification by CO_2 , H_2 and H_2O. Wurzenberger [41] used a three-step approach very similar to Thunman work. While Yang [60] used a single step mechanisms to model char combustion. In all these models, the kinetic rate for conversion of fuel is limited by mass transfer. Almost in all models, in order to predict the ratio CO/CO_2, experimental correlations from the literature including the data reported in [40, 60, 63] are applied.

- Nitrogen chemistry:

N-release and N precursors are considered in some models including Yang work [65]. In the present thesis, nitrogen release is considered for two models, although it is assumed that N-release during the propagation of the reaction front is in the shapes of HCN and NH_3 only. Simulations of N-chemistry in fixed bed models are few and scarce. Modeling of pollutant species reaction such as NO_x and SO_x is not considered in this work. Only in the last two models, as an example, two of the most common NO_x precursors, including NH_3 and HCN, are introduced. However, NO_x emissions chemistry is not studied in details.

3.2.1.3 Model Configuration:

The model configuration includes the dimensions of the model, boundary conditions and the assumptions that are applied to the model. All models employed in the present thesis are 0-D and

1-D only. In 0-D models, the whole bed is considered as one control volume in which no species transport in any direction is assumed [27, 46]. Figure 3.1 displays a schematic view of different conversion zones in grate-firing biomass furnace bed. General assumptions applied for developing the four bed models in this thesis are summarized as follows [19, 20, 62]:

1. Nitrogen in the supplied air is considered inert at temperatures below 1200 °C.
2. Ash-free fuel (AF) is injected from the top of the bed, and dry primary air (PA) is also supplied from the bottom of the grate.
3. Steady state is considered for all bed models.
4. $C_6H_6(\ Benzen)$ is the only species representing tar.
5. No heat loss to ambient and surroundings through the furnace walls is considered.
6. Pressure remains constant at 1 bar within the bed throughout the entire conversion processes.
7. Gravitational force has a negligible effect on the flow through the bed.
8. Fuel bed is considered a heterogeneous, continuous porous layer consisting of gas and solid phases.
9. Fuel particles are thermally thin, so intra particles' temperature gradients are negligible.
10. Gas flow is incompressible.
11. Pressure drop along the bed height is neglected.
12. Effective thermal conductivity represents the radiation heat inside the bed.

For packed bed modeling, because of significant difference between the temperatures of solid and gas phases, it is recommended to use heterogeneous modeling [51]. In the heterogeneous approach, the solid phase can be considered as either continuous zone (e.g., [31, 66, 67]), or individual particles zone (e.g., [25, 68]). Continuous models consider the bed as an evenly

distributed domain. Also, since there exists no published experimental work on the investigation of flow resistance in the fuel bed, pressure has been completely disregarded [26].

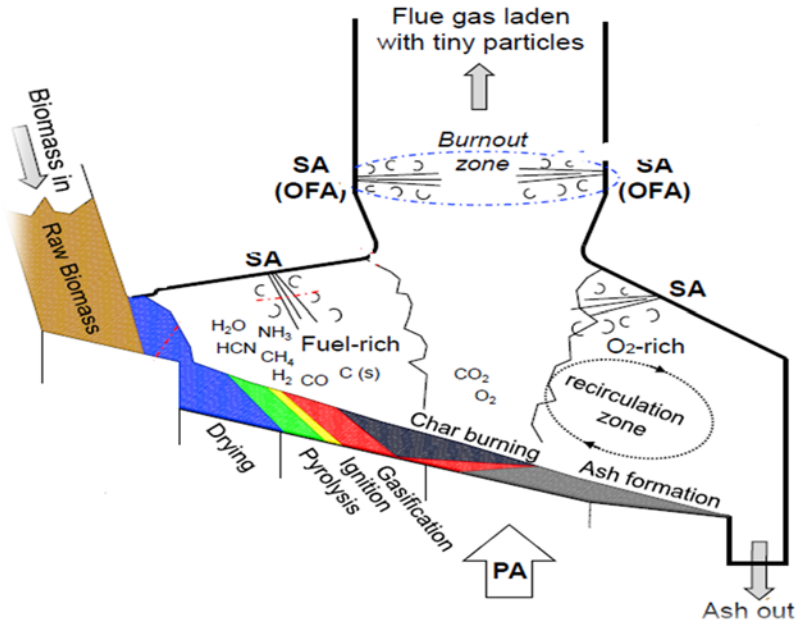

Figure 3.1. A schematic of air supply and different resulted zones in a grate firing biomass boiler [26].

3.2.2 Mathematical description of bed models:

First, the equations for these models are presented in their general forms. Then, for each model, the corresponding equations are used and described, followed by the solution approaches and the numerical methods.

3.2.2.1 Governing equations: General form

A combustion process is controlled by conservation laws of mass, species, energy and momentum. Generally, these conservation laws are described by a system of partial differential equations known as governing equations [26].

$$\partial \frac{\varepsilon \rho \emptyset}{\partial t} + \nabla . (\varepsilon \, \rho \, V) = \nabla . (\Gamma \, \nabla \emptyset) + S_{\emptyset} \tag{3.3}$$

Equation (3.3), is known as transport equation where ε [-] is porosity, ρ [Kg/m^3] is density, V [m/s] is the velocity vector, ∅ is the transported scalar, Γ is the diffusion coefficient and finally $S_\emptyset$ is representing the source terms. Also the term of ε ρ is defined as bulk density. By applying the proper variables over equation (3.3) instead of Γ, ∅ and $S_\emptyset$, the specific governing equation for mass, energy and species transport for combustion process will be generated. These variables are introduced in Table 3.1. Moreover, as explained earlier in this thesis, models with both solid and gas phases are called heterogeneous for which if temperature and species concentration gradients at the fuel bed surface are negligible (continuous fuel layer beds) then the bed model can be treated as homogenous model (one phase) [26].

Table 3.1.Proper variables substitution for general transport equation.

Equation name	**∅**	**Γ**	$\boldsymbol{S_\emptyset}$
Continuity (3.4)	1	0	Sum of reaction rates (r)
Species (3.5)	Mass fraction of species (Y_i)	Bulk density times by Effective mass dispersion ($\varepsilon\ \rho D$)	Rates of species consumption and production
Energy (3.6)	Enthalpy (h_i)	Thermal conductivity divided by specific heat capacity (λ/c_p)	Heat transfer rates

In Table 3.1, the enthalpy of bed (h), the species enthalpy (h_i) and the specific heat capacity (C_p) are defined and implemented as follows:

$$h = \sum Y_i\ h_i \tag{3.7}$$

where

$$h_i = \int_{T_{ref}}^{T} c_{pi}\ dT + h_i^0 \tag{3.8}$$

$$Cp(T) = a + bT + CT^2 + dT^3 \tag{3.9}$$

where, h_i^0 is the enthalpy of i species at standard pressure and room temperature. The standard temperature is T_{ref} = 300.19 K; T is the species temperature in (K) and a, b, c and d are the specific coefficients of each species released from the bed. These coefficients can be picked up from thermodynamic tables [69].

3.2.2.2 Boundary conditions:

Boundary conditions at the grate are provided by the operating conditions, i.e., primary air enthalpy (temperature), mass flux and concentrations of species (Table 3.2), where zero enthalpy gradients are applied for the fuel solid phase. At the bed top, zero gradients are assumed for gas enthalpy and species mass fraction.

3.2.3 Biomass fuel properties:

In biomass combustion system design and modeling, there are some basic parameters that must be considered which include fuel composition, lower heating value, bulk density and sometimes the particles dimensions. These parameters for different types of biomass fuels are available in the literature sources and online databases [26]. A brief list of all biomass properties that are needed for the calculation of coefficients in the governing equations in this work is introduced as follows:

1. Fuel composition (Ultimate and proximate)
2. Fuel bulk density
3. Thermal conductivity of gas and solid fuel
4. Mass dispersion coefficient
5. Specific heat capacities
6. Emissivity of fuel particles

7. Fuel bed porosity
8. Mixing rate (related to empirical formula)
9. Inlet rate of fuel and primary air

Table 3.2 gives the biomass fuel characteristics. The simulations in this work are conducted based on the following fuel features [4].

Table 3.2. Characteristics and chemical analysis of the applied biomass fuel.

Proximate analysis	***(% dry basis)***	***Ultimate analysis***	***(% wet basis)***
Moisture	7.3	C	46.4
Fixed Carbon	14.2	H	5.7
Volatile matter	78	O	39.6
Ash	0.5	N	1
		Moisture	7.3
LHV of fuel	16.47 [MJ/Kg]	*Primary air mass flow*	0.4637 [Kg/s]
Fuel mass flow	0.1108 [Kg/s]	*Bulk density*	690 [Kg/m^3]
Emissivity of bed	0.6 [-]		

3.3 Bed models:

Bed models presented in this work, are 0-D and 1-D, for which MATLAB codes (Appendix A-F) are developed. MATLAB codes solve the chemical, transport, mass and energy conservation equations over the bed domain using numerical methods applying proper assumptions for chemical reactions in each bed model. In 0-D bed models, no physical gradient in any geometrical direction is considered and the equations are solved while considering the whole bed as one control volume. However, in 1-D bed model the mass, energy and transport equations are solved by considering mass and energy gradient along the length of the bed (x axis) only.

3.3.1 Semi-empirical 0-D, one zone model:

For this model, in addition to the general assumptions (Sec.3.2.2), the following specific assumptions are made based on experimental results and published studies [5, 46]. Figure 3.2 shows a simple schematic view of this model.

0-D one-zone model assumptions are:

1. The whole bed is one control volume, meaning the bed is not divided into different conversion zones, and all the species are released from one zone which is the entire bed.
2. No NO_x emission and tar is considered in the released volatiles.
3. Average temperature is considered for all the released volatiles.
4. There is no temperature gradient and density shrinkage along any direction of the bed.
5. The evaporation is assumed partial which means not all the moisture dries up.

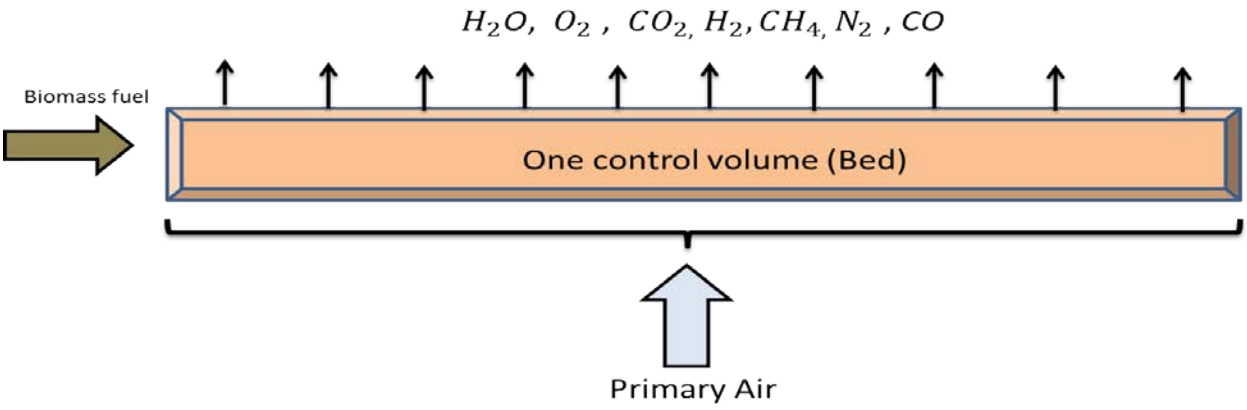

Figure 3.2. Schematic shape of 0-D one zone bed model

Chemical conversion of biomass fuel and the released emissions from the whole bed are considered as in (3.10). The right side coefficients of the chemical equation in (3.10) are defined by the experimental correlations (Eqs. 3.11, 3.12) and chemical equilibrium, while the left side coefficients are determined through biomass fuel chemical analysis (Table 3.2).

$$\alpha\, C_a H_b O_c N_d + \beta\, air \rightarrow \gamma_1 H_2O + \gamma_2 O_2 + \gamma_3 CO_2 + \gamma_4 H_2 + \gamma_5 CH_4 + \gamma_6 N_2 + \gamma_7 CO \quad (3.10)$$

The volatile species in (3.10) are seven while the number of equations obtained from element conservation is only four. To solve the system of equations; $CO, CO_2\ and\ CH_4$ amounts are obtained from published experimental correlations [5, 46].

$$\frac{CO}{CO_2} = 1.94 * 10^{-6} * T_s^{1.87} \quad (3.11)$$

$$\frac{CH_4}{CO_2} = 1.305 * 10^{-11} * T_s^{3.39} \quad (3.12)$$

Applying the mass conservation law over the bed control volume [5] gives us:

$$\dot{m}_{total} = \dot{m}_{fuel} + \dot{m}_{primary\ air} \quad (3.13)$$

$$\dot{m}_{moisture} = Y_{moisture}.\dot{m}_{fuel} \quad (3.14)$$

$$\dot{m}_{fuel-daf} = (1 - Y_{moisture} - Y_{ash}).\dot{m}_{fuel} \quad (3.15)$$

where $\dot{m}_{total}$ is the entire mass flow into the furnace, $\dot{m}_{moisture}$ is the mass flow rate of the moisture in the fuel, $Y_{moisture}$ is the mass fraction of the water in side fuel, Y_{ash} is the mass fraction of inorganic materials in the fuel also known as ash. The mass fraction of elements of species in the fuel is calculated by applying the species conservation equation over the bed as:

$$Y_i = \frac{Y_{if}.m_{fuel-daf}}{m_{total}} \quad (3.16)$$

$$\sum Y_i = 1 \quad (3.17)$$

where i is the number of gas species released from the bed (3.10). Once the concentration of the volatile species leaving the bed is determined, the enthalpy of the released gases can be calculated using the energy conservation law over the bed control volume. This calculation will

also decide the temperature for the released gases over the bed [5, 46]. A simplified version of the energy conservation law (3.6) in table 3.1, which is used in this section, is expressed as:

$$\dot{m}_{fuel} LHV + \dot{m}_{primary\ air} h_{primary\ air} = \dot{m}_{total} \sum_i Y_i h_i \quad (3.18)$$

where LHV is the lower heating value of the fuel in [MJ/kg].

The solution algorithm for the 0-D one-zone model is summarized in Figure 3.3. This algorithm indicates the process of developing the MATLAB (Appendix A) code for modeling the bed in 0-D one-zone condition. An overall description of 0-D algorithms is presented in section 3.6.1 of this chapter. According to the Figure 3.3, the mass flow rate of the primary air, and the ash free biomass fuel along with their physical and chemical properties are applied as inputs of the MATLAB code (Appendix A). The second part of the code is about the species assumptions for the 0-D one zone model. The species are estimated based on the chemical equilibriums. In the third section of the code, mass and element conservation equations (3.15-3.19) are applied on the whole bed to find the mass flow rate of each gas emissions. The final part of the code is about developing a temperature dependent loop over the bed length to solve and find the temperature of the released gases from the bed via trial and error. This loop stops if the energy conservation law (3.18) is confirmed. Upon meeting these conditions the code converges.

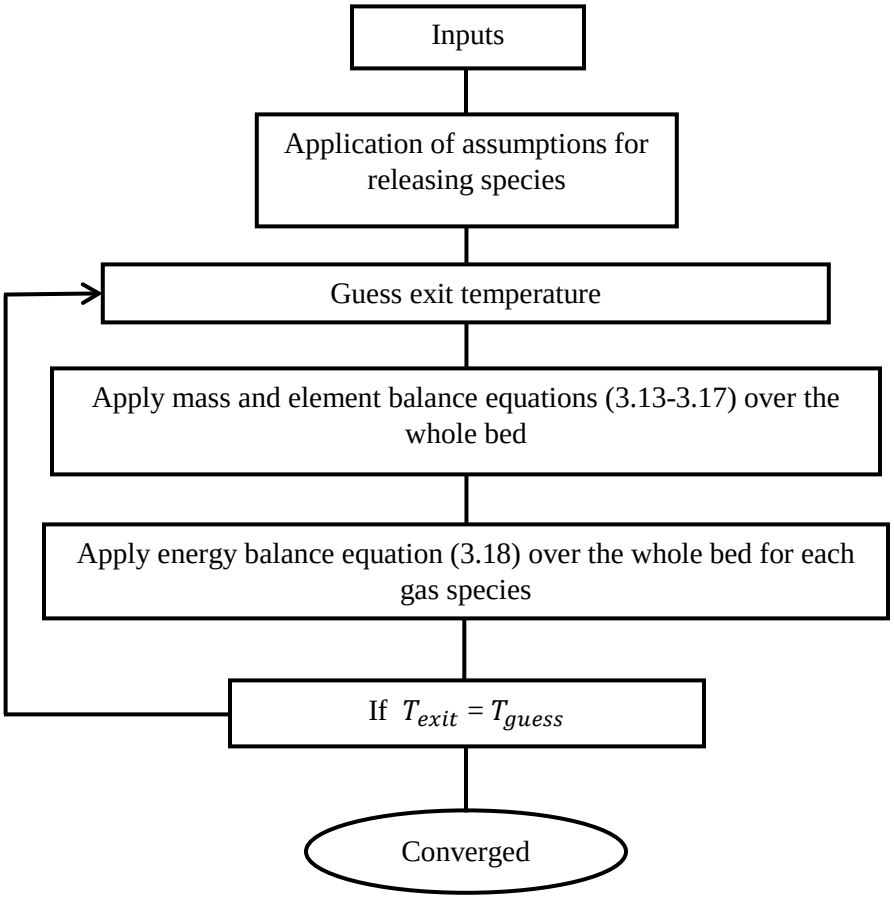

Figure 3.3. 0-D one zone model; solution algorithm

3.3.2 Semi-empirical 0-D, two-zone model:

A zero-dimensional two-zone steady bed model, which first was proposed by Deydier [46], is developed and applied to the biomass furnace bed. The 0-D one-zone model is modified by dividing the chemical length of the bed into two separate conversion zones. Steady state condition and atmospheric pressure are assumed in developing the model. Additionally, the gas emissions which leave the bed are in thermal equilibrium [46].

- Conversion sub model:

The conversion sub model considered in this model is described here. The surface of the bed is divided into two zones to simulate chemical behavior and reactions of the solid biomass on the

bed; drying zone and conversion zone [46]. Figure 3.4 displays a simple schematic view of this model and its assumed sub models. For this model, the following specific assumptions are made:

1. The whole bed is one control volume which is divided into two separate chemical zones: drying and conversion (devolatilization & char combustion).
2. No NO_x emission and tar is considered in the released volatiles.
3. Average temperature is considered for all the released volatiles.
4. There is no temperature gradient and density change along any direction of the bed.

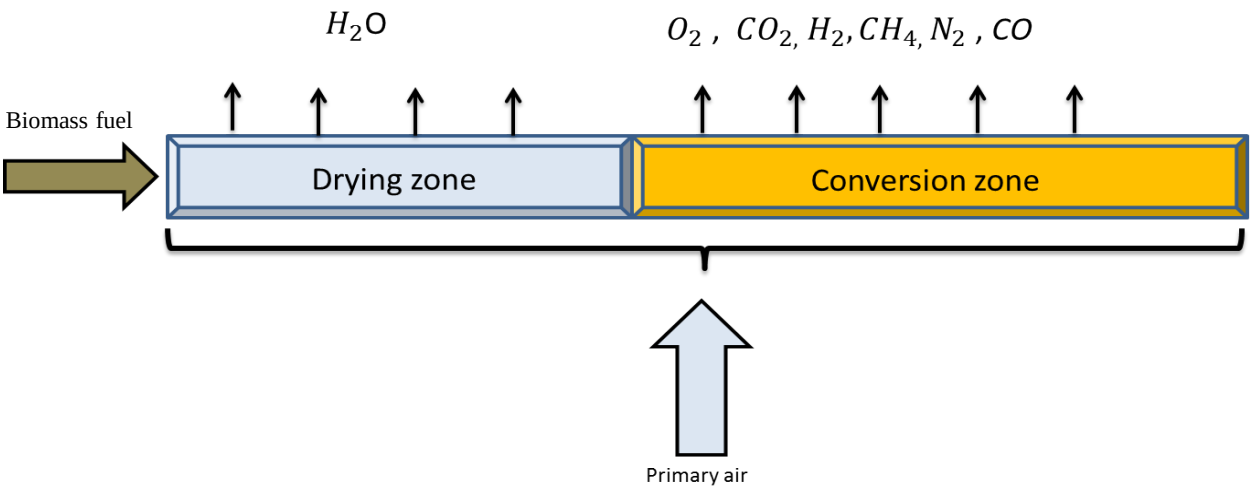

Figure 3.4. Schematic shape of 0-D two zone bed model

The chemical conversion of the biomass fuel in the 0-D two-zone model is assumed as expressed in equations (3.19) and (3.20).

$$1.\ \alpha C_a H_b O_c N_d \xrightarrow{Heat} (\alpha C_a H_{b'} O_{c'} N_d)_{dry} \tag{3.19}$$

$$2.\ (\alpha C_a H_{b'} O_{c'} N_d)_{dry} + \beta air \rightarrow \gamma_1 H_2O + \gamma_2 O_2 + \gamma_3 CO_2 + \gamma_4 H_2 + \gamma_5 CH_4 + \gamma_6 N_2 + \gamma_7 CO \tag{3.20}$$

The left side coefficients in equations (3.19) and (3.20) are defined using the ultimate and proximate analysis of biomass in Table (3.2). The right side coefficients of the chemical reactions in equations (3.19) and (3.20) will be estimated via correlations and empirical ratios the same as 0-D one zone model.

- Chemical sub models:

Drying: For 0-D two-zone model, complete drying assumption is considered. For complete evaporation, the entire moisture turns into water vapor and leaves the feedstock in the bed. Mass and energy balance equations are solved by developing a MATLAB code (Appendix B) for this section [46].

$$H_2O_L \xrightarrow{Freeboard\ heat} H_2O_g \tag{3.21}$$

Mass conservation equation:

$$m_{H_2O}^{moisture} = m_{H_2O}^{dry} \tag{3.22}$$

Energy conservation equation:

$$m_{fuel}h_{fuel} + q_{radiation} = m_{moisture}h_{moisture} + m_{daf}h_{daf} \tag{3.23}$$

where $q_{radiation}$ is the heat which is gained from the freeboard reactions through radiation heat transfer which is needed for fuel drying.

Conversion: Conversion zone includes de-volatilization, gasification and char combustion processes. In this zone, the dried biomass fuel converts into permanent gas emissions, tar (liquid hydrocarbons), and char (fixed carbon), subsequently through gasification tar cracks to gas and via char combustion, char oxidizes and turns in to permanent gases. Therefore, the results of this zone are several different gases released from the solid biomass fuel [46]. In this 0-D model, it is

assumed that mixtures of six gases are released into the freeboard. These gases are:$N_2, H_2, CO_2, CO, CH_4, O_2$. Primary air is supplied to both zones from the bottom of the bed. Nitrogen (N_2) of primary air in the condition of bed temperature below 1200 °C is featured as inert. To solve conversion zone, atomic conversion for C, H, N, O is required in addition of mass and energy conservation. The atomic system of equations for conservation is solved by considering experimental correlations in equations (3.11) and (3.12) for some of the species and then use chemical equilibrium concept for the rest.

$$m_{daf} + m_{primary\ air} = \sum_{i=1}^{i=6} y_i \tag{3.24}$$

where y_i is the mass fraction of released gases. The solution method for the 0-D, two-zone model, is presented in the algorithm of Figure 3.5. Also the equation for the energy conservation is applied as:

$$\dot{m}_{daf} LHV + \dot{m}_{primary\ air} h_{primary\ air} = \dot{m}_{daf} \sum_i Y_i h_i \tag{3. 25}$$

Figure 3.5 briefly indicates how the MATLAB code for the 0-D two zone model works (Appendix B). In this code, the solving procedure is the same as the 0-D one zone. Although in this bed model, the surface of the furnace bed is separated into two separate zones: drying and conversion (devolatilization and gasification, char combustion). The mass conservation equation of (3.22) is applied for the drying section while for the conversion zone (3.24) is used. There are two energy conservation loops in this code to find the temperature of the released gases from each zone. Equations (3.23) and (3.25) are used as the energy conservation laws over each zone. T_{guess} is the temperature that the code keeps guessing in a defined range to find the corresponding temperature for each gas. This range is based on the literature review and experimental measurements.

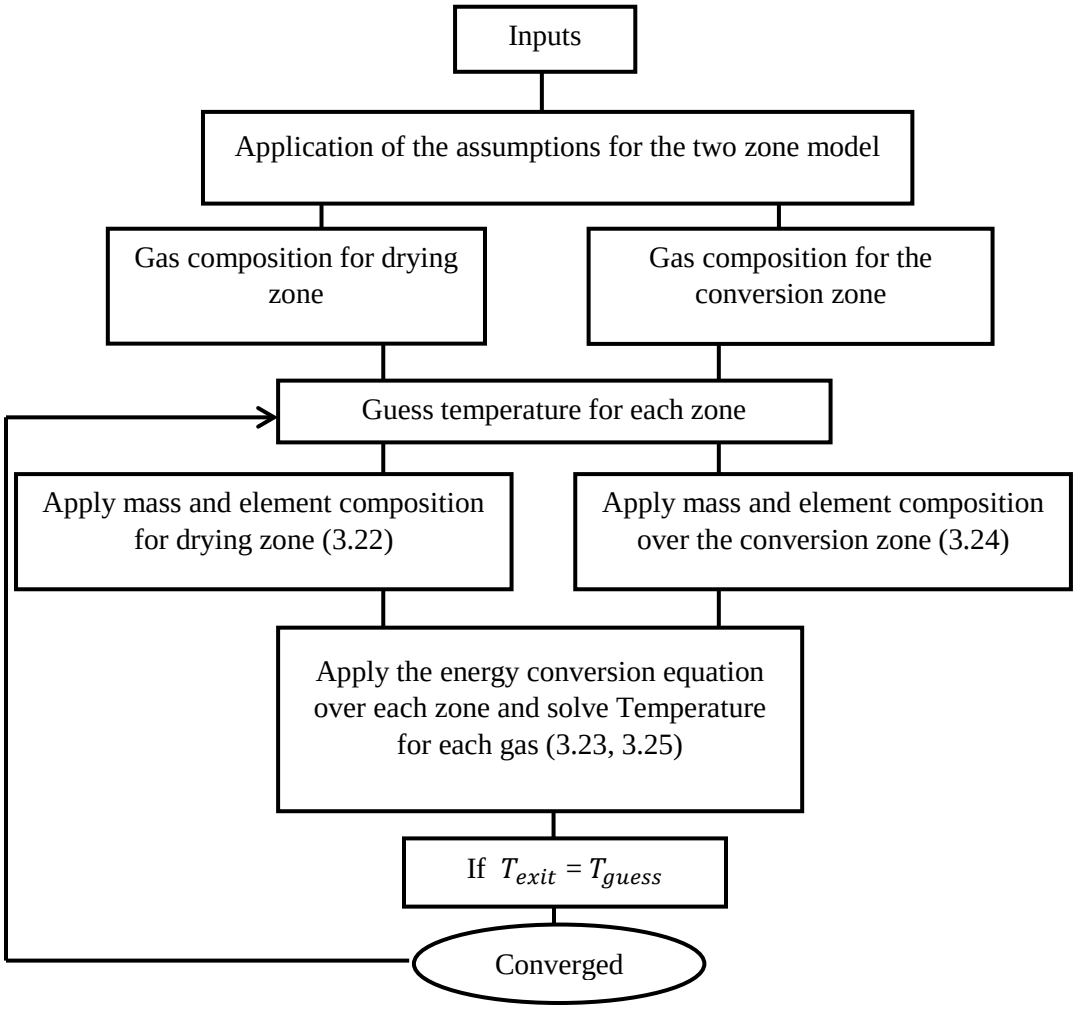

Figure 3.5.0-D two zone model; solution algorithm

3.3.3 Semi-empirical 0-D, three-zone model:

In this model, the biomass fuel bed is divided into three separate zones based on chemical reactions occurring in fuel bed as follows: drying, de-volatilization and char oxidization [4]. Similar to previous models, in this model also primary air is supplied from the bed bottom and the solid fuel is injected from the top. Figure 3.4 shows a schematic view of the model and its associated submodels. Mass, energy and element conservation laws are applied to each zone separately to determine the mass flow rate, species concentration and the temperature of released gases from each zone of the bed [4].

For 0-D three-zone model, it is specifically assumed that:

1. The whole bed is a single control volume which is separated into three different chemical/conversion zones: Drying, Devolatilization and Char combustion.
2. Different species are released from each zone. (Figure 3.4)
3. Average temperature is considered for all the released volatiles.
4. There is no temperature gradient and density shrinkage along any direction of the bed.
5. C_6H_6 represents the released tar from devolatilization zone.
6. Primary air is only applied on the char combustion zone.
7. This model is developed once with considering no NO_x precursors ($HCN\ and\ NH_3$) and then with considering NO_x precursors among the released emissions.

The reason for assuming only the primary air injection for the char combustion zone is that the dense flow of the released gases from the devolatilization zone would not allow the primary air to penetrate into this zone.

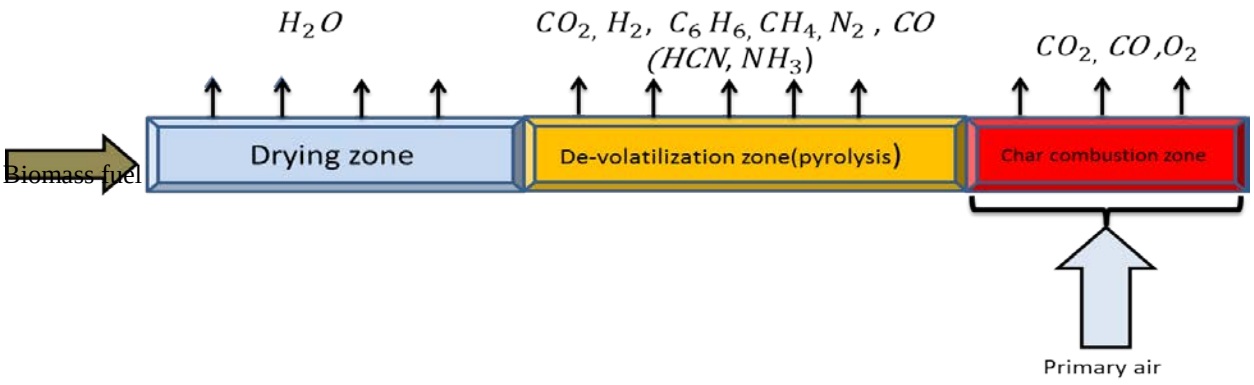

Figure 3.6. Schematic shape of 0-D three zone bed model

- Chemical submodels

Drying: There exist a lot of approaches in the literature to describe the drying process of the solid fuel in the bed [4, 20]. Drying is simulated by the Arrhenius model [20] in 0-D three-zone bed model. Arrhenius drying model is a first-order kinetic rate model which has been used to describe moisture vaporization [20, 70, 71, 72]. According to this concept, biomass moisture only contains pure water and evaporation process is only limited by the amount of moisture in the solid fuel [4].

$$Moisture\ (H_2O_l) \xrightarrow{Evaporation} Vapor\ (H_2O_g) \tag{3.26}$$

De-volatilization: As mentioned in previous sections of this thesis, biomass fuel contains significant amounts of volatile species which are released as gases in the devolatilization zone. The oxygen in the primary air injected from the bottom of the bed into this zone cannot completely infiltrate into this zone. Therefore, de-volatilization is also known as pyrolysis [4]. This model has been solved, with the application of two different assumptions for released gases from the de-volatilization zone; i) NO_x precursors including NH_3 and HCN which are not considered in the group of the released gases of de-volatilization zone, ii) NH_3 and HCN are considered among the released gases from the bed in the second chemical zone. The other gases released from de-volatilization are the same as in the previous models except for the oxygen which is assumed zero since the process is pyrolysis.

$$Wood \xrightleftharpoons{pyrolysis} Volatile + char \tag{3.27}$$

$$Volatile \rightarrow \gamma_1 CO + \gamma_2 CO_2 + \gamma_3 H_2 + \gamma_4 CH_4 + \gamma_5 C_6H_6 + \gamma_6 N_2 \tag{3.28}$$

$$Volatile \rightarrow \gamma_1 CO + \gamma_2 CO_2 + \gamma_3 H_2 + \gamma_4 CH_4 + \gamma_5 C_6H_6 + \gamma_6 N_2 + \gamma_7 NH_3 + \gamma_8 HCN \tag{3.29}$$

Also, in this model, it is assumed that de-volatilization is a one-step process to release volatile gases to the freeboard as a result of radiation heat from combustion of gases in the upper surface of the bed [20, 27, 32, 41]. In this model, to describe the chemical behavior of the solid fuel on the bed, experimental correlations from the literature are applied to the (3.28), and (3.29) chemical equations. Then, using element conservation law, the species concentrations are determined in the volatile matter [73, 65]. The experimental correlations are as follows [4]:

$$\varphi_1 = \frac{CO}{CO_2} = \frac{\gamma_1}{\gamma_2} \quad (3.31) \qquad \varphi_2 = \frac{CH_4}{CO_2} = \frac{\gamma_4}{\gamma_2} \quad (3.30)$$

$$\varphi_1 = 1.94 * 10^{-6} * T_s^{1.87} \quad (3.33) \qquad \varphi_2 = 1.305 * 10^{-11} * T_s^{3.39} \quad (3.32)$$

$$\frac{N}{NH_3} = 1.11 \quad (3.35) \qquad \frac{N}{HCN} = 9.7 \quad (3.34)$$

where T_s stands for the bed surface temperature in devolatilization zone, which is expressed in Kelvin.

Char combustion: The products of char oxidization are considered as $CO\ and\ CO_2$. A published experimental correlation for char oxidization is used to determine species amount released from char zone. This correlation is dependent of the bed temperature in the char combustion zone. Char oxidization is governed by the following equations [4]:

$$C_s + \alpha O_2 \implies 2(1-\alpha)CO + (2\alpha - 1)CO_2 \quad (3.36)$$

$$\frac{CO}{CO_2} = 2500\exp(-\frac{6420}{T_s}) \quad (3.37)$$

In the models, it is assumed that char oxidization reaction is limited and controlled by diffusion, and the amount of char in the bed. For solving and determining the physical behavior of the solid fuel in the bed, the mass and energy conservation laws are applied on each zone as follows [4]:

$$\sum m_{in} = \sum_{i}^{species} m_{out_i} \tag{3.38}$$

$$m_i h_i + q_{rad} + LHV = m_o(h_{o+} h_{combustion}) \tag{3.39}$$

where q_{rad} is the radiation heat flux produced by combustion in freeboard, LHV is the amount of heat which is releasing while the solid biomass is burned, $h_{combustion}$ is the heat released due to the conversion of states and chemical compositions of the species, m_i and m_o represent the inlet and outlet mass flow, respectively, and h_i and h_o are the sensible and standard enthalpy which are defined as in equations (3.7) and (3.8). The solution algorithm for the 0-D, three-zone model, is presented in Figure 3.7. This figure, introduces a summary of the MATLAB code algorithm for the 0-D three zone bed model (Appendix C). The physical and chemical properties of the biomass fuel and the primary air are given as inputs. The 0-D three zone model assumptions are applied on the chemical reactions and emissions. The chemical length of the bed is divided into three sections. The mass, element and energy conservation equations are solved on each zone separately while their solutions are coupled to each other via trial and error loop in MATLAB. The loop solves the equations over the bed zones until a conservation of mass and energy are reached over each zone.

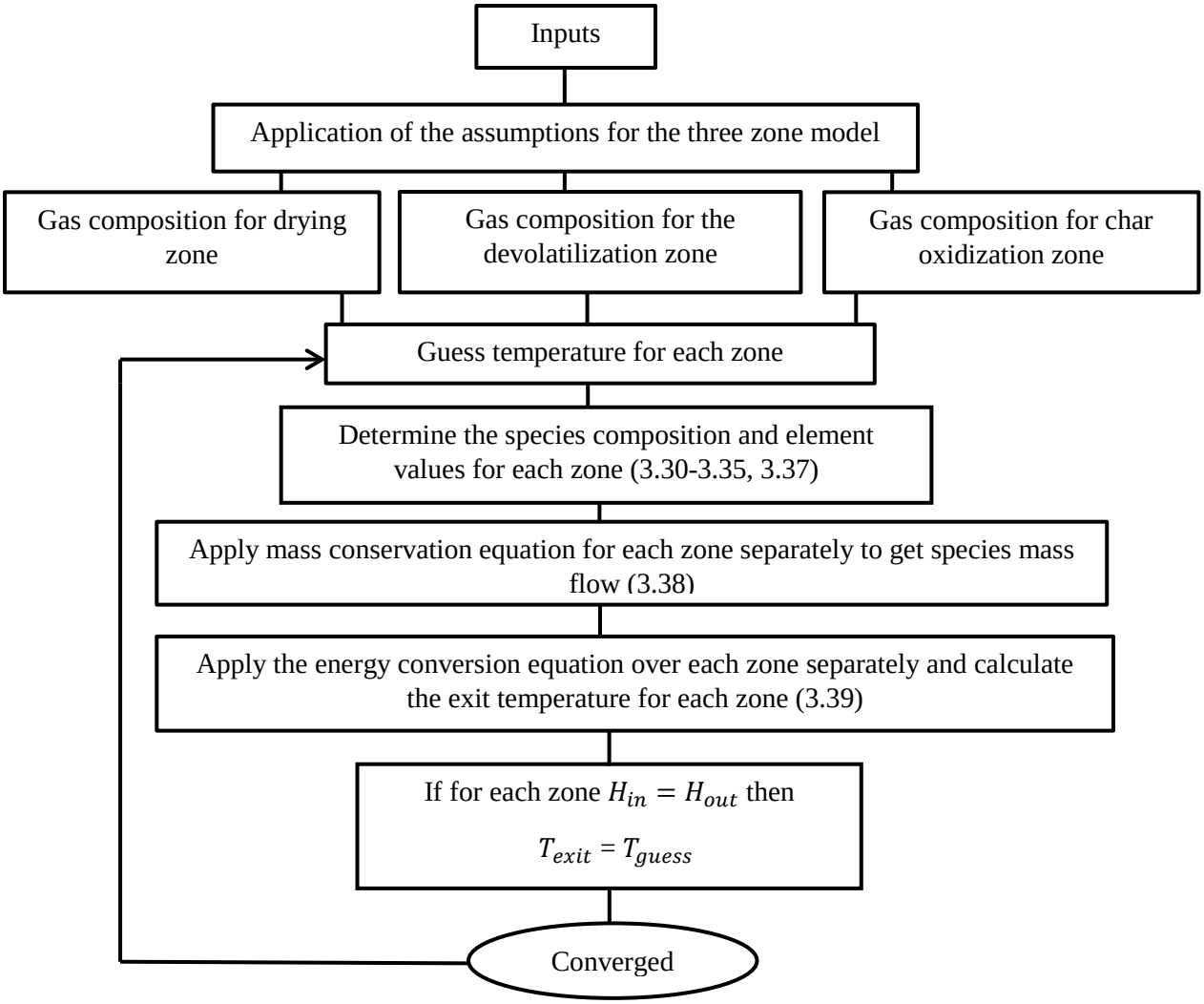

Figure 3.7. 0-D three zone model; solution algorithm

3.3.4 One dimensional, steady, three-zone model:

In this model, chemical conversion zones and released species from the bed are similar to the zero-dimensional model that was described in section 3.5.3. However, more detailed chemical conversion submodels are applied in zones [26]. These submodels are based on conversion rates in each zone which these converion rates are introduced via the equations obtaind from experiments reported in literature. By considering chemical kinetic rates, it means that the released gases from the bed are not uniform and are generated while moving forward along the

bed. Figure 3.5 illustrates a schematic view of the 1-D three zone model together with the assumed sub-models.

For 1-D three zone model, it is specifically assumed that:

1. The whole bed is a control volume which is separated into three different chemical zones: Drying, Devolatilization and Char combustion.
2. Different species are released from each zone (Figure 3.4)
3. Chemical reactions determine the conversion length of the bed.
4. The temperature and mass gradient are assumed only along the length direction of the bed.
5. No heat loss through the wall of the furnace is considered [26].
6. C_6H_6 is considered as a representative of the released tar in devolatilization zone.

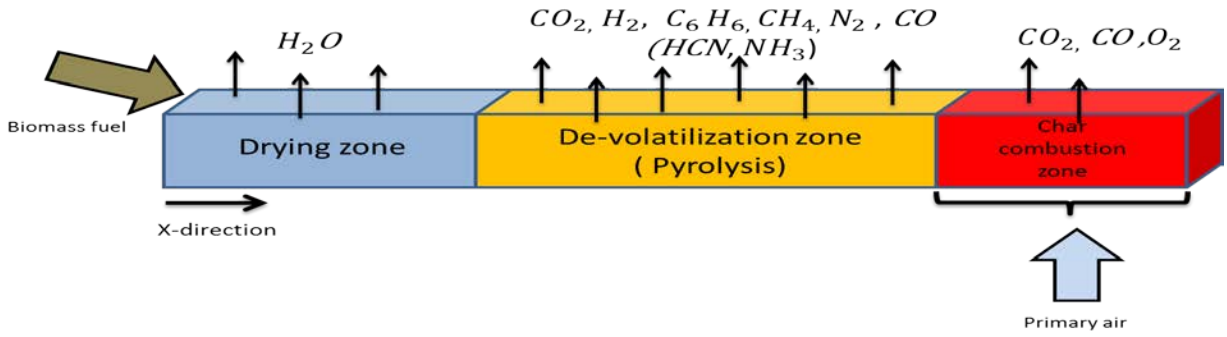

Figure 3.8. Schematic shape of 1-D three zone bed model

3.3.4.1 Governing equations:

The governing equations for the 1-D bed model are derived from the general transport equations of mass, species and energy presented in equations (3.3) and ultimately from equations (3.4), (3.5) and (3.6). The 1-D governing equations are the simplified form of the general transport

equations. These simplifications are carried based on the assumption and initial conditions that are considered for 1-D bed model in 3.5.4 section of this work.

Governing equations of 1-D steady packed bed model are formulated as follows [26]:

$$\frac{\partial(\epsilon_b\,\rho_g v_g)}{\partial x} = r_{dry} + r_{pyr} + r_{char} \qquad [\frac{kg}{m^3 s}] \tag{3.40}$$

$$\frac{\partial(\epsilon_b\,\rho_g v_g Y_{g,i})}{\partial x} = \frac{\partial}{\partial x}\left(\epsilon_b \frac{\rho_g D_{g,i}\partial Y_{g,i}}{\partial x}\right) + r_i + \epsilon_b \sum r_{i.} \qquad [\frac{kg}{m^3 s}] \tag{3.41}$$

$$\frac{\partial(\epsilon_b\,\rho_g v_g h_g)}{\partial x} = \frac{\partial}{\partial x}\left(\epsilon_b \frac{\lambda_g \partial h_g}{c_{p,i}\partial x}\right) + h_c A_p(T_s - T_g) + (r_{dry} + r_{pyr} + r_{char})h_s - \epsilon_b \sum_{j=1}^{G} \Delta h_j r_j \qquad [\frac{W}{m^3}] \tag{3.42}$$

where the right side term in the continuity equation (3.40) introduces the total kinetic rate of the species formation in fuel bed processes. The continuity equation for species in equation (3.41) term is written for the *i-th* gas species which are produced in each section of the bed. The source terms in the energy transport equation are described as follows:

- $h_c A_p(T_s - T_g)$ heat gained from the interphase convective heat transfer
- $(r_{dry} + r_{pyr} + r_{char})h_s$ heat transfer due to mass transfer in bed
- $\epsilon_b \sum_{j=1}^{G} \Delta h_j r_j$ heat released from the homogeneous reaction in the freeboard

Sensible enthalpies are related to temperature through temperature-dependent specific heat capacity which is introduced in equations (3.8) and (3.9).

3.3.4.2 Coefficients of process rates:

Coefficients of these conversion kinetic rates must be determined accurately and adequately to solve mass, species and energy equations in (3.40), (3.41) and (3.42). Conversion kinetic rates are obtained through experimental measutments and correlations and are defined as follows [26]:

$$r_{drying} = \ 2.822 * 10^{-4} \exp\left(-\frac{10584}{T_s}\right)(1-\varepsilon_b)\rho * YH_2O * (T_s - 475)^7 \qquad \left[\frac{kg}{m^3 s}\right] \quad (3.43)$$

$$r_{pyr} = 1.56 * 10^{10} \exp\left(-\frac{16600}{T_s}\right)(1-\varepsilon_b)\rho Y_{volatile} \qquad \left[\frac{kg}{m^3 s}\right] \quad (3.44)$$

$$r_{char} = 12 * \exp\left(-\frac{3300}{T_s}\right) \qquad \left[\frac{kg}{m^3 s}\right] \quad (3.45)$$

For drying rate, first-order kinetic rate model, as in (3.43), is used and implemented in the MATLAB code (Appendix E-F). The temperature dependence of the kinetic rate is presented in equation (3.43). For temperatures higher than 457 K, the equation (3.43) results in unrealistic rates. Thus, this model is deemed not suitable for high drying temperatures unless the evaporation completes below 475 K) [26]. Pyrolysis rate (devolatilization rate) is given as a first-order reaction rate with Arrhenius constant (3.44). $Y_{volatile}$ [kg/kg] is the mass fraction of volatile species $\in \{ CO_2, CO, CH_4, H_2, N_2, O_2, C_xH_y \}$ [26]. For char burning, it is assumed that char oxidizes according to equation (3.45). It can be realized from the above equations that the conversion rates are temperature dependent. The mass, energy, momentum and element conservation equations are solved for each zone in this model, based on spatial differential along the bed length. Therefore, the model is referred to as one dimensional [4]. Figure 3.9 presents a summary of the solution algorithm which is used in developing the MATLAB codes (Appendix E-F) for the 1-D three zone bed model. This solution algorithm describes how the code initiates and runs, and detailed explanation of the code solution procedure is presented in the following section 3.6.2 of this chapter.

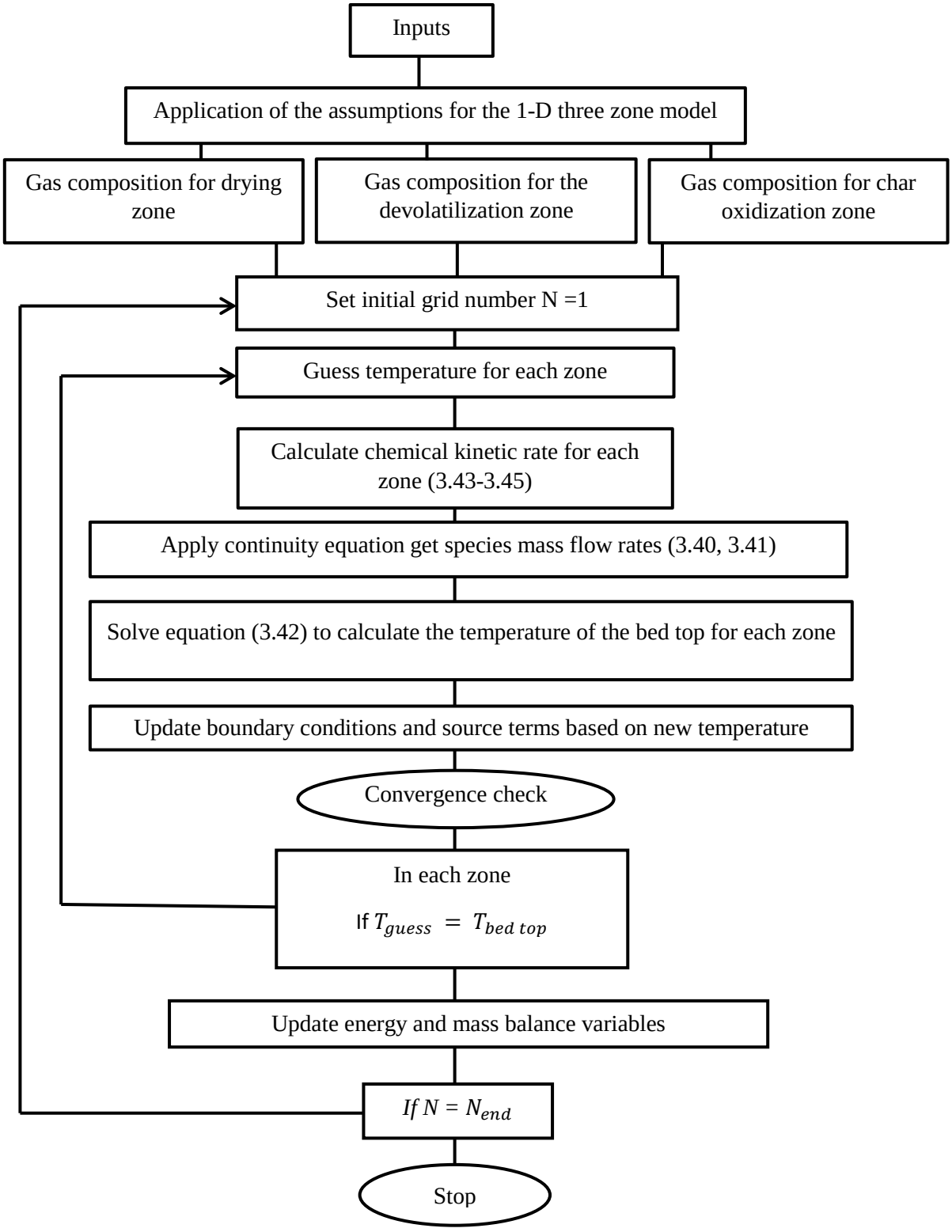

Figure 3.9. Solution algorithm of 1-D three-zone model

3.3.4.3 Discretization of the 1-D model governing equations:

The governing equations in (3.40-3.42) are discretized and solved using finite volume method. Finite volume is a standard approach in CFD platforms for solving equations involving mass and energy transport. Also finite volume method is a discretization technique for partial differential equations which present conservation laws of energy and mass. A short description of the governing equation discretization is presented in this section. The discretization in this section shows the 1-D bed model special case when the transport is one dimensional steady and velocity is already known. The bed is presented as a rectangular and the computational domain for each chemical conversion zone is divided into a number of control volumes which form a uniform grid [26], as shown in the figure 3.10.

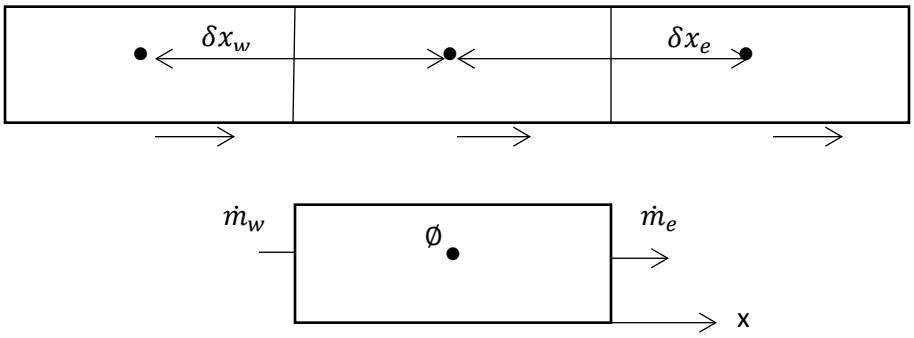

Figure 3.10. One dimensional computational grid

In the following equations (3.46), (3.47), the transport scalar is considered as $\emptyset$ in convective term which represents mass, species concentration Y_i and the species enthalpy $h_g$in mass, species and energy conservation equations in (3.40), (3.41) and (3.42). $S_\emptyset$ represents the source terms in the governing equations in section 3.5.4.1. The source terms are the outlets of the chemical reactions that are happening within the bed and therefore they are dependent of the conversion

zones. Γ represents the constant parameters in the diffusion terms, which is equal to $(\epsilon_b \rho_g D_{g,i})$ in equation (3.40) and to $\left(\epsilon_b \frac{\lambda_g}{c_{p,i}}\right)$ in equation (3.42). The equation for mass conservation and transport of ∅ are considered as (3.46) and (3.47), respectively.

$$\frac{d(\rho U \emptyset)}{dx} = 0 \tag{3.46}$$

$$\frac{d(\rho U \emptyset)}{dx} = \frac{d\left(\Gamma \frac{d\emptyset}{dx}\right)}{dx} + S_{\emptyset} \tag{3.47}$$

$$\dot{m} = \rho U A \tag{3.48}$$

Equation (3.47) is integrated over a typical control volume as shown in Figure 3.10.

$$\int \frac{d(\rho U \emptyset)}{dx} d\forall = \frac{d\left(\Gamma \frac{d\emptyset}{dx}\right)}{dx} d\forall \tag{3.49}$$

Performing the integration leads to:

$$\Gamma_e A_e \left(\frac{d\emptyset}{dx}\right)_e - \Gamma_w A_w \left(\frac{d\emptyset}{dx}\right)_w = \frac{\Gamma_e A_e}{\delta x} (\emptyset_E - \emptyset_P) - \frac{\Gamma_w A_w}{\delta x} (\emptyset_P - \emptyset_W) \tag{3.50}$$

Finally, equation (3.50) can be written as:

$$\Gamma_e A_e \left(\frac{d\emptyset}{dx}\right)_e - \Gamma_w A_w \left(\frac{d\emptyset}{dx}\right)_w = D_e (\emptyset_E - \emptyset_P) - D_w (\emptyset_P - \emptyset_W) \tag{3.51}$$

Where $D_e = \frac{\Gamma_e A_e}{\delta x}$ (3.52)

And $D_w = \frac{\Gamma_w A_w}{\delta x}$ (3.53)

Since the domain grid is uniformly spaced, a linear interpolation is used to obtain the face values of the transport scalar ∅. This linear interpolation is referred to as the central differencing schemes (CDS) in numerical methods.

$$\emptyset_e = \frac{1}{2}(\emptyset_P + \emptyset_E) \;\&\; \emptyset_W = \frac{1}{2}(\emptyset_P + \emptyset_W) \tag{3.54}$$

By substitution and rearranging, equation (3.54) can be written as:

$$a_P \emptyset_P = a_W \emptyset_W + a_E \emptyset_E \tag{3.55}$$

where

$$a_W = D_w + \frac{1}{2}\dot{m}_w \tag{3.56}$$

$$a_E = D_e - \frac{1}{2}\dot{m}_e \tag{3.57}$$

Therefore

$$a_P = a_W + a_E + S_\emptyset \tag{3.58}$$

The transport equation is discretized and solved using the MATLAB code (Appendix E-F).

3.4 Overall solution algorithms:

The overall solution algorithm for all the four bed models is described below. Since the energy equation applied on the bed models is solved with respect to the enthalpies, temperature must be calculated using heat capacities over a few iterations. Bed top temperature is the solution to the equation (3.42).

3.4.1 0-D bed models flow algorithm:

1. Setting inputs : Mass fluxes for fuel and primary air, ultimate and proximate properties of fuel and air (table 3.2), bed geometry, $T_{ref} = 300.19\ (K)$.
2. Applying model chemical assumption over the bed.
    a. One zone model
    b. Two zone model
    c. Three zone model

3. Considering chemical gas composition for each zone.
4. Applying element equilibrium over each zone for the corresponding gases and calculate mole of the species.
5. Guessing the exit temperature for bed top in each zone.
6. Solving mass conservation equation for each zone.
7. Solving energy conservation equation for each zone and calculating temperature of the new exit temperature for gases.
8. Checking the convergence criteria ($T_{guess} = T_{exit}$).
9. If the solution diverges return to number five.

3.4.2 1-D bed model flow algorithm:

In the 1-D algorithm, the flow field is obtained directly from the continuity equation. This algorithm is as follows:

1) Setup 1-D domain grid.
2) Initialize solution variables such as boundary conditions and source terms.
3) Initialize variables for solving mass and energy equations.
4) Start grid loop for $N=0...N_{end}$
    a) Set initial value to the grid.
    b) Calculate kinetic rate according to the equation (3.43-3.45).
    c) Start outer loop.
        i. Solve gas continuity equation to gain mass flow rate and velocities.
        ii. Update boundary conditions.
        iii. Solve (3.43) to get the bed top temperature.

iv. Update coefficients and source terms.

v. Check for convergence.

d) Update mass and energy balance variables.

e) If the $N \neq N_{end}$, then returns to step number four. Otherwise move to the next step.

5) Evaluate mass and energy balance conservation.

3.5 Gas- phase combustion modeling: Freeboard

To further test the performance of these models, and due to the lack of experimental data for the species released from the bed, the simulated bed outlets were put as boundary conditions for the simulation of the combustion in the freeboard and predicted results are compared with the experimental measurements. Since this simulation of the freeboard was the scope of a PhD thesis performed on the same project details about the CFD platform is not reported here and can be found in Farokhi [61]. A computational fluid dynamic (CFD) platform is used to predict the gas-phase changes in the freeboard [61]. The combustion of volatile gases within the freeboard is simulated using Reynolds Averaged Navier-Stokes (RANS) conservation equations of continuity, momentum, energy and species transport along with the assumption of incompressible ideal gas law. P1-approximation model together with the domain based weight-sum-of-gray-gas (WSGG) method is employed to account for radiation. The effect of the chemical reaction mechanism is accounted for using a four-step reduced reaction mechanism of methane combined with a two-step reaction mechanism of benzene with CO as the common species. Eddy dissipation concept (EDC) approach is employed to model the gas-phase combustion process within the freeboard [4]. The CFD simulation of the freeboard is performed using ANSYS-FLUENT 15.0, and second-order upwind spatial discretization scheme is applied to solve the conservation equations. A SIMPLE method is also used as the pressure-velocity

coupling algorithm. [4] The computational domain includes nearly 1.2 million cells covering from the top of the bed until the entrance of the boiler. (i.e., flue gas exhausts). A 1.8 MW small industrial grate firing biomass burner, as shown in Figure 3.11, is utilized for the present work. The biomass fuel type is wood-pellet that its chemical and physical properties were introduced in section 3.3. The wood-pellet supplies the furnace bed with the mass flow rate of 0.1108 [Kg/s]. The primary air is injected into the furnace from the bottom of the bed with the mass flow rate of 0.464 [Kg/s]. Excessive air, which is known as secondary and tertiary air flow, is applied into the freeboard with the mass flow rate of 0.348 [Kg/s]. The pressure and temperature for all air flows are assumed 100 kPa and 298 K, respectively.

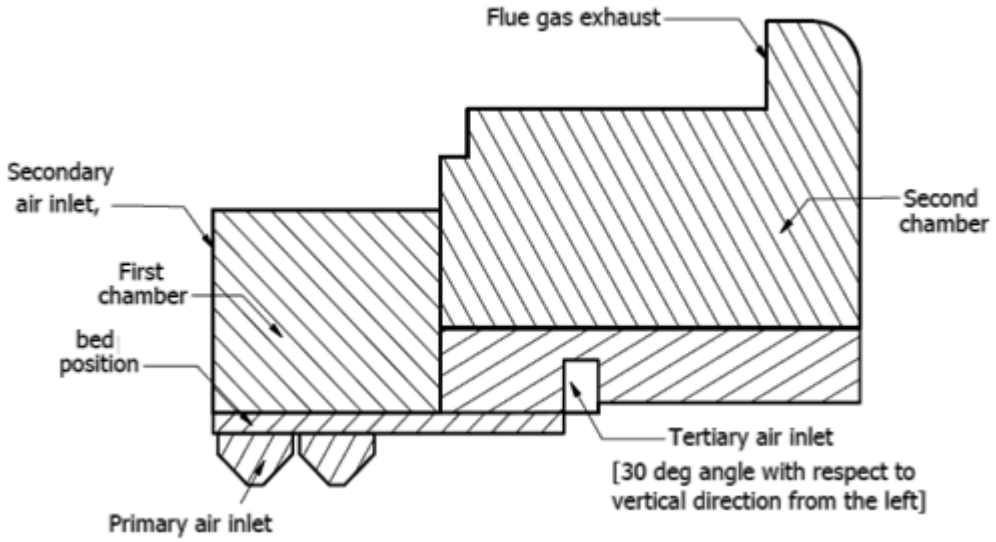

Figure 3.11. Schematic view of the small-scale commercial biomass furnace **[4]**

CHAPTER 4: RESULTS & DISCUSSION

4. Results and Discussion

4.1 Results and discussion:

Different types of bed models with distinctive assumptions are analyzed in this thesis. When applying the bed models presented in section (3.3) to predict the conversion features of a biomass fuel bed on a grate, (i.e., anticipate the gas flow leaving the fuel bed into the freeboard), some considerations must be kept into account. The temperature computed by 0-D models is an average value not an exact representation of the real energy content; the equilibrium assumption usually results in high conversion of the fuel which is not realistic. Thus, only the models with a geometric configuration nearly similar to the actual furnace and time scales of the chemical conversion processes that allow a better representation are considered. Nevertheless, a 0-D model provides some initial information which are valuable for development of more complicated bed models [46]. Another issue that requires discussion is the need to examine the performance of fuel bed models on the ground of experimental measurements obtained from the top of the fuel bed. Conducting experimental measurements for gases composition in the grate-firing furnaces in real operations has many hardships. The difficulties are due to the strong coupling between the fuel bed and freeboard as well as instabilities inside the grate combustor [46]. As a result, no experimental measurements of fuel bed are available in the literature. For this reason, the present work aims at comparing the way each model describes the fuel thermal conversion on the bed. Also, each bed model is applied as boundary conditions for the homogeneous gas-phase simulation of freeboard of an industrial scale biomass furnace, and these results are compared with the experimental measurements at the freeboard outlet of the industrial biomass furnace.

4.1.1 Results of bed models:

A comparison between the four bed models presented in Chapter 3 is made for the biomass fuel which has the composition reported in Table 3.2. The biomass fuel which is at room temperature ($T_{ref} = 300.19\ K$) enters a 1.8 MW grate firing industrial furnace with a mass flow rate of 0.11080 kg/s while the primary air is supplied from under the grate with a mass flow rate of 0.4637 kg/s at the same temperature. The results obtained from MATLAB codes (Appendix A-F) are presented in the following section. In the semi-empirical approaches, the produced gases are considered as a mixture of water vapor, volatiles gases and char burnout products (i.e., $CO_2\ and\ CO$) as shown in figures 3.2, 3.4, 3.6 and 3.8. In general, because of the different kinetic and chemical schemes considered for each individual bed model, different values of mass flow rate (for each individual species) and temperature are obtained. These values are presented in the following diagrams.

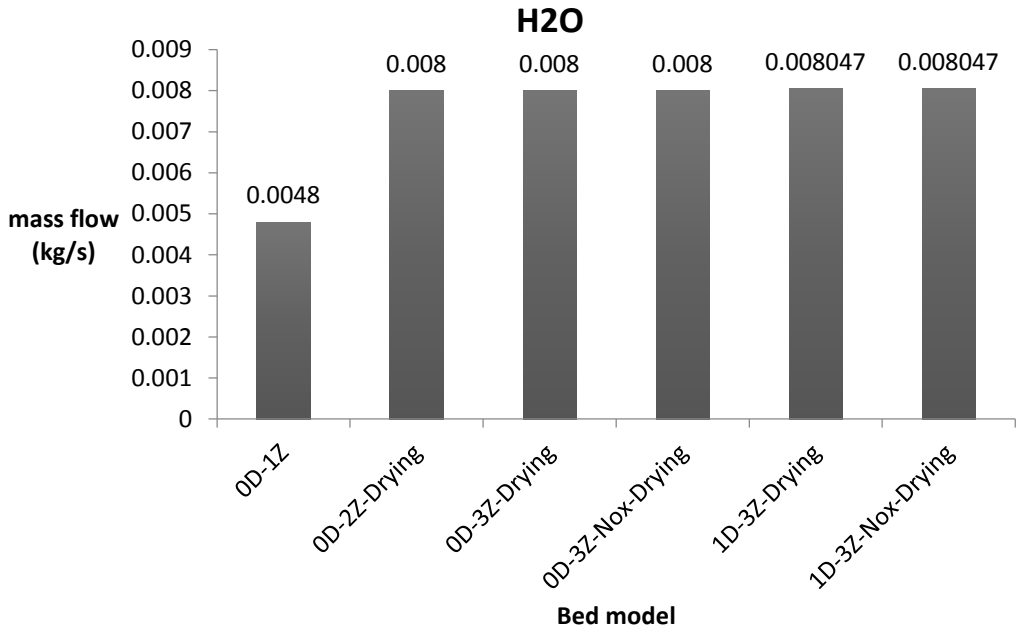

Figure 4.1. Mass flow rate of released $\boldsymbol{H_2O}$ from the investigated furnace bed.(0D-1Z: zero dimensional one zone; 0D-2Z: zero dimensional two zone; 0D-3Z: zero dimensional three zone; 0D-3Z-$\boldsymbol{NO_x}$: zero dimensional three zone with $\boldsymbol{NO_x}$; 1D-3Z: one dimensional three zone; 1D-3Z-$\boldsymbol{NO_x}$: one dimensional three zone with $\boldsymbol{NO_x}$)

Figure 4.1 shows the amount of released moisture which is assumed to be pure water (H_2O) from the bed for each model. The mass flow rate of the moisture is nearly similar for all the bed models except for the 0-D one zone model. According to the H_2O diagram in figure 4.1, the mass flow rate of the released moisture from the 0-D one zone model is less than that of the other models beside the fact that similar test conditions are used for all the bed models. The reason for this difference is the evaporation process which is not complete in the 0-D one-zone model and as a result, part of fuel moisture content is converted to H_2 and O_2. According to the diagrams in figures 4.6 and 4.7, the released hydrogen and oxygen gases from the bed in the 0-D one zone model are more than the 0-D two zone model for hydrogen and the 0-D two zone and 1-D three zone NOx models for the oxygen gas. The reason for these phenomena is the different chemical conversion mechanisms adopted for each bed model.

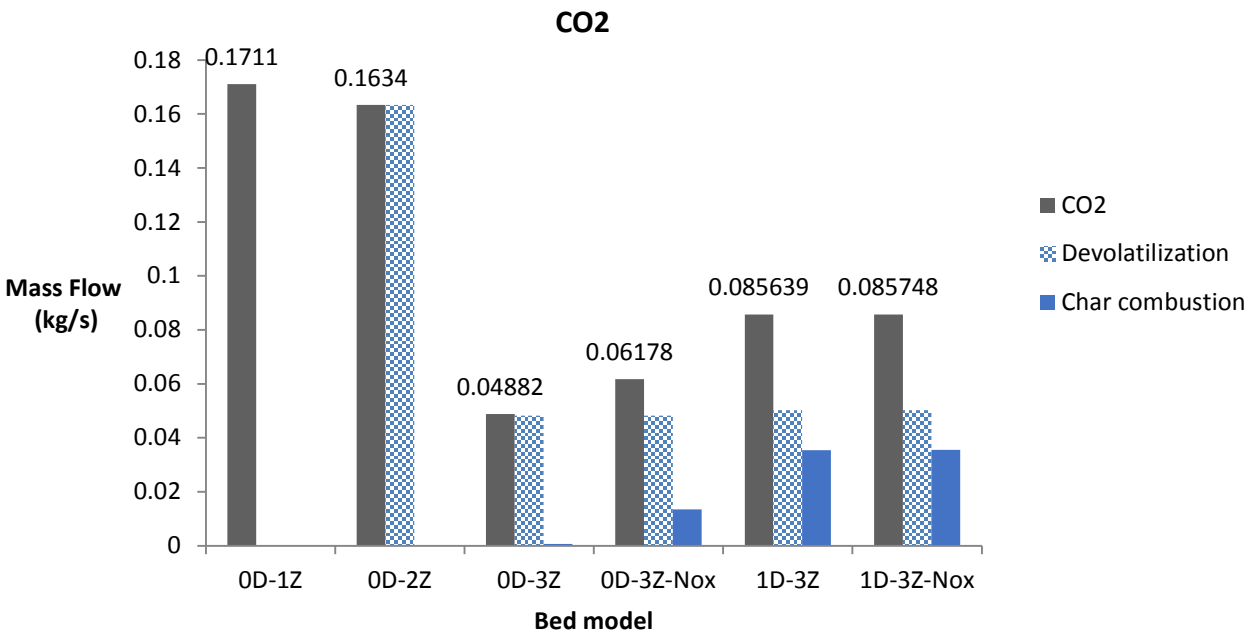

Figure 4.2. Mass flow rate of released $\boldsymbol{CO_2}$ from the investigated furnace bed.(0D-1Z: zero dimensional one zone; 0D-2Z: zero dimensional two zone; 0D-3Z: zero dimensional three zone; 0D-3Z-$\boldsymbol{NO_x}$: zero dimensional three zone with $\boldsymbol{NO_x}$; 1D-3Z: one dimensional three zone; 1D-3Z-$\boldsymbol{NO_x}$: one dimensional three zone with $\boldsymbol{NO_x}$)

The diagram in Figure 4.2 displays the mass flow rate of the released CO_2 gas for each model. In 0-D one zone model, all CO_2 comes out of the entire bed. The 0-D one zone model predicts the highest amount of CO_2 gas. This is mainly due to partial evaporation and conversion of water to hydrogen and oxygen, which consequently leads to more available oxygen for reaction with carbon in this model. In the 0-D two-zone model, there are only two zones, drying zone and the other one is the combination of devolatilization and char combustion. Since the drying zone releases only water vapor, the other species are released from devolatilization-char combustion. The 0-D two-zone model prediction for CO_2 is very close to the 0-D one zone model. This can be explained by the fact that similar chemical submodels and assumptions were applied for both 0-D two zone and 0-D one zone bed models. According to Figure 4.2, by comparing the 0-D three zone and 1-D three-zone models, it can also be seen that there exist differences in the prediction of CO_2. The 0-D three zone model with no NO_x precursors (HCN, NH_3) predicts the lowest amount of CO_2, while the 0-D three zone model with NO_x precursors predicts higher amounts. Also, in the 0-D three-zone model without NO_x precursors, the released CO_2 comes out mostly from the devolatilization zone while char oxidizatio has a very small share of CO_2. The reason is that according to Figure 4.3, the 0-D three zone model predicts higher amount of *CO* released from the char zone where due to oxygen shortage in this zone almost all carbon is converted to *CO* instead of CO_2.

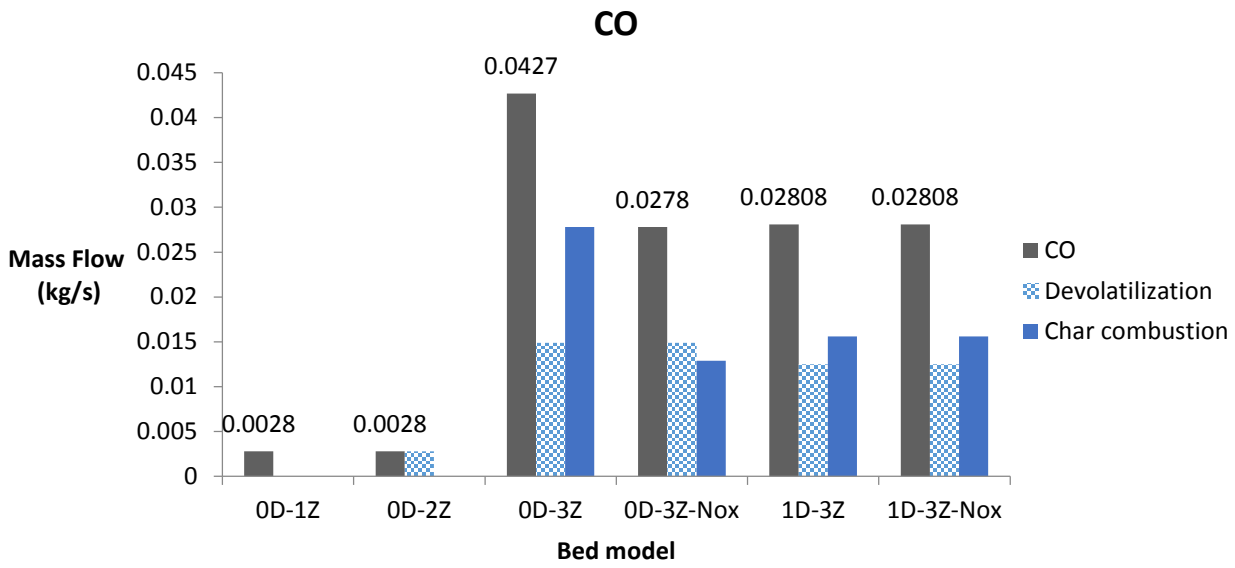

Figure 4.3. Mass flow rate of released *CO* from the investigated furnace bed.(0D-1Z: zero dimensional one zone; 0D-2Z: zero dimensional two zone; 0D-3Z: zero dimensional three zone; 0D-3Z-$\boldsymbol{NO_x}$: zero dimensional three zone with $\boldsymbol{NO_x}$; 1D-3Z: one dimensional three zone; 1D-3Z-$\boldsymbol{NO_x}$: one dimensional three zone with $\boldsymbol{NO_x}$)

The diagram in Figure 4.3 provides information regarding the bed models predictions of CO. According to this diagram, the lowest amount of mass flow rate for CO is predicted by the 0-D one zone and the 0-D two-zone models. The expected amount of CO in these two models is almost the same. These two bed models predict a small amount of CO and convert most of the fuel carbon to CO_2 (Figure 4.2). The highest predicted amount of CO is by the 0-D three-zone model. According to Figure 4.2, this model has the lowest CO_2 while it predicts the highestCO. This suggests that this model converts most of the biomass fuel carbon into CO rather than CO_2 which is due to insufficient oxygen in devolatilization and char combustion zones. In the 0-D three-zone bed model, the predicted mass flow rate for CO with NO_x precursors and without NO_x precursors are not similar. The fact that the 0-D three-zone model predicts more CO than CO_2 is the major reason for these fluctuations in Figure 4.3. The reason that the 0-D three-zone model releases higher CO than the 0-D three-zone with NO_x precursors is because all carbon in

0-D three-zone is converted to either CO or CO_2, while in 0-D three-zone with NO_x precursors, some of the fuel carbon reacts with nitrogen to produce HCN.

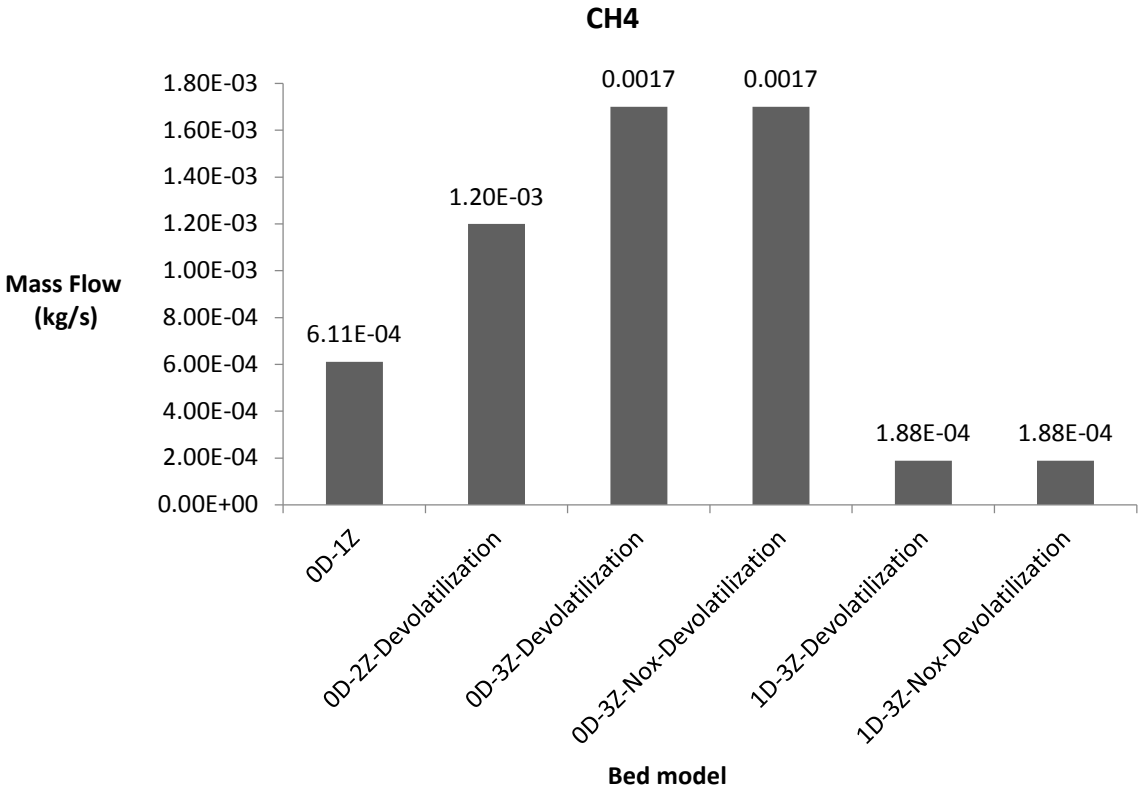

Figure 4.4. Mass flow rate of released $\boldsymbol{CH_4}$ from the investigated furnace bed.(0D-1Z: zero dimensional one zone; 0D-2Z: zero dimensional two zone; 0D-3Z: zero dimensional three zone; 0D-3Z-$\boldsymbol{NO_x}$: zero dimensional three zone with $\boldsymbol{NO_x}$; 1D-3Z: one dimensional three zone; 1D-3Z-$\boldsymbol{NO_x}$: one dimensional three zone with $\boldsymbol{NO_x}$)

The diagram in Figure 4.4 illustrates the mass flow rate of CH_4 gas leaving the bed. In the bed models with more than one conversion zone, CH_4 is released from the devolatilization (pyrolysis) section. CH_4 is an important representative of hydrocarbon group which is a major part of the biomass fuel. According to Figure 4.4, the amount of CH_4 released from the bed models varies. The lowest mass flow rate is predicted by the 1-D three-zone mode, while the 0-D three-zone bed model predicts the highest mass flow. The 0-D one-zone model compared to 0-D two-zone model predicts a smaller mass flow rate of CH_4. This can be explained through the

diagram of CO_2 in Figure 4.2, where the 0-D one-zone model predicts the highest CO_2 which justifies how this model converts most of carbon to CO_2 rather than other species. 0-D three-zone model and 1-D three-zone with NO_x and without NO_x precursors predict almost the same value of the mass flow rate of CH_4. Comparing the results obtained for CH_4 from the 0-D three-zone and 1-D three-zone model, it is noticeable that there is a significant difference between these two models. One explanation is that the 1-D three-zone bed model converts more carbon to CO_2 (Figure 4.2), while it produces similar CO compared to 0-D three-zone (Figure 4.3) and higher C_6H_6 (Figure 4.5).

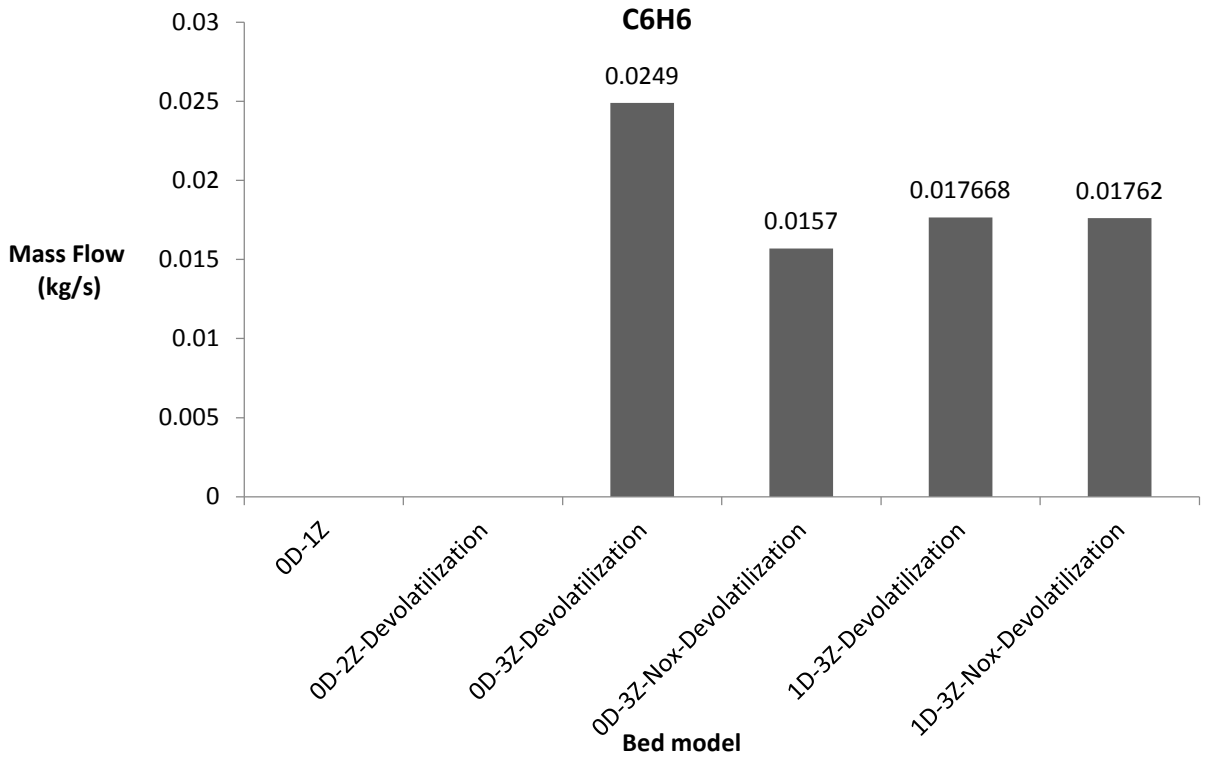

Figure 4.5. Mass flow rate of released $\boldsymbol{C_6H_6}$ from the investigated furnace bed.(0D-1Z: zero dimensional one zone; 0D-2Z: zero dimensional two zone; 0D-3Z: zero dimensional three zone; 0D-3Z-$\boldsymbol{NO_x}$: zero dimensional three zone with $\boldsymbol{NO_x}$; 1D-3Z: one dimensional three zone; 1D-3Z-$\boldsymbol{NO_x}$: one dimensional three zone with $\boldsymbol{NO_x}$)

Figure 4.5 shows the mass flow rate of released benzene (C_6H_6) from devolatilization zone of different bed models. C_6H_6 is a representative of tar, which is released from solid fuel during the

devolatilization process. For the 0-D one-zone and 0-D two-zone bed models, it is assumed that no tar is released from the fuel [46]. The reason could be that no separate pyrolysis zone is considered in these two models. Amongst the models that predict C_6H_6 for the conversion of fuel, the 0-D three-zone without NO_x precursors predicts the highest amount of mass flux for benzene (tar). The 0-D three-zone with NO_x precursors bed model predicts a lower mass flow rate. One explanation for this is that the 0-D three zone with NO_x precursors converts most of the carbon to CO_2 and also some carbon to *HCN*. The 1-D three zone bed models produces almost similar results to 0-D three zone regarding the mass flow rate of C_6H_6 released from the bed. However, the amount of mass flux predicted by the 1-D three-zone bed model without NO_x precursors is higher than the other one with a small approximation.

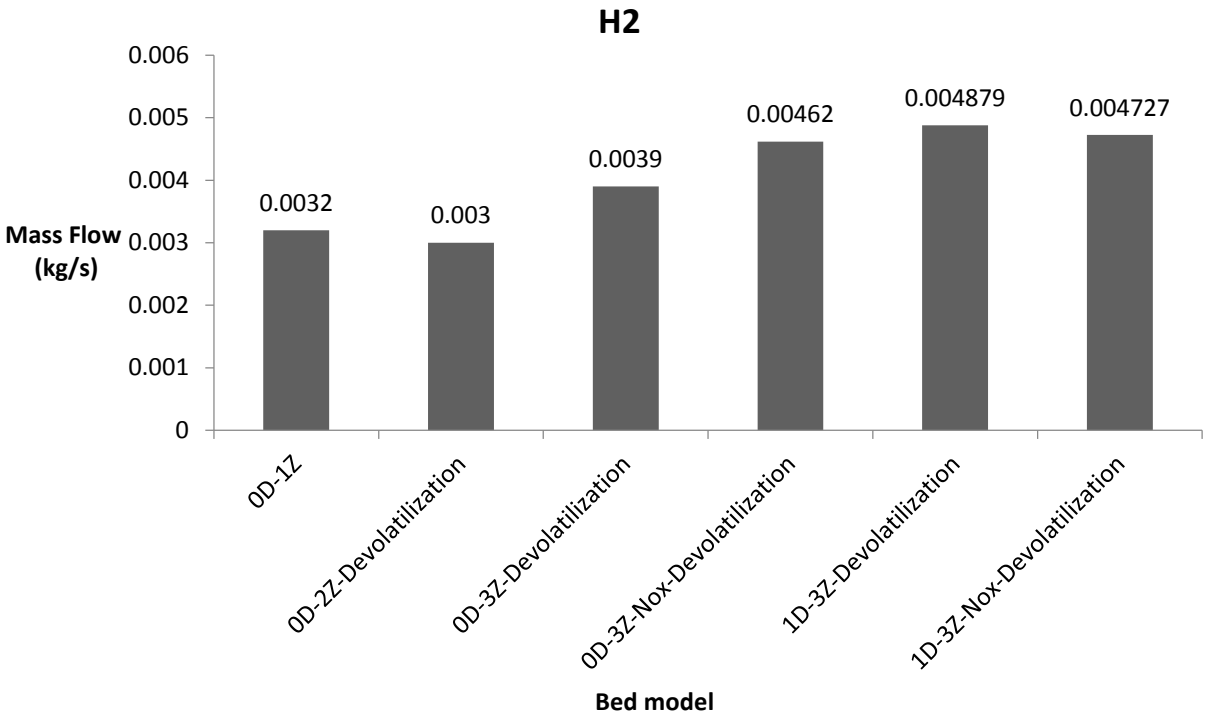

Figure 4.6. Mass flow rate of released $\boldsymbol{H_2}$ from the investigated furnace bed. .(0D-1Z: zero dimensional one zone; 0D-2Z: zero dimensional two zone; 0D-3Z: zero dimensional three zone; 0D-3Z-$\boldsymbol{NO_x}$: zero dimensional three zone with $\boldsymbol{NO_x}$; 1D-3Z: one dimensional three zone; 1D-3Z-$\boldsymbol{NO_x}$: one dimensional three zone with $\boldsymbol{NO_x}$)

The diagram in Figure 4.6 describes the information regarding the mass flow rate of hydrogen (H_2) gas coming out of the fuel bed during devolatilization. According to Figure 4.6, the predicted H_2 differs from one model to another. The lowest predicted value of hydrogen mass flow is for the 0-D two-zone model which is due to the fact that this model converts the majority of hydrogen to methane and moisture compared to 0-D one zone model. The 0-D three zone models produce less amount of mass flow rate for H_2 than the 1-D three zone models. This could be attributed to the fact that the 0-D three zone bed models use considerably more hydrogen for the conversion to benzene and methane than the 1-D three zone models. Therefore a smaller amount of H_2 is left for the 0-D three zone model which can come out of the bed. For the 0-D three zone models with NO_x and without NO_x precursors, there is a small difference in the mass flow rate of the hydrogen, which is due to the difference between the mass flow rates of benzene in Figure 4.5. Subsequently, for 1-D three zone bed models, there exist also a slight difference between the two aforementioned types of with NO_x and without NO_x precursors which is possibly caused by differences in the mass flow rates predicted in Figures 4.4 and 4.5 for these models.

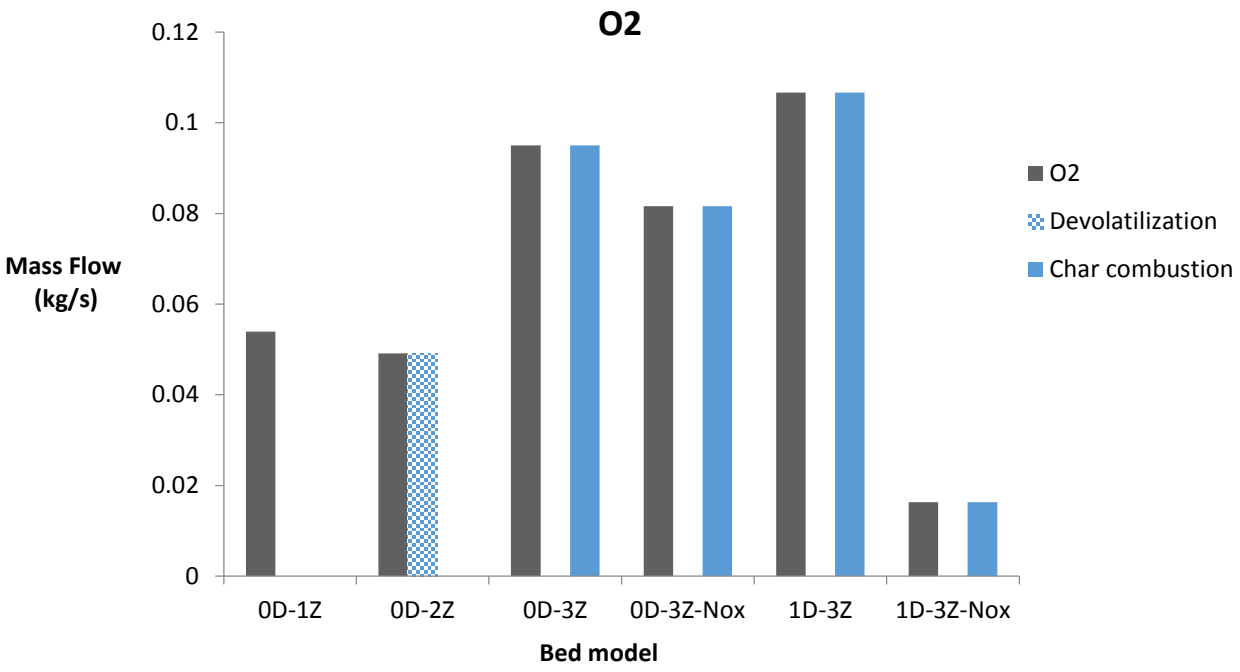

Figure 4.7. Mass flow rate of released $\boldsymbol{O_2}$ from the investigated furnace bed. (0D-1Z: zero dimensional one zone; 0D-2Z: zero dimensional two zone; 0D-3Z: zero dimensional three zone; 0D-3Z-$\boldsymbol{NO_x}$: zero dimensional three zone with $\boldsymbol{NO_x}$; 1D-3Z: one dimensional three zone; 1D-3Z-$\boldsymbol{NO_x}$: one dimensional three zone with $\boldsymbol{NO_x}$)

The illustrated diagram in Figure 4.7 describes the mass flow of oxygen O_2. The O_2 can either be originted from the air or from the devolatilization of the fuel. According to Figure 4.7, between the first two bed models, the released mass flow of O_2 when using the 0-D one zone model is slightly higher than that of the 0-D two zone model. The reason for this can be explained by the fact that, in the 0-D one zone model, not all the moisture is vaporized and some water converts to hydrogen and oxygen species. Also in the 0-D one zone and 0-D two zone models, unlike the other bed models, the O_2 gas is released from either the entire fuel bed or the devolatilization zone. In three zone bed models of both 0-D and 1-D, the excessive mass flow rate of O_2 leaves the bed in the char combustion zone only. The reason for this is that, in three zone bed models and due to high concentration of released volatiles from the devolatilization zone, the oxygen can not influence the converion in this zone, and as a result, the devolatilization section is also called pyrolysis since the penetration of air oxygen into that area is very low. The fuel O_2 converts to

other species including CO_2 and CO, therefore, no oxygen is almost produced from the fuel. Among three zone models, the 1-D three zone with NO_x precursors bed model predicts the lowest amount of excessive O_2. This is likely because, for this model, most of the oxygen in char combustion zone reacts with carbon and nitrogen and produce more CO_2 and NO than the other three zone models. The difference between the models with NO_x and without NO_x precursors in the three zone models is negligible because NO_x precursors do not react with any O_2 for their production.

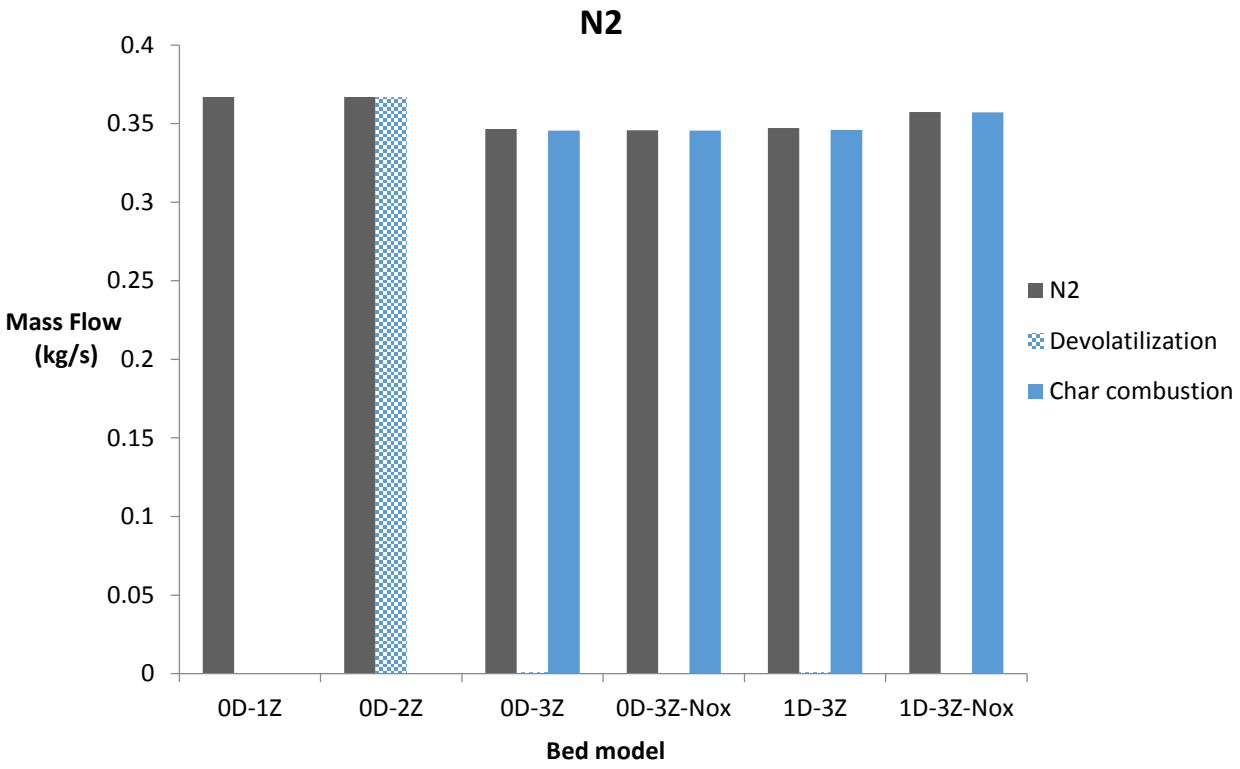

Figure 4.8. Mass flow rate of released $\boldsymbol{N_2}$ from the investigated furnace bed. .(0D-1Z: zero dimensional one zone; 0D-2Z: zero dimensional two zone; 0D-3Z: zero dimensional three zone; 0D-3Z-$\boldsymbol{NO_x}$: zero dimensional three zone with $\boldsymbol{NO_x}$; 1D-3Z: one dimensional three zone; 1D-3Z-$\boldsymbol{NO_x}$: one dimensional three zone with $\boldsymbol{NO_x}$)

Figure 4.8 shows the mass flow rate for the N_2 gas. The same as for O_2 diagram in Figure 4.7, for the 0-D one zone and 0-D two zone models, N_2 releases from the entire bed or from the de-volatilization zone. While in three zone bed models of both 0-D and 1-D, the released nitrogen

only comes out from the char combustion zone. The explanation for this phenomenon is that air is not able to infiltrate into devolatilization zone due to the high concentration of released volatiles from this zone. Therefore N_2 in the air only generates from the char burning zone. Regarding the N_2 in biomass fuel, it is assumed for the three zone bed models that this nitrogen is not able to leave the fuel at temperatures as low as those in the devolatilization zones, while in 0-D one zone and 0-D two zone, since the temperature of the bed is higher compared to the temperature predicted by three zone bed models, the NO_x precursors can be released from the fuel. Between the three zone bed models with NO_x precursors and without NO_x precursors, there is a small difference that is due to the fact that very little amount of N_2 converts to NO_x precursors.

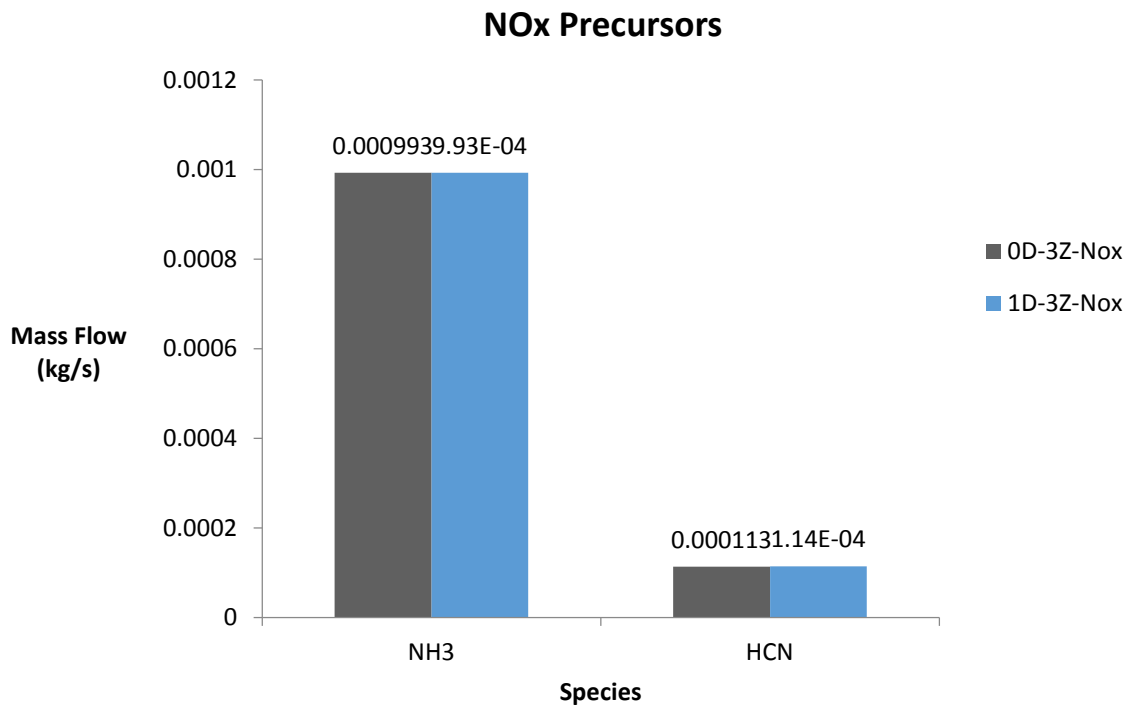

Figure 4.9. Mass flow rate of $\boldsymbol{NO_x}$ precursors from the bed.

Figure 4.9 displays the mass flow rates of NO_x precursors which are assumed to be HCN and NH_3 species in the 0-D three zone and 1-D three zone models. There is a very small difference between the predicted amounts of HCN and NH_3 in the 0-D three zone and 1-D three zone bed models. This small difference can be due to the fact that according to equations (3.34, 3.35) in Chapter 3, similar experimental ratios are used in developing these two models with NO_x precursors and without NO_x. Therefore in the scale of these emissions the difference is not very noticeable.

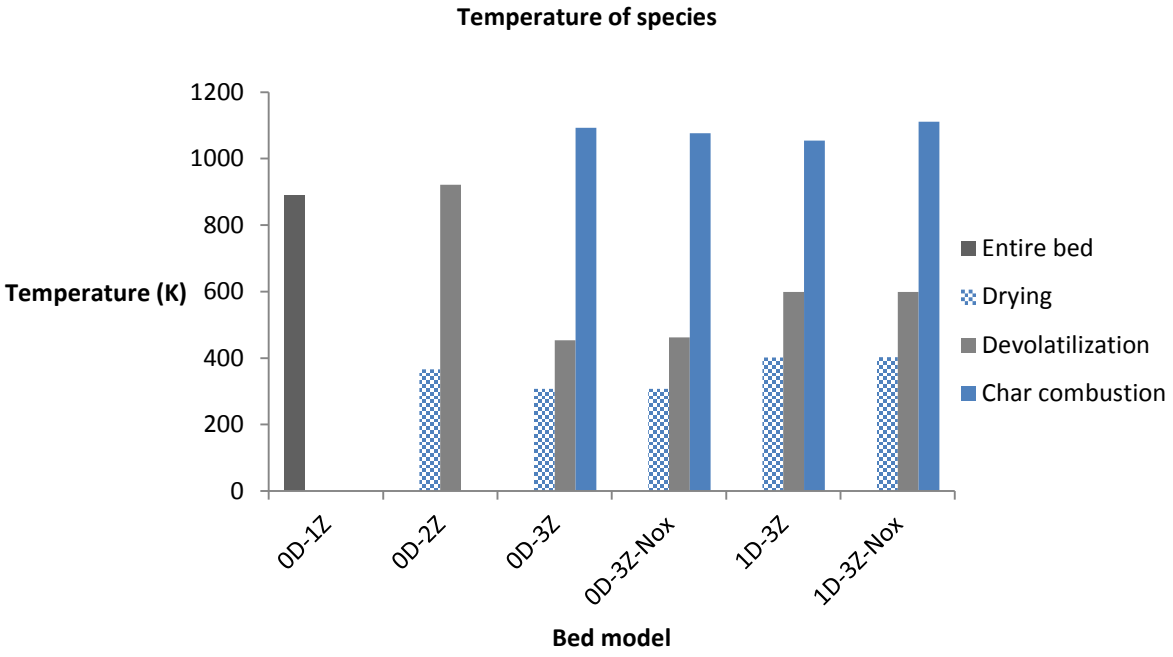

Figure 4.10. Temperature of released species from the investigated furnace bed.(0D-1Z: zero dimensional one zone; 0D-2Z: zero dimensional two zone; 0D-3Z: zero dimensional three zone; 0D-3Z-$\boldsymbol{NO_x}$: zero dimensional three zone with $\boldsymbol{NO_x}$; 1D-3Z: one dimensional three zone; 1D-3Z-$\boldsymbol{NO_x}$: one dimensional three zone with $\boldsymbol{NO_x}$)

The diagram in Figure 4.10 contains information regarding the predicted temperature in each chemical zone. According to this bar chart, each species that leaves the bed includes some energy and a specific temperature which is resulted from the conversion processes and chemical reaction in the bed. For the 0-D one zone model, the temperature of the species that are released

from the entire bed is the same because no separate conversion zones are considered for this model. The 0-D one zone model shows that the average predicted temperature of all released gases is lower than that of the other models. The drying section is defined for all the models except for the 0-D one zone model. The temperature in the drying zone varies for each model, where the highest temperature is for the 1-D three zone bed model. In this model, the difference in temperature between the model with NO_x precursors and without is slightly noticeable. Nevertheless, these two 1-D three zone bed models predict almost the same temperature for the moisture in the drying section. It must be noted that, in 1-D three zone bed models, the temperature of the released species from the bed is an average value and the real value changes along the length of the bed. The 0-D three zone bed models predict the lowest temperature for the vapor in the drying zone. Similar to the 1-D three zone models, the difference in the predicated temperature between two 0-D three zone bed with and without NO_x precursors is negligible. The devolatilization zone is also introduced for all the models except for the first bed model. Compared to drying temperature, the devolatilization temperature is much higher which is due to the released volatiles and thermochemical pyrolysis which produces heat and energy. The temperature in the char combustion zone, which is the third conversion section in three zone bed models, differs slightly between these models. The maximum predicted temperature of the char burning zone is predicted by the 1-D three-zone with NO_x precursors models. The temperature of char oxidization predicted by this model is the highest probably due to higher combustion enthalpy of the released gases. The difference in the average temperature for the char zones between the three zone bed models is due to the difference in the mass flow rate of gases released when using different model, which ultimately affects the energy and enthalpy.

4.1.2 Results of 1-D three zone bed model:

Based on mass and temperature gradient along the bed length for 1-D three-zone model, the results are also presented versus bed length. These results from the 1-D three-zone bed model along the bed's length are obtained by applying the model over a small 1.8 MW industrial biomass furnace (Figure 3.10). The dimensions of the fuel bed are introduced as follows: length 1.2 (m) and width 0.9398 (m). The fuel bed emissivity is considered as 0.6 with a density of 690 $\left(\frac{Kg}{m^3}\right)$. The height of the fuel bed is also assumed as 0.012 (m).

- Without NO_x precursors

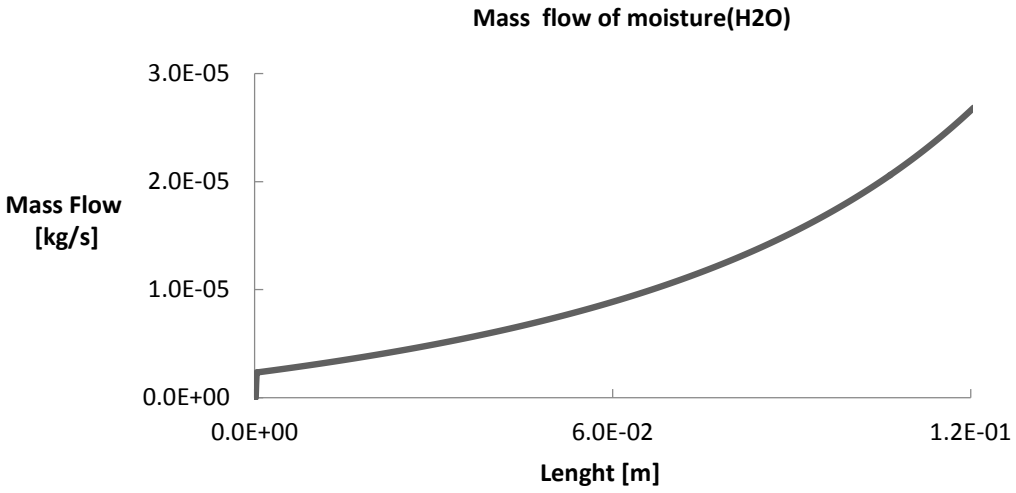

Figure 4.11. Mass flow rate of released moisture.

The mass flow rate of the released moisture from the fuel bed is shown in Figure 4.11. According to this figure, after the injection of the fuel into the bed, the evaporation process starts from the bed inlet. In the beginning, the drying rate and the amount of released moisture are the least. As the fuel moves farther on the bed, the drying rate increases and continues until almost all the water in fuel vaporizes. At the end of this process, the biomass fuel is completely dry, and all the moisture in the fuel is released. In this model, the Arrhenius drying kinetic rate (equation

(3.43)) for evaporation is applied to the drying process in order to determine the length of the bed at which drying ends. The 1-D three-zone model determines the drying conversion rate along the bed length of 0.12 (m). By this length, the drying process is completed. The 0.12 (m) also indicates the length of the fuel bed that is occupied by drying process for the specific biomass fuel burning in the 1.8MW furnace.

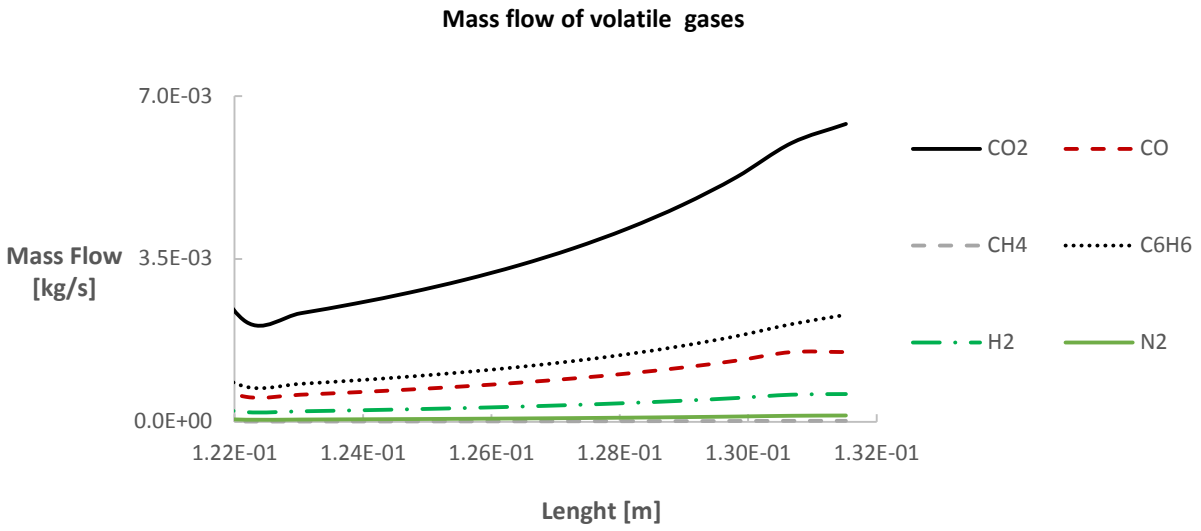

Figure 4.12. Mass flow rate of released volatiles.

Figure 4.12 shows the mass flow rate of the released volatile gases from the bed. The volatile gases as described in the previous chapter consist of tar (C_6H_6), light hydrocarbon (CH_4), hydrogen (H_2), nitrogen (N_2), carbon monoxide and carbon dioxide. Devolatilization process begins at x= 0.122(m) from the inlet along the bed. The conversion rate at the beginning of the process is low and the mass flow rate of released volatiles from the bed increases farther down along the bed. The pyrolysis conversion kinetic rate (3.44) determines the length of the bed too. For this conversion process, the defined bed length according to figure 4.1 2 is <0.01 (m), which

means that the chemical conversion process of devolatilization continues along the bed length for 0.01 (m). This process stops when the bed length is at x= 0.132 (m).

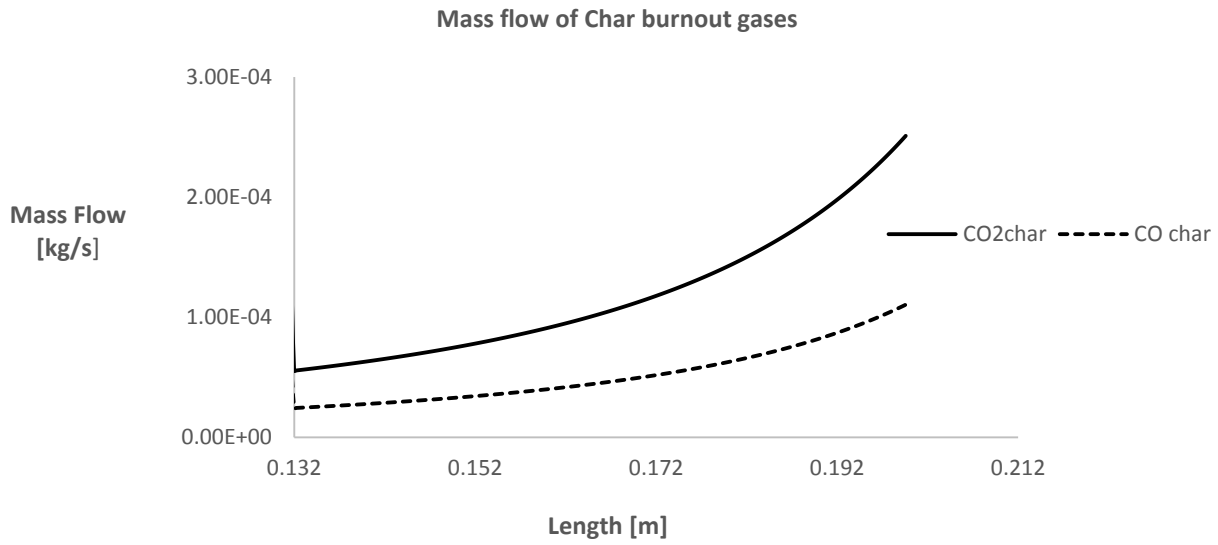

Figure 4.13. Mass flow rate of char burnouts.

Figure 4.13 describes the emissions of char oxidization zone. As shown in this figure, CO and CO_2 start releasing from the bed after the devolatilization zone is complete where the char zone length begins. According to Figure 4.13, char burning zone length is determined by the chemical kinetic rate of the char combustion process (3.45). These results show that the oxidization process of the char occupies only 0.08(m) of the bed length. Therefore the total length of the bed involved in drying and the chemical conversions of the biomass fuel is 0.212 (m). No chemical conversion occurs beyond this point.

- With NO_x precursors

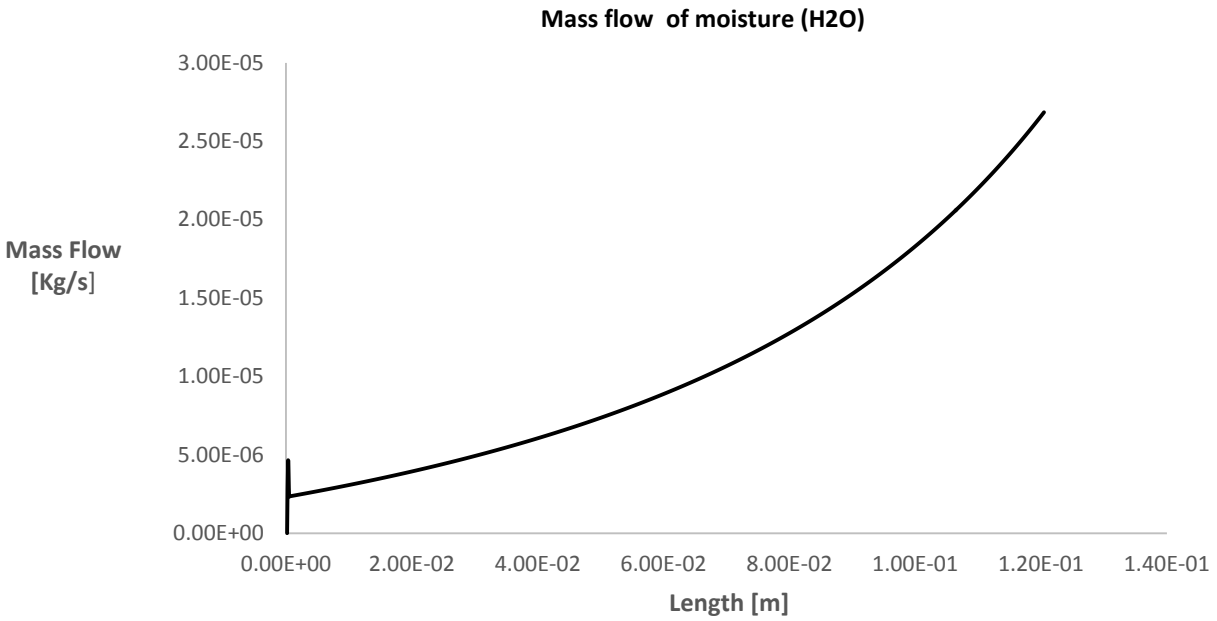

Figure 4.14. Mass flow rate of released moisture.

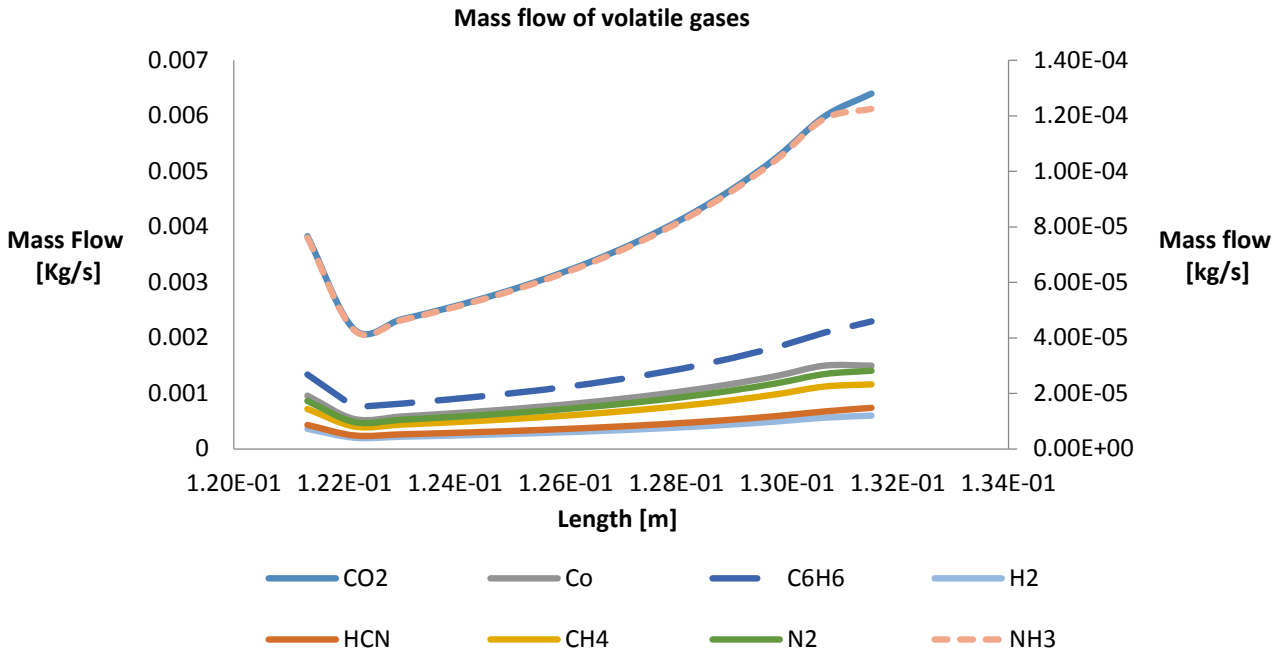

Figure 4.15. Mass flow rate of released volatiles.

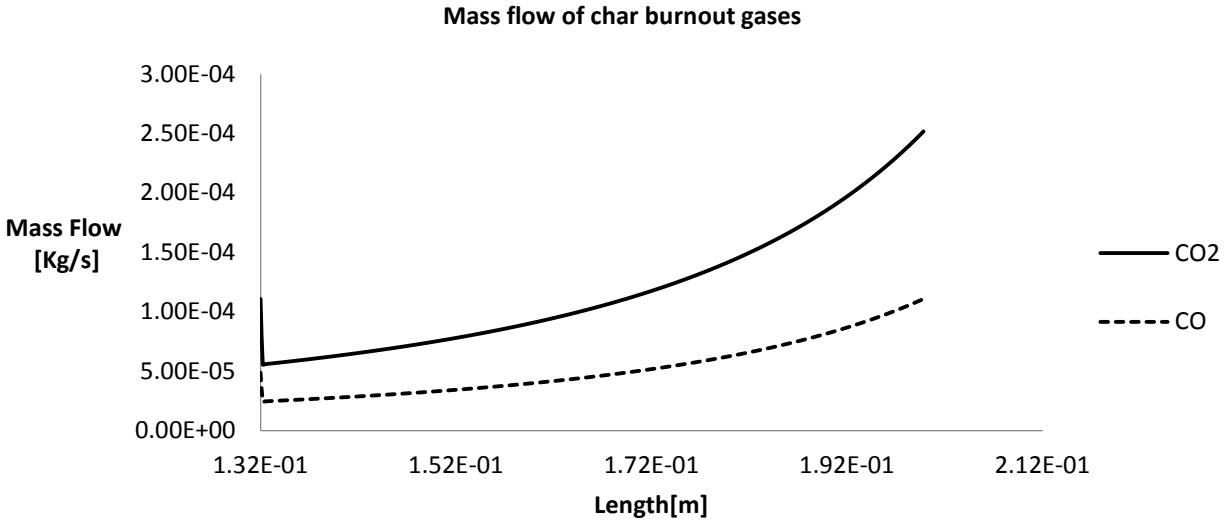

Figure 4.16. Mass flow rate of released char burnouts.

Figures 4.14 - 4.16 display the mass flow rate of the released gases from individual zones in 1-D three zone model with NO_x precursors. According to these figures, for each reaction zone, the conversion bed length, which is the length of the bed occupied by the drying and the chemical conversion processes, is determined by the chemical conversion kinetic rates obtained from experimental measurements and correlations [26] for each process and are presented earlier in equations (3.43), (3.44) and (3.45).

4.2 Performance of bed models:

The results presented above concern solid fuel conversion. However, to evaluate bed models, experimental data from the bed section of the industrial furnaces are required. To do so, the two bed models with more chemical and physical details are selected to be applied as boundary conditions for the simulation of the combustion of the released gases in the grate firing furnace freeboard. The **1.8MW** small-scale industrial furnace which is introduced in section 3.6 of this

thesis is used. Two different bed inflow boundary conditions are tested, namely the 0-D three zone bed model and the 1-D bed model. These simulations are performed using ANSYS FLUENT 15.0, and the calculations are compared with experimental measurements.

4.2.1 Temperature contours within the freeboard:

Figure 4.17(a) and (b) presents the temperature contours within the freeboard of the 1.8 MW industrial furnace by applying 0-D and 1-D bed models, respectively [4].

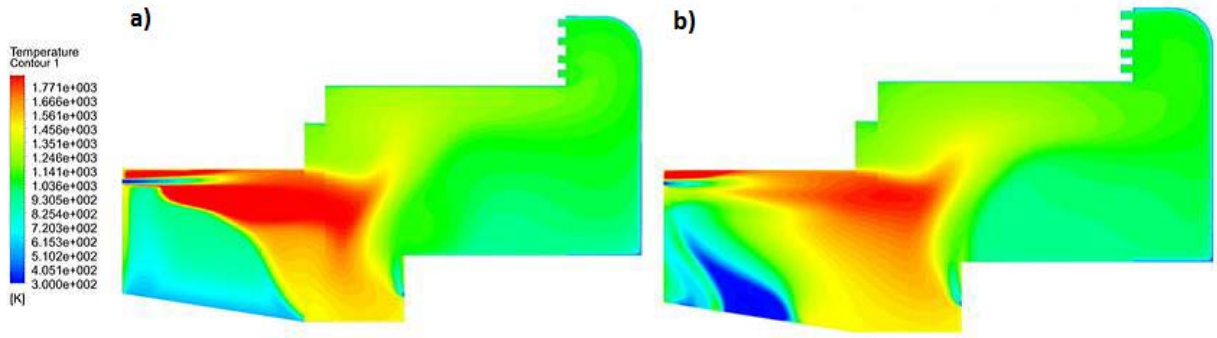

Figure 4.17. Freeboard temperature distribution contours; a) With 0-D bed model application. b) With 1-D bed model application [4].

Comparing the temperature contours in Figure 4.17 (a) and (b) reveals that the 1-D bed model produces a broader distribution of temperature within the furnace. Moreover, the local temperature close to the back wall of the furnace is relatively higher compared to that of 0-D bed model.

The predictions of species concentrations exhausting from the furnace freeboard, and their average temperature are compared with experimental measurements. The mole fraction of species (e.g., O_2, N_2, CO_2 and CO) and the average temperature are available at the outlet of the furnace freeboard. Table 4.1 displays the predicted and measured species mole fraction (reported on dry basis biomass fuel) and temperature.

Table 4.1. Comparison between bed models predictions and experimental measurements.

Species	CO_2 [-]	O_2[-]	N_2[-]	CO[ppm]	$Temperature[K]$
Experiment	0.105	0.10	0.79	200	928.15
0-D bed model	0.104	0.102	0.793	700	1000.0
1-D bed model	0.107	0.099	0.792	408	935.0

From Table 4.1, it can be realized that both 0-D and 1-D models predictions are in good agreement with experimental measurements. However, the best predictions are accomplished using 1-D bed model. This is due to the fact that this bed model introduces more reasonable fuel bed boundary conditions to freeboard since it predicts better the length of the bed where kinetic conversion rates are considered.

CHAPTER 5: CONCLUSIONS & FUTURE WORK

5. Conclusions & Future work

The present work is concerned with numerical modeling of grate firing combustion of woody biomass fuels. The scope of this thesis is restricted to the numerical modeling of processes that take place within the fuel bed. The information concerning the conversion processes occurring in the bed is fundamental for optimization and development of the grate-firing systems. Also, this importance is emphasized by the fact that the obtained results from CFD simulations in grate combustors strongly depend on the accuracy of the input boundary conditions including temperature, mass fluxes and species composition of the releasing gas from the bed.

In this study, a set of zero dimensional bed models (with different conversion sub models) and a one dimensional bed model were developed and applied on a small scale industrial biomass furnace with 1.8MW capacity. The fuel bed is treated as a continuous layer that consists of both gas and solid phases.

5.1 Bed models performance without freeboard:

The main conclusions obtained from the numerical solutions of bed models for gas concentrations and average temperature of gas species in bed outlet are

- The predicted released moisture (H_2O) is nearly similar for all bed models. This is because all models use the same drying model (Arrhenius expression) except for 0-D one-zone model in which partial evaporation is assumed.
- Devolatilization holds a higher share in the production of CO_2 than char combustion, while char combustion produces most of CO rather than devolatilization for all bed models.

- The prediction of the other released volatile gases depends on the applied chemical and thermal conversion sub models.
- 0-D and 1-D three-zone bed models provide a more detailed view of biomass solid conversion including temperature and mass flow rate of species for each chemical zone.
- 1-D three-zone considers temperature and mass gradient along the bed length, and hence it is more detailed biomass fuel conversion model than 0-D three-zone.

5.2 Bed models performance in the simulation of freeboard:

Comparison between the zero-dimension three-zone and one-dimension three-zone bed models is carried out in terms of their influence on the performance freeboard combustion. The main findings are:

- Both 0-D and 1-D bed approaches produced reasonable average temperature at the exit of the grate-firing furnace. However, the major difference between the two models is in the temperature distribution within the freeboard. This is an indication that the boundary conditions between the bed section and freeboard, which depends on the bed model, has a significant impact on the flame in the freeboard.
- Another difference between the 0-D and 1-D bed models is in the prediction of CO concentration at the exit of the furnace. While both bed models are in close agreement with the experimental measurements, the 1-D bed model prediction is much closer to the experiment, which is an indication of its superiority over the other model.
- Finally, for grate firing biomass furnace studies in which the major focus is on the system optimization, simplified bed models such as 0-D and 1-D models can be used without substantial errors.

5.3 Future work:

- The 1-D steady bed model should be coupled with freeboard combustion modeling. The coupling can be done through user defined functions in the commercial code ANSYS FLUENT. The mass and transport equations should be solved in the CFD platform and only the chemical kinetic rates need to be introduced to the platform via user developed codes and functions. Coupling makes the conversion of fuel bed directly dependants of freeboard reactions which ultimately provide a more detailed engineering view of biomass furnace combustion processes.
- A more detailed NO-chemistry may be considered for bed models to provide a better understanding of NO_x pollutant emissions from the outlet of the bed and ultimately grate-firing furnace.
- The 1-D steady bed model can be extended to 2-D bed model to describe the gas species behaviour and gradients along the height of the bed on their way to the freeboard. Although there exist some 2-D bed models in the literature, much work has yet to be performed in order to modify and improve the numerical stability of the existing 2-D bed models.

References

[1] J. Cambell and Laherrere, "The end of cheap oil," *Scientific American,* pp. 60-65, 3/1998.

[2] R. Bentley, "Global oil and gas depletion; An overview," *Energy Policy 30,* pp. 189-205, 2002.

[3] U. Bardi, "The mineral economy: a model for the shape of production curve," *ENERGY POLICY 33,* pp. 53-61, 2005.

[4] Z. Taban, M. Farokhi and M. Birouk, "The influence of empirical bed modeling on CO emissions in a small scale grate firing biomass furnace," in *Combustion Institude Canadian Section*, Montreal, 2017.

[5] T. Klason, "Modelling of Biomass combustion in Furnaces," PhD thesis, Lund Institude of Technology, May 2006.

[6] Available: Energy.gov./energybasics/articles/biomass/resource-basics.

[7] A. Demirbas, "Biomass resources facilities and biomass conversion processing for fuels and chemicals," *Energy conversion and Management,* vol. 42, September2000.

[8] Available: energy.techno-science.ca/en/energy101/biomass.php.

[9] J. Chen, W. Ju, J. Cihlar, D. Price, J. Liue, W. Chen, J. Pan, A. Black and A. Barr, "Spacial distribution of carbon sourcesand sinks in Canada forests.," *Taylor & Francis,* vol. 55i2.16711, pp. 622-641, 2003.

[10] V. Stansilave and Vasiileve, "An Overview of thechemical composition of biomass," *Fuel,* 2010.

[11] "Biomass Burn Characteristics," Ministry of Agriculture, Food and rural affairs.

[12] M. Nakamura, "Methematical and Physical Modeling of Mixing and Flow Phenomena of Municipal Solid Waste Particles on a Reverse Acting Grate," Engineering and Applied Science, Columbia University, 2008.

[13] J. Parikh, "A Correlation for calculating elemental composition from proximate analysis of biomass materials," *Fuel,* 2007.

[14] C. Huang, Z. Yang and X. Liu, "Ultimate analysis and heating value prediction of straw by near infrared spectroscopy," *Waste Management,* 2009.

[15] H. Goyal, D. Seal and R. Saxena, "Bio fuels from thermochemical conversion of renewable resources," in *Indian Institude of Petroleum*, India, 2006.

[16] M. Kucuk and e. al, "Biomass Conversion Process," *Energy Conversion Management*, vol. 38, no. 2, pp. 151-165, 1995.

[17] R. Overend, "Thermochemical conversion of biomass," National Renewable Energy Laboratory,

Colorado,USA.

[18] H. Knoef, Handbook of Biomass Gasification.

[19] C. Yin, L. A. Rosendahl and S. K. Kaer, "Grate-firing of biomass for heat and power production," *Progress in energy and Combustion Science,* vol. 34, pp. 725-754, 2008.

[20] H. Khodaie, Y. Al-Abdeli, F. Guzzomi and G. Yeoh, "An Overview of processes and considerations in the modelling of fixed-bed biomass combustion," *Energy,* vol. 88, pp. 946-972, 2015.

[21] C. Yin and S. Li, "Advancing grate-firing for greater enviromental impacts and efficiency for decentralized biomass/wastes combustion," *Energy Procedia,* vol. 120, pp. 373-379, 2017.

[22] N. Paces and M. Kozek, "Modeling of a grate firing biomass furnace for real time application," in *Institude of Mechanics and Mechatronics*, Vienna, Austria.

[23] F. Al-Mansour and J. Zuwala, "An evaluation of biomass co-firing in Europe," *Biomass Bioenergy,* vol. 34, pp. 620-629, 2010.

[24] X. Zhang, "Numerical modeling of biomass combustion in a stoker boiler," PhD thesis, University of Iowa, USA, 2011.

[25] R. Mehrabian, "CFD simulation of biomass grate furnaces with a comprehensive 3D packed bed model," in *25th German flame day*, Karlsruhe, Germany, 2011.

[26] T. Jurena, "Numerical Modeling of Grate Combustion," PhD thesis, Brno University of Technology, 2012.

[27] H. Van Kuijk, "Grate Furnace Combustion : A model for the solid fuel layer," PhD thesis, Eindhoven University of Technology, 2008.

[28] Y. Yang, C. Ryu, A. Khor, N. Yates, V. Sharifi and J. & Swithenbank, "Effects of fuel properties on biomass combustion. Part 2. Modeling approach - identification of the controlling factors," *Fuel,* vol. 84, pp. 2116-2130, 2005.

[29] R. F. M. B. M. B. T. &. O. I. Scharler, "Advanced CFD analysis of large fixed bed biomass boilerswith special focus on convective section.," in *Proceedings of the 2nd World Conference and Exihibition on Biomass for Energy Industry and Climate Protection,* ISBN 88-89407-04-2, 2004.

[30] R. a. O. I. Scharler, "Numerical modeling of biomass grate furnaces," in *Proceedings of the 5th European Conference on Industrial furnaces and boilers*, ISBN 972-8034-04-0, 2000.

[31] J. Collazo, J. Porteiro, D. Patino and E. Granasa, "Numerical modeling of the combustion of densified wood under fixed bed conditions," *Fuel,* vol. 93, pp. 149-159, 2012.

[32] J. Chaney, H. Liu and J. Li., "An overview of CFD modeling of small-scale fixed-bed biomass pellet boilers with preliminary results from a simplified approach," *Energy Conversion and Management,* vol. 63, pp. 149-156, 2012.

[33] H. &. J. Thuman, "Combustion of wood particles- a particle model for eulerian calculations," *Combustion and Flame,* vol. 129, pp. 30-46, 2002.

[34] W. Yang, C. Ryu and S. & Choi, "Unsteady one-dimensional model for bed combustion of solid fuels," *Proceeding of the Insitute of Mchanical Engineers,Part A : Journal of Power and Energy,* vol. 218, pp. 589-598, 2004.

[35] H. Zhou, A. D. Jensen, P. Glarborg, J. P.A. and A. & Kavaliauskas, "Numerical modeling of starw combustion in a fixed bed," *Fuel,* vol. 84, pp. 389-403, 2004.

[36] R. Gort and J. Brouwers, "Theoretical analysis of the propagation of a reaction front in a packed bed," *Combustion and Flame,* vol. 124, no. 1-2, pp. 1-13, 2001.

[37] D. Lozinski and J. Buckmaster, "Quenching of reverse smolder," *Combustion and Flame,* vol. 102, no. 1-2, pp. 87-100, 1995.

[38] D. M. V. V.-P. A. Schult, "Propagation and extinction of forced opposed flow smolder waves," *Combustion and Flame,* vol. 101, no. 4, pp. 471-490, 1995.

[39] T. Ohlemiller, "Modeling of smoldering combustion propagation," *Progress in Energy and Combustion,* vol. 11, no. 4, pp. 277-310, 1985.

[40] H. L. B. Thunman, "Co-current and counter-current fixed bed combustion of biofuel : A comparison," *Fuel,* vol. 82, no. 3, pp. 275-283, 2003.

[41] J. Wurzenberger, S. Wallner, H. Raupenstrauch and J. Khinast, "Thermal conversion of biomass: Comprehensive reactor and particle modeling," *AIChE,* vol. 48, no. 10, pp. 2398-2411, 2002.

[42] C. Bruch, B. Peters and T. Nussbaumer, "Modelling of wood combustion under fixed bed conditions," *Fuel,* vol. 82, pp. 729-738, 2003.

[43] R. Johansson, h. Thunman and B. Leckner, "Influence of intraparticle gradients in modeling of fixed bed combustion," *Combustion and Flame,* vol. 149, no. 1-2, pp. 49-62, 2007.

[44] G. Debenest, V. Mourzenko and J. Thovert, "Smouldering in fixed beds of oil shale grains. Governing parameters and global regimes," *Combustion Theory and Modelling,* vol. 9, no. 2, pp. 301-321, 2005.

[45] G. Debenest, V. Mourzenko and J. Thovert, "Smouldering in fixed beds of oil shale grains. A three dimensional microscale numerical model," *Combustion Theory and Modelling,* vol. 9, no. 1, pp. 113-135, 2005.

[46] M. Costa, N. Massarotti, V. Indrizzi, B. Rajh, C. Yin and N. Samec, "Engineering bed models for solid fuel conversion process in grate fired boilers," *Energy,* vol. 77, pp. 244-253, 2014.

[47] J. Porteiro, J. Collazo, D. Patino, E. Granda, J. Gonzalez and L. Miguez, "Numerical modeling of a biomass pellet boiler," *Energy Fuels,* vol. 23, pp. 1067-1075, 2009.

[48] M. Purvis, E. Tadulan and A. Tariq, "NOx control by air staging in a small biomass fuelled

underfeed stoker.," *Energy Res,* vol. 24, pp. 917-933, 2000.

[49] C. Yin, L. Rosendahl, S. Kaer, C. Sonnik, Hvid and T. Hille, "Mathematical modeling and experimental study of biomass combustion in a 108 MW Grate-fired boiler," *Energy Fuels,* vol. 22, pp. 1380-1390, 2008.

[50] W. Smith, S. Morrin and Timoney.D.J., "Effects of operating condition on particulate matter emission factor for a domestic biomass boiler," *Proc.Inst Mech Eng Part A: J Power Energy,* vol. 225, pp. 614-618, 2011.

[51] M. Karim and J. Naser, "Progress in numerical modeling of packed bed biomass combustion," in *19th Australian Fluid Mechanics,* Melbourne Australia, December 2014.

[52] M. Hobbs, P. Radulovic and L. Smoot, "Combustion and gasification of coals in fixed beds," *Progress in Energy and Combustion Science,* vol. 19, pp. 505-586, 1993.

[53] D. Giltrap, R. Mcjibbin and G. Barnes, "A steady state model of gas-char reactions in a downdraft biomass gasifier," *Solar Energy,* vol. 74, pp. 85-91, 2003.

[54] D. Shin and S. Choi, "The combustion of simulated waste particles in a fixed bed," *Combustion and Flame,* vol. 121, pp. 167-180, 2000.

[55] H. Thunman and B. Leckner, "Modeling of Combustion front in a countercurrent fuel converter," in *29th Symposium on Combustion, The Combustion Institute,* 2002.

[56] N. Ford, M. Cooke and M. Pettit, *Energy,* pp. 65-137, 1992.

[57] M. Beckman and R. Scholz, "Simplified mathematical model of combustion in stoker systems," in *3rd European Conference of Industrial Furnaces and Boilers*, 1995.

[58] Y. Yang, R. Naewman, V. Sharifi, J. Swithenbank and J. & Ariss, "Mathematical modeling of starw combustion in a 38 MWe power plant furnace and effect of operation conditions," *Fuel,* vol. 86, pp. 129-142, 2007.

[59] N. Wakao, "Heat and mass transfer in packed beds," *Gordon and Breach Science*, 1982.

[60] Y. Yang, H. Yamauchi, V. Sharifi and J. Swithenbank, "Effects of fuel de-volatilization on the combustion of wood chips and incineration of simulated municipal solid wastesin a packd bed," *Fuels,* vol. 82, pp. 2205-2221, 2003.

[61] M. Farokhi, "Numerical study of biomass combustion of a grate-firing furnace with emphasis on gas-phase combustion modeling, Ph.D Thesis;," The University of Manitoba, 2018.

[62] J. Collazo, J. Porteiro, J. Miguez, E. Granada and M. Gomez, "Numerical simulation of a small-scale biomass boiler," *Energy Conversion and Management,* vol. 64, pp. 87-96, 2012.

[63] R. Johansson, "Modelling of biofuel combustion in fixed beds," Chalmers University of Technology, 2006.

[64] R. Scharler, E. Widmann and I. Obernberger, "CFD modelling of NOx formation in biomass grate furnaces with detailed chemistry," in *Science in thermal and chemical biomass conversion,* Victoria, Vamcouver Island,BC,Canada, 30 August to 2 September 2004.

[65] C. Yin, S. Kaer, L. Resendahl and S. Hvid, "Co-firing straw with coal in a swirl stablized dual feed burner modeling and experimental validation," *Bioresource technology,* vol. 101, pp. 4169-4178, 2010.

[66] N. Duffy and J. Eaton, "Investigation of factors affecting chennelling in fixed bed solid fuel combustion using CFD," *Combustion and Flame,* vol. 160, no. 10, pp. 2204-2220, 2013.

[67] S. Hermansson and H. Thuman, "CFD modeling of bed shrinkage and channelling in fied-bed combustion," *Combustion and Flame,* vol. 158, no. 5, pp. 988-999, 2011.

[68] B. Peters, "Measurments and application of a discrete particle model (DPM) to simulate combustion of a packed bed of individual fuel particles," *Combustion and Flame,* vol. 131, no. 1-2, pp. 132-146, 2002.

[69] Y. B. Cengel, "Ideal gases specific heat as a function of temperature, Table A-2," in *Thermodynamics, An Engineering Approach,* McGraw-Hill, 2008.

[70] M. Miltner, A. Makaruk, M. Harasek and A. Friedl, "Computational fluid dynamic simulation of a solid biomass combustor: Modeling appraoches,," *Clean technology and Enviromental Policy,* vol. 10, no. 2, pp. 165-174, 2008.

[71] B. Peters, B. Schroder, C. Brunch and T. Nussbaumer, "Measurments and particle resolved modeling of heat up and drying of a packed bed," *Biomass and Bioenergy,* vol. 23, no. 4, pp. 291-306, 2002.

[72] K. Bryden, K. Ragland and C. Rutland, "Modelling thermally thick pyrolysis of wood.," *Biomass and Bioenergy,* vol. 22, no. 1, pp. 41-53, 2002.

[73] H. Thunman, F. Niklasson, F. Johnsson and B. Leckner, "Composition of volatile gases and thermochemical properties of wood for modeling of fixed bed or fluidized beds," *Energy and Fuels,* vol. 15, pp. 1488-1497, 2001.

Appendix:

A.1. Introduction:

In this section, the MATLAB codes which were developed and ran to solve the chemical and physical conversion equations for the bed models are presented. Each code has been generated based on the assumptions and conditions which are considered in that.

In the codes developed for bed models, the initial step is to code the chemical conversion model to identify the specific chemical mass and mole fraction using experimental and empirical correlations and ratios. The next step is to solve the conservation equations of physics through MATLAB tool via numerical methods.

The following sections present each bed model MATLAB code.

A.2. MATLAB codes for presented bed models:

Appendix A – Zero dimensional one zone bed model code

```
% 0 Zone - one CV model

Mashf = Mf - Mf.*Yash ;
B = Ma ./ 28.92 ;
b2 = Ymoist*2/18 ;
bt = b1 + b2 ;
c2= Ymoist/18 ;
ct = c1 + c2 ;
Sw = 12.*a + bt + 16.*ct + 14.*d ;
A = Mashf/Sw ;
Mt = Mashf + Ma ;
Mmoist = Ymoist*Mashf;

M = [1 0 0 0 ; 0 1 0 0 ; 4 2 2 0 ; 0 0 0 2];

YCf=a;
YHf=b1 + (.4)*Ymoist*(2/18);
YOf=c1 + (.4)*Ymoist*(16/18);
YNf=d;

YH2O = Mashf*(.6*Ymoist);
YN2 = 0.5*((2*Ma*0.79) +(YNf*Mashf));
YCO2 = (Mashf*YCf)/1.0892;
```

```
YCO = YCO2*.086;
YCH4 = YCO2*.0032;
YOt = (0.21*2*Ma) + (Mashf*YOf);
YOconsume = YCO2*(32/44) + YCO*(16/28);
YO2 = (YOt - YOconsume)/2;
YHt=Mashf*YHf;
YHconsume = YCH4*(4/16);
YH2 = (YHt - YHconsume)/2;

Mout = YCO2 + YCO + YCH4 + YH2O + YO2 + YH2 + YN2 ;
Min = Mashf + Ma ;

YCout = YCO2*0.272 + YCO*0.428 + YCH4*0.67 ;
YHout = YCH4*0.25 + YH2O*.11 + YH2*0.5 ;
YOout = YCO2*0.363 + YCO*0.571 + YO2./2 + YH2O*0.88;

YHin = A.*bt.*1 ;
YCin = 12.*A.*a  ;
YOin = 16.*A.*ct + 0.46.*B.*16 ;

erC = YCin - YCout ;
erH = YHin - YHout ;
erO = YOin - YOout ;

Tg = Tref ;
Tref = 300;
Qrad = 21.6;
%All the enthalpies are in Kj/Kg
HcomCO = 10104;
HcomCH4 = 55514;
HcomH2 = 141584;
HfCO2 = 17314;

for T=300:2000
hCO2 = .45 + 1.67*(T/1000) - 1.27*(T/1000)^2 + .39*(T/1000)^3;
hCO = 1.10 -.46*(T/1000) +1*(T/1000)^2 -.454*(T/1000)^3 ;
hCH4 =  1.2 + 3.25*(T/1000) - 1.27*(T/1000)^2 + .39*(T/1000)^3;
hO2 =  .45 + 1.67*(T/1000) +.75*(T/1000)^2 -.71*(T/1000)^3;
hH2 =  13.46 + 4.6*(T/1000) - 6.85*(T/1000)^2 + 3.79*(T/1000)^3;
hN2 = 1.11 -.48*(T/1000) +.96*(T/1000)^2 -.42*(T/1000)^3;
CpH2O =  1.79 + .107*(Tg/1000) +.586*(Tg/1000)^2 -.2*(Tg/1000)^3;


    Qout = ((T)*(YCO2*hCO2 + (YCO*hCO) + YCH4*hCH4 + YO2*hO2 + YH2*hH2 +
YN2*hN2 + CpH2O*YH2O))+ YCO*10104 + YCH4*55514 + YCO2*17314
   Qin = (Mashf - Mmoist)*LHV +Ma*300.19 +Qrad - 2257*Mmoist - YCO2*17314 -
YCO*1326 - YCH4*1192 ;
    S =abs(Qout) - abs(Qin);

    if (0<S)&&(S<1);

     break;
```

```
     end
end
```

Appendix B – Zero dimensional two zone bed model code

```
%Zero Dimensioanl-2 Zone :


%Drying Section :

Qrad = 21.75;
Mashf = Mf - Mf.*Yash ;
YH2O = Ymoist*Mashf;
Mashfd = Mashf - YH2O ;
for TH2O= 300:400

    CpH2O =  1.79 + .107*(TH2O/1000) +.586*(TH2O/1000)^2 -.2*(TH2O/1000)^3;
    Q1out= CpH2O*YH2O*TH2O ;
    Q1in =  -YH2O*LvH2O + Qrad;
    S1 = Q1out-Q1in;

       if (2<S1)&&(S1<3);

        break;
       end
    end



%Conversion Section(Gasification):
YCf=a;
YHf=b;
YOf=c;
YNf=d;

%Experimental correlations:
%CO/CO2=x1
%CH4/CO2=x2
Ts=TH2O;

x1= 1.97*10^(-6)*Ts^(1.87);
x2= 1.305*10^(-11)*Ts^(3.39);


YN2 = 0.5*((2*Ma*0.79) +(YNf*Mashf));
YCO2star = (Mashf*YCf*44)/12;
YCO = YCO2star*x1;
```

```
YCH4 = YCO2star*x2;
YCO2 = YCO2star-(YCO + YCH4);
YOt = (0.21*2*Ma) + (Mashf*YOf);
YOconsume = YCO2*(32/44) + YCO*(16/28);
YO2 = (YOt - YOconsume)/2;
YHt=Mashf*YHf;
YHconsume = YCH4*(4/16);
YH2 = (YHt - YHconsume)/2;



% Enthalpy of outlet gases

Z = 1- YH2O - Yash ;
LHVmo = LHV/Z + YH2O*LvH2O/Z ;
Tg = TH2O;
CpH2O =  1.79 + .107*(Tg/1000) +.586*(Tg/1000)^2 -.2*(Tg/1000)^3;;
DeltaT = 173;
% if we consider the radiation heat amount using for drying we can
% mathematically calculate it since we do not have data from experiment for
% the Q rad ,we can calculate it with this assumption that
Qdry = Mashf.*Ymoist.*CpH2O*Tg  ;

%All the enthalpies are in Kj/Kg
HcomCO = 10104;
HcomCH4 = 55514;
HcomH2 = 141584;
HfCO2 = 17314;
Mmoist = YH2O*Mashf;

for T = 300:2000
hCO2 = .45 + 1.67*(T/1000) - 1.27*(T/1000)^2 + .39*(T/1000)^3;
hCO = 1.10 -.46*(T/1000) +1*(T/1000)^2 -.454*(T/1000)^3;
hCH4 =  1.2 + 3.25*(T/1000) - 1.27*(T/1000)^2 + .39*(T/1000)^3;
hO2 =  .45 + 1.67*(T/1000) +.75*(T/1000)^2 -.71*(T/1000)^3;
hH2 =  13.46 + 4.6*(T/1000) - 6.85*(T/1000)^2 + 3.79*(T/1000)^3;
hN2 = 1.11 -.48*(T/1000) +.96*(T/1000)^2 -.42*(T/1000)^3;


h1CO2 = .45 + 1.67*(Tg/1000) - 1.27*(Tg/1000)^2 + .39*(Tg/1000)^3;
h1CO = 1.10 -.46*(Tg/1000) +1*(Tg/1000)^2 -.454*(Tg/1000)^3;
h1CH4 =  1.2 + 3.25*(Tg/1000) - 1.27*(Tg/1000)^2 + .39*(Tg/1000)^3;
h1O2 =  .45 + 1.67*(Tg/1000) +.75*(Tg/1000)^2 -.71*(Tg/1000)^3;
h1H2 =  13.46 + 4.6*(Tg/1000) - 6.85*(Tg/1000)^2 + 3.79*(Tg/1000)^3;
h1N2 = 1.11 -.48*(Tg/1000) +.96*(Tg/1000)^2 -.42*(Tg/1000)^3;

    Qout = T*(YCO2*hCO2 + YCO*hCO + YCH4*hCH4 + YO2*hO2 + YH2*(hH2) +
YN2*(hN2))+YCO*10104 +  YCH4*55514 ;
   Qin = (Mashfd)*(LHV) - YCH4*1192 - YCO*1326 +Ma*300.19 - YCO2*17292  ;

    S =abs(Qin) -abs(Qout);

    if (0<S)&&(S<1)
```

```
      ;

        break;
    end


end
```

Appendix C – Zero dimensional three zone bed model code (withoutNO_x)

```
% Drying :
Ldry = Lb*Ymoist ;
Qdry = Ldry*Qrad/Lb ;
% Mass balance :
YH2O = Ymoist*Mf ;
Mmoist = Ymoist*Mf ;
MH2O = Mmoist ;
Tsdry1 = Qdry/(.90*Boltz*Ldry*W) + 300.19^4 ;
Tsdry = Tsdry1^.25;
% To see how much this radiation can increase the tempreture of the water.

% Devolitilazation Zone ;
% We assume CO ,CO2 ,H2 ,CH4 and C6H6 as our volatile gases.
% Volatile = A1CO + A2CO2 + A3H2 + A4CH4 + A5C6H6
% We assume Volatile to have this formation : CmHnOp
% According to Mass balance law we have :

% For Carbon : m = 12*A1/28 + 12*A2/44 + 12*A4/18 + 72*A5/78 ;
% For Hydrogen : n = A3 + 4*A4/18 + 6*A5/78 ;
% For Oxygen : p = 16*A1/28 + 32*A2/44 ;
% we have 5 unknowns and 3 equation

Ldev = Lb*Yvol ;
Qdev =Ldev*Qrad/Lb ;
Tsdev1 = Qdev/(Evol*Boltz*Ldev*W) + Tref^4 ;
Tsdev = Tsdev1^0.25 + Tsdry ;
% This is the temp of surface in 2nd zone
R1 = 1.94*10^-6*Tsdev^1.87 ;
R2 = 1.305*10^-11*Tsdev^3.39 ;
syms A2
S1 = vpasolve( 16*R1*A2/28 + 32*A2/44 ==p,A2);
A2 = S1;
A1 = R1*A2 ;
A4 = R2*A2;
syms A5
S2 = vpasolve(12*A1/28 + 12*A2/44 + 12*A4/18 +72*A5/78 == m ,A5);
A5 = S2;
syms A3
S3 = vpasolve(A3 + 4*A4/18 + 6*A5/78 == n,A3);
A3 = S3;
Y1CO = A1*Mf ;
Y1CO2 =A2*Mf ;
```

```
YCH4 = A4*Mf ;
YH2 = A3*Mf ;
YC6H6 = A5*Mf ;
Y1N2 = Y1pN2*Mf;

% Char Combustin Zone :
% kC + zO2 = B1CO + B2CO2 ;
Lchar = Lb*Ychar ;
Qcharrad = Qrad*Lchar/Lb ;
Tschar1 = Qcharrad/Echar*Boltz*Lchar + Tref^4 ;
Tschar = Tschar1^0.25  + Tsdev;
U = exp(-6420/Tschar);
R3 = 2500*U;
% Mass balance ;
syms B2
S4 = vpasolve(B2*R3*12/28 + 12*B2/44 == k ,B2);
B2 = S4 ;
B1 = R3*B2 ;
z = 16*B1/28 + 32*B2/44 ;
% this is the consumed oxygen in char burning
% Mass of O2 leaving the Bed :
z1 = 0.46*Ma - z ;

Y2CO = B1*Mf ;
Y2CO2 = B2*Mf ;
YO2 = z1*Ma;

% Now we have the mass of all the species leaving the bed
% Here We estimate the flow of species leaving the Bed :
%DRYING :

MH2Og = Mf*Ymoist ;
% with the assumption of having uniform release from bed otherwise we need
% to calculate rate.

%Devolatilization :
Mvol = Yvol*Mf;
M1CO = Y1CO*Yvol*Mf ;
M1CO2 = Y1CO2*Yvol*Mf ;
MH2 = YH2*Yvol*Mf ;
MCH4 = YCH4*Yvol*Mf;
MC6H6 = YC6H6*Yvol*Mf ;

%Char Combustion :
Mchar = Ychar*Mf ;
M2CO = Y2CO*Ychar*Mf ;
M2CO2 = Y2CO2*Ychar*Mf ;
MO2 = z1 ;

% Tempreture of the leaving gases :
% we solve this part for the three zones and we use Energy balance:
% Tgj = Qtotal/Mgj*Cpg + Trefg ;

% Qt = Qrad + Qcharcombustion - Qevap
%Hchar = 16.7*10^6 + 2.93*10^6/1-Yvol  ;
```

```
Mchar = Ychar*Mf ;
%Qcharcom = Hchar*Mchar ;
Qevap = Hevap*MH2O ;
Qtd = Qdry  - Qevap ;
Qtdev = Qdev;
Qtchar = Qcharrad + LHV.*Mchar + Ha*Ma;
%first We use the correlation in thermodynamic to calculate Cp of gases for
%different gases
%H2O:
T = 300:4000 ;
CpH2O = 32.24 + 0.1923e-2.*T + 1.055e-5.*T.^2 - 3.595e-9.*T.^3 ;
TH2O = Qtd./(MH2O.*CpH2O) + 300.19 ;
ErH2O=abs(TH2O - T);
[a,b]=min(ErH2O);
Finalcalctemp=TH2O(b);
Fianlabstemp=T(b);
```

Appendix D - Zero dimensional three zone bed model code (with NO_x)

```
% Drying :
Ldry = Lb*Ymoist ;
Qdry = Ldry*Qrad ;
% Mass balance :
YH2O = Ymoist*Mfaf ;
Mmoist = Ymoist*Mfaf ;
MH2O = Mmoist ;
Tsdry1 = Qdry/(.95*Boltz*Ldry*W) + 300.19^4 ;
Tsdry = Tsdry1^.25;
% To see how much this radiation can increase the tempreture of the water.

% Devolitilazation Zone ;
% We assume CO ,CO2 ,H2 ,CH4 and C6H6 as our volatile gases.
% Volatile = A1CO + A2CO2 + A3H2 + A4CH4 + A5C6H6
% We assume Volatile to have this formation : CmHnOp
% According to Mass balance law we have :

% For Carbon : m = 12*A1/28 + 12*A2/44 + 12*A4/16 + 72*A5/78 ;
% For Hydrogen : n = A3 + 4*A4/16 + 6*A5/78 ;
% For Oxygen : p = 16*A1/28 + 32*A2/44 ;
% we have 5 unknowns and 3 equation

Ldev = Lb*Yvol ;
Qdev =Ldev*Qrad ;
Tsdev1 = Qdev/(Ef*Boltz*Ldev*W) + Tref^4 ;
Tsdev = Tsdev1^0.25 + Tsdry ;
% This is the temp of surface in 2nd zone
R1 = 1.94*10^-6*Tsdev^1.87 ;
R2 = 1.305*10^-11*Tsdev^3.39 ;
Y1N2 = Y1pN2*Mfaf;
YNH3=Y1N2/1.11;
YHCN = Y1N2/9.7;
Y1N2f = Y1N2 - (YNH3*(14/17) + YHCN*(14/27));
```

```
syms A2
S1 = vpasolve( 16*R1*A2/28 + 32*A2/44 ==p,A2);
A2 = S1;
A1 = R1*A2 ;
A4 = R2*A2;
syms A5
S2 = vpasolve(12*A1/28 + 12*A2/44 + 12*A4/16 +72*A5/78 == m ,A5);
A5 = S2;
syms A3
S3 = vpasolve(A3 + 4*A4/16 + 6*A5/78 == n,A3);
A3 = S3;
Y1CO = A1*Mfaf ;
Y1CO2 =A2*Mfaf ;
YCH4 = A4*Mfaf ;
YH2 = A3*Mfaf ;
YC6H6 = A5*Mfaf ;

% Char Combustin Zone :
% kC + zO2 = B1CO + B2CO2 ;
Lchar = Lb*Ychar ;
Qcharrad = Qrad*Lchar ;
Tschar1 = Qcharrad/Ef*Boltz*Lchar + Tref^4 ;
Tschar =max( Tschar1)^0.25  + Tsdev;
U = exp(-6420/Tschar);
R3 = 2500*U;
% Mass balance ;
syms B2
S4 = vpasolve(B2*R3*12/28 + 12*B2/44 == k ,B2);
B2 = S4 ;
B1 = R3*B2 ;
z = 16*B1/28 + 32*B2/44 ;
% this is the consumed oxygen in char burning
% Mass of O2 leaving the Bed :
Mchar = Ychar*Mfaf;
z1 = .23*Ma - z*Ma*.23 ;

Y2CO = B1*Mfaf ;
Y2CO2 = B2*Mfaf ;
YO2 = z1;
Y2N2 = Y2pN2*Ma;

% Now we have the mass of all the species leaving the bed
% Here We estimate the flow of species leaving the Bed :
%DRYING :

MH2Og = Mfaf*Ymoist ;
% with the assumption of having uniform release from bed otherwise we need
% to calculate rate.

%Devolatilization :
Mvol = Yvol*Mfaf;
M1CO = Y1CO*Yvol*Mfaf ;
M1CO2 = Y1CO2*Yvol*Mfaf ;
MH2 = YH2*Yvol*Mfaf ;
MCH4 = YCH4*Yvol*Mfaf;
MC6H6 = YC6H6*Yvol*Mfaf ;
```

```
%Char Combustion :
Mchar = Ychar*Mfaf ;
M2CO = Y2CO*Ychar*Mfaf ;
M2CO2 = Y2CO2*Ychar*Mfaf ;
MO2 = z1 ;

% Tempreture of the leaving gases :
% we solve this part for the three zones and we use Energy balance:
% Tgj = Qtotal/Mgj*Cpg + Trefg ;

% Qt = Qrad + Qcharcombustion - Qevap
%Hchar = 16.7*10^6 + 2.93*10^6/1-Yvol  ;
Mchar = Ychar*Mfaf ;
%Qcharcom = Hchar*Mchar ;
Qevap = Hevap*MH2O ;
Qtd = Qdry ;
Qtdev = Qdev;
LHVMO = LHV*Mf*(1-Yash) - Hevap*Ymoist;
Qtchar = Qcharrad + LHVMO.*Mchar + Ha*Ma;
%first We use the correlation in thermodynamic to calculate Cp of gases for
%different gases
%H2O:
T = 300:4000 ;
CpH2O = 32.24 + 0.1923e-2.*T + 1.055e-5.*T.^2 - 3.595e-9.*T.^3 ;
TH2O = Qtd./(MH2O.*CpH2O) + 300.19 ;
ErH2O=abs(TH2O - T);
[a,b]=min(ErH2O);
Finalcalctemp=TH2O(b);
Fianlabstemp=T(b);

%Cp mix in volatile:
T = 300:4000 ;
Cpmixvol = Y1CO*(28.16 + 0.1675e-2.*T + 0.5372e-5.*T.^2 - 2.222e-9.*T.^3) +
Y1CO2*(22.26 + 5.981e-2.*T - 3.501e-5.*T.^2 + 7.469e-9.*T.^3) + YCH4*(19.89 +
2.024e-2.*T + 1.269e-5*T.^2 - 11.01e-9.*T.^3) + YC6H6*(6.9 + 17.27e-2.*T -
6.406e-5.*T.^2 + 7.285e-9.*T.^3) + YH2*(29.11 - 0.1916e-2.*T + 0.4003e-
5.*T.^2 - 0.8704e-9.*T.^3) + YNH3*(27.568 + 2.5630*10.^(-2)*T +
0.99072*10.^(-5)*T.^2 - 6.6909*10.^(-9)*T.^3) + YHCN*43.806 + Y1N2f*(28.90  -
0.1571*10.^(-2)*T + 0.8081*10.^(-5)*T.^2 - 2.873*10.^(-9)*T.^3);
Tvol =Qtdev./(Mvol.*Cpmixvol) + 400.19;
Ervol=abs(Tvol - T) ;
[a1,b1]=min(Ervol) ;
Finalcalctemp1=Tvol(b1) ;
Finalabstemp1=T(b1);

%
% % Cp mix in char :
Cpmix1 = Y2CO*(28.16 + 0.1675e-2*T + 0.5372e-5*T.^2 - 2.222e-9*T.^3) +
Y2CO2*(22.26 + 5.981e-2.*T -3.501e-5.*T.^2 + 7.469e-9.*T.^3) + YO2*(25.48 +
1.52e-2.*T - 0.7155e-5.*T.^2 + 1.312e-9.*T.^3) + Y2N2*(28.90 - .001571*T +
0.000008081*T.^2 - 0.000000002873*T.^3) ;
Tchar = Qtchar./(Mchar.*Cpmix1) + 400.19;
Erchar=abs(Tchar - T);
[a2,b2]=min(Erchar);
Finalcalctemp2=Tchar(b2);
```

```
Finalabstemp2=T(b2);
```

Appendix E - One dimensional three zone bed model code (without NO_x)

```
clc
close all
clear

% Code:
Ychem = Yvol + Ychar + Ymoist ;
Mfaf = Mf*(1-Yash);
% Evaporation zone:
YH2O = Ymoist*Mfaf;
Mevap = Ymoist*Mfaf;
Levap = Lb*Ymoist/Ychem;
K = Eg/(1-Eg)*4*Boltz*dp*Tfl^3 ;
%Radiation:
Qradevap = Qrad*Levap/Lb ;
syms T
S1 = vpasolve(Qradevap == Alfa*Boltz*(- Eg*Tfl^4 + Es*T^4 ),T );
Ts1evap = abs(max(S1));
%Convection:
Aconvevap = Wb*Levap;
Pevap = 2*(Levap + Wb);
Rhevap = Aconvevap/Pevap ;
deqevap = 2*Rhevap ;
Acevap = Hevap*Wb;
Reyevap = Mevap*Rhevap/(Acevap*Viscos);
Nuevap = 2 + Pr^(1/3)*1.1*Reyevap^0.6 ;
htevap = Nuevap*K/deqevap ;
syms T
S2 = vpasolve(Qradevap == htevap*Aconvevap*(Tgevap - T),T);
Ts2evap = S2;
Tsevap =eval( Ts1evap - Ts2evap) ;


%Devolatilization zone:
Mdev = Mfaf*Yvol ;
Ldev = Lb*Yvol/Ychem;
%Radiation:
Qraddev = Qrad*Ldev/Lb;
syms T
S3 =  vpasolve(Qraddev == Alfa*Boltz*(-Eg*Tfl^4 + Es*T^4 ),T );
Ts1dev =abs(max(S3));
%Convection :
Aconvdev = Wb*Ldev ;
Pdev = 2*(Ldev + Wb );
Rhdev = Aconvdev/Pdev ;
deqdev = 2*Rhdev ;
Acdev = Hdev*Wb ;
Reydev = Mdev*Rhdev/(Acdev*Viscos);
Nudev = 2+Pr^(1/3)*1.1*Reydev^0.6;
```

```
htdev = Nudev*K/deqdev ;
syms T
S4 = vpasolve(Qraddev == htevap*Aconvdev*(Tgdev - T),T);
Ts2dev = max(S4);
%Conduction:
Deltaxdev = Ldev/2 + Levap/2 ;
syms T
S5 = vpasolve(Alfa*Boltz*(-Eg*Tfl^4 + Es*T^4)*exp(Alfa*(Z0 - Z)) -
Eg*4*Boltz*dp*T^(3)*(T - Tsevap)*Acdev/Deltaxdev ==0 ,T);
Ts3dev = abs(max(S5));
Tsdev =eval( Ts1dev + Ts2dev - Ts3dev ) ;

%Char Zone:Tsdev
Mchar = Ychar*Mfaf;
Lchar = Ychar*Lb/Ychem;
%Radiation:
Qradchar = Qrad*Lchar/Lb;
syms T
S6 =  vpasolve(Qradchar == Alfa*Boltz*(Eg*Tfl^4 - Es*T^4 ),T );
Ts1char = abs(max(S6));
%Convection:
Aconvchar = Lchar*Wb;
Pchar = 2*(Wb + Lchar);
Rhchar = Aconvchar/Pchar;
deqchar = 2*Rhchar ;
Acchar = Wb*Hchar;
Reychar = Mchar*Rhchar/(Acchar*Viscos);
Nuchar = 2 + Pr^(1/3)*1.1*Reychar^0.6 ;
htchar = Nuchar*K/deqchar ;
syms T
S7 = vpasolve(Qradchar==htchar*Aconvchar*(Tgchar - T),T);
Ts2char = S7 ;
%Conduction;
Deltaxchar = Levap + Ldev + Lchar/2 - (Levap + Ldev/2);
syms T
S8 = vpasolve(Alfa*Boltz*(Eg*Tfl^4 - Es*T^4)*exp(Alfa*(Z0 - Z)) -
Eg*4*Boltz*dp*T^(3)*(T - Tsdev)*Acchar/Deltaxchar ==0 ,T);
Ts3char = max(S8);
% Char combustion heat :
%Experimental correlation:
Qcomb = Mchar*LHV ;
syms T
S9 = vpasolve(Qcomb== Mchar*(28.16 + 0.001675*T + 0.0000053*T^(2) -
0.0000000022*T^(3) +22.6 + 0.05981*T - 0.000035*T^(2) +
0.0000000074*T^(3))*(T - Tgchar),T);
Ts4char =abs( max(S9));
Tschar = eval(Ts1char + Ts2char + Ts3char - Ts2dev - Ts3dev);% + Ts4char;

% Next step is to derive the kinetic rates:
%Evaporation :
YH2O = Ymoist*Mfaf;
rdry = 2.822*10^(-4)*exp(-10584/Tsevap)*(1-Eb)*160*YH2O*abs((Tsevap - 475)^7)
;

%Devolatilization;
%Experimental Correlation:
```

```
Z1 = 1.94*10^(-6)*Tsdev^1.84;
Z2 = 1.305*10^(-11)*Tsdev^3.39;
syms G2
S10 = vpasolve(Mfaf*p==16*Z1*G2/28 + 32*G2/44 , G2);
G2 = eval(S10) ;
G1 = Z1*G2;
G3 = Z2*G2*Mfaf;
syms G4
S11 = vpasolve(Mfaf*m== 12*G1/28 + 12*G2/44 + 12*G3/16 + 72*G4/78,G4);
G4 =eval( S11);
G6 =Mfaf*k;
syms G5
S12 = vpasolve(Mfaf*n==4*G3/16 + 6*G4/78 +G5,G5);
G5 = eval(S12) ;
% Mass fraction of volatiles:
Y1COs = G1;
Y1CO2s = G2;
YCH4s =G3;
YC6H6s =G4;
YH2s = G5;
YN2s =G6;
%Kinetic rate for all the species(CO2,CO,CH4,C6H6,H2,N2);
r1CO = 1.56*10^(10)*exp(-16600/Tsdev)*(1-0.58)*1.165*Y1COs ;
r1CO2 = 1.56*10^(10)*exp(-16600/Tsdev)*(1-Eb)*1.842*Y1CO2s;
rCH4 = 1.56*10^(10)*exp(-16600/Tsdev)*(1-Eb)*0.668*YCH4s ;
rC6H6 = 1.56*10^(10)*exp(-16600/Tsdev)*(1-Eb)*3.486*YC6H6s ;
rH2 = 1.56*10^(10)*exp(-16600/Tsdev)*(1-Eb)*0.089*YH2s ;
rN2 = 1.56*10^(10)*exp(-16600/Tsdev)*(1-Eb)*1.165*YN2s ;
rvol = r1CO2 + r1CO + rCH4 + rC6H6 + rH2 + rN2 ;
Kvol = 1.56*10^(10)*exp(-16600/Tsdev);
rdev = Kvol*Mdev;
% Char :
% Species in solid :
rc = 12*exp(-3300/Tschar);
Fy = (1+1/rc)/(1/2 + 1/rc);
Y2COs = Mchar*2*(1-1/Fy);
Y2CO2s = Mchar*((2/Fy) - 1) ;
YO2consump =Mair*0.23*(32/28.92)*1/Fy;
YO2s = 0.23*Mair*(32/28.92) - YO2consump;
% Kinetic rate Modelling :
kc = 8620*exp(-15900/Tschar);
rchar = kc*Mchar*PO2;
r2CO = rchar*Y2COs;
r2CO2 = rchar*Y2COs;
rO2 = rchar*YO2s;
% Conservation laws:
%Solid :
while rdev + rchar + rdry == 0 + (rdev + rchar + rdry )*.01;
   continue;
end
% Continuity in gas phase:
rf = rdev + rchar + rdry ;
x = zeros (1,N);
Ab = Wb*Lb;
for i= 1:N;
   x(i) = i*Lb/N ;
   M(:,i) =  -Ab*rf*x(i) + Mfaf ;
```

```
end

   % Species equation:
%Evaporation:
%H2Og:
for i=2:N;
        x1(i) = i*Levap/N ;

    YH2Os(:,i) = YH2O - rdry*(x1(i))^2/(2*row)- x1(i)*(YH2O/Levap -
rdry*Levap/(2*row));
      YH2Og(:,i) =-( rdry*x1(i)^2/(2*row)- x1(i)*(YH2O/Levap -
rdry*Levap/(2*row)));
end
% Devolatilization:
for i=1:N ;
    x(i) = i*Ldev/N ;
    Y1CO2g1(:,i) =Y1CO2s -  r1CO2*x(i)^2/(2*row)- x(i)*(Y1CO2s/Ldev -
r1CO2*Ldev/(2*row));
    Y1CO2g2(:,i) = - ( r1CO2*x(i)^2/(2*row)- x(i)*(Y1CO2s/Ldev -
r1CO2*Ldev/(2*row)));
    Y1COg1(:,i) = Y1COs - r1CO*x(i)^2/(2*row)- x(i)*(Y1COs/Ldev -
r1CO*Ldev/(2*row));
    Y1COg2(:,i) =  -( r1CO*x(i)^2/(2*row)- x(i)*(Y1COs/Ldev -
r1CO*Ldev/(2*row)));
    YCH4g1(:,i) = YCH4s - rCH4*x(i)^2/(2*row)- x(i)*(YCH4s/Ldev -
rCH4*Ldev/(2*row));
    YCH4g2(:,i) =  -( rCH4*x(i)^2/(2*row)- x(i)*(YCH4s/Ldev -
rCH4*Ldev/(2*row)));
    YC6H6g1(:,i) = YC6H6s - rC6H6*x(i)^2/(2*row)- x(i)*(YC6H6s/Ldev -
rC6H6*Ldev/(2*row));
    YC6H6g2(:,i) =  -( rC6H6*x(i)^2/(2*row)- x(i)*(YC6H6s/Ldev -
rC6H6*Ldev/(2*row)));
    YH2g1(:,i) = YH2s - rH2*x(i)^2/(2*row)- x(i)*(YH2s/Ldev -
rH2*Ldev/(2*row));
    YH2g2(:,i) = -( rH2*x(i)^2/(2*row)- x(i)*(YH2s/Ldev - rH2*Ldev/(2*row)));
    YN2g1(:,i) = YN2s - rN2*x(i)^2/(2*row)- x(i)*(YN2s/Ldev -
rN2*Ldev/(2*row));
    YN2g2(:,i) =  -( rN2*x(i)^2/(2*row)- x(i)*(YN2s/Ldev -
rN2*Ldev/(2*row)));
end
% char combustion:
for i=1:N ;
    x(i) = i*Lchar/N;
    Y2CO2g1(:,i) = Y2CO2s - r2CO2*x(i)^2/(2*row)- x(i)*(Y2CO2s/Lchar -
r2CO2*Lchar/(2*row));
    Y2CO2g2(:,i) =  -( r2CO2*x(i)^2/(2*row)- x(i)*(Y2CO2s/Lchar -
r2CO2*Lchar/(2*row)));
    Y2COg1(:,i) = Y2COs - r2CO*x(i)^2/(2*row)- x(i)*(Y2COs/Lchar -
r2CO*Lchar/(2*row));
    Y2COg2(:,i) = -( r2CO*x(i)^2/(2*row)- x(i)*(Y2COs/Lchar -
r2CO*Lchar/(2*row)));
    YO2g1(:,i) = YO2s - rO2*x(i)^2/(2*row)- x(i)*(YO2s/Lchar -
rO2*Lchar/(2*row));
   YO2g2(:,i) = - (rO2*x(i)^2/(2*row)- x(i)*(YO2s/Lchar -
rO2*Lchar/(2*row)));
end
```

```
%Energy Conservation:
%Gas phase
%Evaporation zone:
Aevap = Levap*Wb;
for i=1:N ;
    x1(i) = i*Levap/N ;
    T1g(i) = Tsevap + .001*Tsevap;

      % T1g(t,i) = T1g(T,i)+((TgH2O(T,i) - T1g(T,i)));

       h1f(i) = YH2Og(i)*(32.24 + T1g(i)*0.1923*10.^(-2) +
T1g(i).^2*1.055*10.^(-5) - T1g(i).^3*3.595*10.^(-9) )*(T1g(i) - Tsevap);
       h1(i) = ((0.99 + T1g(i)*1.22*10^(-4) - T1g(i)^(-
2)*5.68*10^3)*10^3)*(T1g(i) - Tsevap);
       TgH2O(i) =( Mevap*h1f(i)/(Aevap*Eb*k))*x1(i) -
x1(i)^2/(2*Eb*k)*(h1(i)*Aevap*(Tsevap - T1g(i))) - x1(i)*(Tsevap -
T1g(i))/(Eb*k) + Tsevap ;

     TfinalH2O(:,i) = TgH2O(i);



end

%Devolatilization zone :
Adev = Ldev*Wb ;
for i =1:N ;
    x2(i) = i*Ldev/N ;
        T2g(i) = Tsdev + 0.00001*Tsdev ;
        h2f(i) = (Y1COg2(i)*(28.16 + T2g(i)*0.1675*10^(-2) +
T2g(i)^2*0.5372*10^(-5) - T2g(i)^3*2.222*10^(-9)) + Y1CO2g2(i)*(22.26 +
T2g(i)*5.981*10^(-2) - T2g(i)^2*3.501*10^(-5) + T2g(i)^3*7.469*10^(-9)) +
YCH4g2(i)*(19.89 + T2g(i)*5.024*10^(-2) + T2g(i)^3*1.269*10^(-5) -
T2g(i)^3*11.01*10^(-9)) + YC6H6g2(i)*(-36.22 + T2g(i)*48.475*10^(-2) -
T2g(i)^2*31.57*10^(-5) + T2g(i)^3*77.62*10^(-9)) + YH2g2(i)*(29.11 -
T2g(i)*0.1916*10^(-2) + T2g(i)^2*0.4003*10^(-5) - T2g(i)^3*0.8704*10^(-9)) +
YN2g2(i)*(28.90 - T2g(i)*0.1571*10^(-2) + T2g(i)^(2)*0.8081*10^(-5) -
T2g(i)^(3)*2.873*10^(-9)))*(T2g(i) - Tsdev);
        h2(i) = ((0.99 + T2g(i)*1.22*10^(-4) - T2g(i)^(-
2)*5.68*10^(3))*10^(3))*(T2g(i) - Tsdev);
        Tgvol(i) = ( Mdev*h2f(i)/(Adev*Eb*k))*x2(i) -
x2(i)^(2)/(2*Eb*k)*(h2(i)*Adev*(Tsdev - T2g(i))) - x2(i)*(Tsdev -
T2g(i))/(Eb*k) + Tsdev ;
        %if abs(Tgvol(i) - T2g(t))<0.1*Tgvol(i,t)
            Tfinalvol(:,i) = Tgvol(i) ;
       % else
          %  T2g(i,t) = T2g(i,t-1) + ((Tgvol(i,t) - T1g(i,t)));
        %end

end

  % Char Combustion zone:
Achar = Lchar*Wb ;
for i=1: N;
```

```
    x3(i) = i*Lchar/N ;
    T3g(i) = Tschar + 0.000005*Tschar;
  %  T3g = zeros(1,M1) ;
  %      T3g(t==1) = T3guess ;
    %    hf = zeros(1,M1);
        h3f(i) = (Y2COg2(i)*(28.16 + T3g(i)*0.1675*10^(-2) +
T3g(i)^(2)*0.5372*10^(-5) - T3g(i)^(3)*2.222*10^(-9)) + Y2CO2g2(i)*(22.26 +
T3g(i)*5.981*10^(-2) - T3g(i)^(2)*3.501*10^(-5) + T3g(i)^(3)*7.469*10^(-9)) +
YO2g2(i)*(25.48 + T3g(i)*1.520*10^(-2) - T3g(i)^(2)*0.7155*10^(-5)+
T3g(i)^(3)*1.312*10^(-9)) + 0.7469*Mair*(28.90 - T3g(i)*0.1571*10^(-2)+
T3g(i)^(2)*0.8081*10^(-5) - T3g(i)^(3)*2.873*10^(-9)))*(T3g(i) - Tschar);

      %  h = zeros(1,M1);
        h3(i) = ((0.99 + T3g(i)*1.22*10^(-4) - T3g(i)^(-
2)*5.68*10^(3))*10^(3))*(T3g(i) - Tschar);
        % Tgchar = [1:N,1:M1];
        Tgchar(i) = (Mchar*h3f(i)/(Eb*Achar*k))*x3(i) -
((x3(i)^(2))*(h3(i)*Achar*(Tschar - T3g(i)) + Qcomb + Mair*Hair ))/(2*Eb*k) -
((Tschar - T3g(i))/Achar - Achar*(Qcomb + Mair*Hair)/((Eb*k)))*x3(i) + Tschar
;
      %  if abs(Tgchar(i,t) - T3g(t))<0.1*Tgchar(i,t)
            Tfinalchar(:,i) = Tgchar(i);
     %   else
                        % T3g(t) = T3g(t-1) + ((Tgchar(i,t) - T2g(t))) ;


end
```

Appendix F - One dimensional three zone bed model code (with NO_x)

```
clc
close all
clear

% first step is to calculate the temperature of surface for each zone:
Mf = 0.11081;
Yash = 0.005;
Lb = 0.8;
Wb = 0.9398;
Ymoist = 0.073;
Qrad = 21.75;
Boltz = 5.670*10^(-8);
Tfl = 800;
Eg = 0.9;
Es = 0.9 ;
Eb = 0.6 ;
Alfa= 0.2;
Hevap = 0.012;
Viscos = 1;
Yvol = 0.78;
Ychar = 0.142;
LHV = 16470;
Z = 0.012;
```

```
Z0 = 0.006;
p = .396;
m = .322 ;
n= 0.057;
k = 0.01;
Dens =690;
Mair = 0.46376;
Hair = 300.19;
M1=10;
Tguess =375;
Pr = 0.0707;
Tgevap = 400 ;
dp = 0.0004;
Tgdev = 600;
Tgchar = 800;
Hdev = 0.012;
Hchar = 0.01;
PO2 = 23.3;
row = 690;
Hb = 0.12;
% Code:
Ychem = Yvol + Ychar + Ymoist ;
Mfaf = Mf*(1-Yash);
% Evaporation zone:
YH2O = Ymoist*Mfaf;
Mevap = Ymoist*Mfaf;
Levap = Lb*Ymoist/Ychem;
K = Eg/(1-Eg)*4*Boltz*dp*Tfl^3 ;
%Radiation:
Qradevap = Qrad*Levap/Lb ;
syms T
S1 = vpasolve(Qradevap == Alfa*Boltz*(- Eg*Tfl^4 + Es*T^4 ),T );
Ts1evap = abs(max(S1));
%Convection:
Aconvevap = Wb*Levap;
Pevap = 2*(Levap + Wb);
Rhevap = Aconvevap/Pevap ;
deqevap = 2*Rhevap ;
Acevap = Hevap*Wb;
Reyevap = Mevap*Rhevap/(Acevap*Viscos);
Nuevap = 2 + Pr^(1/3)*1.1*Reyevap^0.6 ;
htevap = Nuevap*K/deqevap ;
syms T
S2 = vpasolve(Qradevap == htevap*Aconvevap*(Tgevap - T),T);
Ts2evap = S2;
Tsevap =eval( Ts1evap - Ts2evap) ;


%Devolatilization zone:
Mdev = Mfaf*Yvol ;
Ldev = Lb*Yvol/Ychem;
%Radiation:
Qraddev = Qrad*Ldev/Lb;
syms T
S3 =  vpasolve(Qraddev == Alfa*Boltz*(-Eg*Tfl^4 + Es*T^4 ),T );
Ts1dev =abs(max(S3));
```

```
%Convection :
Aconvdev = Wb*Ldev ;
Pdev = 2*(Ldev + Wb );
Rhdev = Aconvdev/Pdev ;
deqdev = 2*Rhdev ;
Acdev = Hdev*Wb ;
Reydev = Mdev*Rhdev/(Acdev*Viscos);
Nudev = 2+Pr^(1/3)*1.1*Reydev^0.6;
htdev = Nudev*K/deqdev ;
syms T
S4 = vpasolve(Qraddev == htevap*Aconvdev*(Tgdev - T),T);
Ts2dev = max(S4);
%Conduction:
Deltaxdev = Ldev/2 + Levap/2 ;
syms T
S5 = vpasolve(Alfa*Boltz*(-Eg*Tfl^4 + Es*T^4)*exp(Alfa*(Z0 - Z)) -
Eg*4*Boltz*dp*T^(3)*(T - Tsevap)*Acdev/Deltaxdev ==0 ,T);
Ts3dev = abs(max(S5));
Tsdev =eval( Ts1dev + Ts2dev - Ts3dev ) ;

%Char Zone:Tsdev
Mchar = Ychar*Mfaf;
Lchar = Ychar*Lb/Ychem;
%Radiation:
Qradchar = Qrad*Lchar/Lb;
syms T
S6 =  vpasolve(Qradchar == Alfa*Boltz*(Eg*Tfl^4 - Es*T^4 ),T );
Ts1char = abs(max(S6));
%Convection:
Aconvchar = Lchar*Wb;
Pchar = 2*(Wb + Lchar);
Rhchar = Aconvchar/Pchar;
deqchar = 2*Rhchar ;
Acchar = Wb*Hchar;

Reychar = Mchar*Rhchar/(Acchar*Viscos);
Nuchar = 2 + Pr^(1/3)*1.1*Reychar^0.6 ;
htchar = Nuchar*K/deqchar ;
syms T
S7 = vpasolve(Qradchar==htchar*Aconvchar*(Tgchar - T),T);
Ts2char = S7 ;
%Conduction;
Deltaxchar = Levap + Ldev + Lchar/2 - (Levap + Ldev/2);
syms T
S8 = vpasolve(Alfa*Boltz*(Eg*Tfl^4 - Es*T^4)*exp(Alfa*(Z0 - Z)) -
Eg*4*Boltz*dp*T^(3)*(T - Tsdev)*Acchar/Deltaxchar ==0 ,T);
Ts3char = max(S8);
% Char combustion heat :
%Experimental correlation:
Qcomb = Mchar*LHV ;
syms T
S9 = vpasolve(Qcomb== Mchar*(28.16 + 0.001675*T + 0.0000053*T^(2) -
0.0000000022*T^(3) +22.6 + 0.05981*T - 0.000035*T^(2) +
0.0000000074*T^(3))*(T - Tgchar),T);
Ts4char =abs( max(S9));
Tschar = eval(Ts1char + Ts2char + Ts3char - Ts2dev - Ts3dev);% + Ts4char;
```

```
% Next step is to derive the kinetic rates:
%Evaporation :
YH2O = Ymoist*Mfaf;
rdry = 2.822*10^(-4)*exp(-10584/Tsevap)*(1-Eb)*160*YH2O*abs((Tsevap - 475)^7)
;

%Devolatilization;
%Experimental Correlation:
YNH3s = k*Mfaf/1.11;
YHCNs = k*Mfaf/9.7 ;

% Now the consumed C and H and N in the above gases is calculated:

Cconsum = YHCNs*12/27;
Hconsum = YHCNs*1/27 + YNH3s*3/17 ;
Nconsum = YHCNs*14/27 + YNH3s*14/17 ;
Cleft = (m*Mfaf) - Cconsum ;
Hleft = (n*Mfaf) - Hconsum ;
Nleft = (k*Mfaf) - Nconsum ;

% Calculating the concentration of other gases in solid biomass :

Z1 = 1.94*10^(-6)*Tsdev^1.84;
Z2 = 1.305*10^(-11)*Tsdev^3.39;
syms G2
S10 = vpasolve(Mfaf*p==16*Z1*G2/28 + 32*G2/44 , G2);
G2 = eval(S10) ;
G1 = Z1*G2;
G3 = Z2*G2*Mfaf;
syms G4
S11 = vpasolve(Cleft== 12*G1/28 + 12*G2/44 + 12*G3/16 + 72*G4/78,G4);
G4 =eval( S11);
G6 =Mfaf*k;
syms G5
S12 = vpasolve(Hleft==4*G3/16 + 6*G4/78 +G5,G5);
G5 = eval(S12) ;
% Mass fraction of volatiles:
Y1COs = G1;
Y1CO2s = G2;
YCH4s =G3;
YC6H6s =G4;
YH2s = G5;
YN2s =Nleft;

%Kinetic rate for all the species(CO2,CO,CH4,C6H6,H2,N2);
r1CO = 1.56*10^(10)*exp(-16600/Tsdev)*(1-0.58)*1.165*Y1COs ;
r1CO2 = 1.56*10^(10)*exp(-16600/Tsdev)*(1-Eb)*1.842*Y1CO2s;
rCH4 = 1.56*10^(10)*exp(-16600/Tsdev)*(1-Eb)*0.668*YCH4s ;
rC6H6 = 1.56*10^(10)*exp(-16600/Tsdev)*(1-Eb)*3.486*YC6H6s ;
rH2 = 1.56*10^(10)*exp(-16600/Tsdev)*(1-Eb)*0.089*YH2s ;
rN2 = 1.56*10^(10)*exp(-16600/Tsdev)*(1-Eb)*1.165*YN2s ;
rNH3 = 1.56*10^(10)*exp(-16600/Tsdev)*(1-Eb)*1.165*YNH3s ;
rHCN = 1.56*10^(10)*exp(-16600/Tsdev)*(1-Eb)*1.165*YHCNs ;
rvol = r1CO2 + r1CO + rCH4 + rC6H6 + rH2 + rN2 + rNH3 + rHCN ;
```

```
Kvol = 1.56*10^(10)*exp(-16600/Tsdev);
rdev = Kvol*Mdev;

% Char :
% Species in solid :
Ct=0.464;
Mtchar = Ct*Mfaf;
rc = 12*exp(-3300/Tschar);
Fy = (1+(1/rc))/(1/2 + (1/rc));
Y2COs = Mtchar*2*(1-1/Fy);
Y2CO2s =Mtchar*((2/Fy) - 1) ;
YO2consump =Mair*.23*(1/Fy);
YO2s = 0.23*Mair - YO2consump;
% Kinetic rate Modelling :
kc = 8620*exp(-15900/Tschar);
rchar = kc*Mchar*PO2;
r2CO = rchar*Y2COs;
r2CO2 = rchar*Y2COs;
rO2 = rchar*YO2s;


% Conservation laws:
%Solid :
while rdev + rchar + rdry == 0 + (rdev + rchar + rdry )*.01;
   continue;
end
% Continuity in gas phase:
N=10;
x = zeros (1,N);
Ab = Wb*Lb;
rt = rchar + rdev + rdry;
D = (1.805*10^(-5))/0.7;

% Continuity Equations:
 %field generation:
 dx = Lb/N;
 dt = 0.01;
 time = 10;
  for t=1:time;
     for i=1:N
         x(i) = i*dx;
     end
 end

%initial conditions:
for t=1;
    for i=1:N
        if i==1;
        M(i,t) = 0;
        M(N,t)= Mfaf;
        else
            M(i,t)=rt*x(i) + (Mfaf-(rt*Lb))*x(i);
        end
    end
end
for t=1:time
```

```
    for i=2:N-1;
        aa(i,t+1)= (1/dt)+(M(i,t)/dx);
         bb(i,t+1)=((M(i+1,t)-M(i,t))/dx) ;
         M(i,t+1)=(-M(i,t)*bb(i,t+1))/aa(i,t+1)+M(i,t);
    end
end

%Species Equation:

%Drying zone:
time1 = 100;
N1 = 5000;
dx1 = Lb/N1;
Aevap = Levap*Wb;
A = Wb*Hb;
Mdry = YH2O;
dt1=1;
% Grid describtion:

  for t=1:time1;
     for i=1:N1
         x1(i) = i*dx1;
     end
 end
%initial condition:

for t=1;
    for i=1:N1
         if i==1
            YH2Og(i,t)=0;
                else

          YH2Og(i,t) = -[(rdry*x1(i)^(2))/2 + (YH2O*(Mdry/A - row*D) -
rdry*Levap/2)*x1(i)]/((Mdry*x1(i)/A) - row*D);
               if  abs(YH2Og(i,t)) > YH2O

              YH2Og(i,t) = 0;
          end
         end

  end
end

%Transport Equation:

for t=1:time1
    for i=2:N1-1
          aa1(i,t+1)= (row*(YH2Og(i,t))/dt1) +((Mevap/Aevap)*YH2Og(i,t)/dx1
);
          bb1(i,t+1)=(D*row*(YH2Og(i+1,t)- YH2Og(i,t)))/dx1 ;
         YH2Og(i,t+1)=((-YH2Og(i,t)*bb1(i,t+1))/aa1(i,t+1) )+ YH2Og(i,t);
         if abs(YH2Og(i+1,t)) > YH2O;
             YH2Og(i+1,t)=0;
         elseif abs(YH2Og(i,t+1))>YH2O
             YH2Og(i,t+1)=0;
```

```
         end

    end
end

YH2Og(isnan(YH2Og))=0  ;
indevap=find(YH2Og==max(max(YH2Og)));
Levapfinal=x1(indevap);

for t=1
    for i=1:indevap
        if i==1
        else
        YH2Ogstar(i,t)=0;
        YH2Ogstar(i,t) = ((YH2Og(i,t) - YH2Og(i-1,t)));
    end
end
end
x1excel=x1';

for i=1:indevap
    x11(i) = i*dx1;
end
x11excel = x11';


%Devolatilization zone:


time2 = 200;
N2=800;
Adev = (Ldev)*Wb;
dx2=(Lb-Levapfinal)/N2;
dt2=0.001;

for t=1:time2;
    for i=1:N2
        x2(i)=i*dx2;

    end
end

%initial conditions:

for t=1
    for i=1:N2
        if i==1
            Y1CO2g(i,t)=0;
            Y1COg(i,t)=0;
            YCH4g(i,t)=0;
            YC6H6g(i,t)=0;
            YH2g(i,t)=0;
            YN2g(i,t)=0;
            YNH3g(i,t) = 0;
```

```
            YHCN(i,t)=0;
%
            else
%
   Y1CO2g(i,t) = -[(r1CO2*x2(i)^(2))/2 + (Y1CO2s*(Mdev/A - row*D) -
r1CO2*Ldev/2)*x2(i)]/((Mdev*x2(i)/A) - row*D);
         if abs(Y1CO2g(i,t)) > Y1CO2s;
           Y1CO2g(i,t) = 0;
        end
   Y1COg(i,t) = -[(r1CO*x2(i)^(2))/2 + (Y1COs*(Mdev/A - row*D) -
r1CO*Ldev/2)*x2(i)]/((Mdev*x2(i)/A) - row*D);
      if abs(Y1COg(i,t)) > Y1COs;
           Y1COg(i,t) = 0;
      end
   YCH4g(i,t) = -[(rCH4*x2(i)^(2))/2 + (YCH4s*(Mdev/A - row*D) -
rCH4*Ldev/2)*x2(i)]/((Mdev*x2(i)/A) - row*D);
     if abs(YCH4g(i,t)) > YCH4s;
           YCH4g(i,t) = 0;
     end
   YC6H6g(i,t) = -[(rC6H6*x2(i)^(2))/2 + (YC6H6s*(Mdev/A - row*D) -
rC6H6*Ldev/2)*x2(i)]/((Mdev*x2(i)/A) - row*D);
        if abs(YC6H6g(i,t)) > YC6H6s;
           YC6H6g(i,t) = 0;
        end
   YH2g(i,t) = -[(rH2*x2(i)^(2))/2 + (YH2s*(Mdev/A - row*D) -
rH2*Ldev/2)*x2(i)]/((Mdev*x2(i)/A) - row*D);
   if  abs(YH2g(i,t)) > YH2s;
           YH2g(i,t) = 0;
       end
   YN2g(i,t) = -[(rN2*x2(i)^(2))/2 + (YN2s*(Mdev/A - row*D) -
rN2*Ldev/2)*x2(i)]/((Mdev*x2(i)/A) - row*D);

      if  abs(YN2g(i,t)) > YN2s;
           YN2g(i,t) = 0;
      end
   YNH3g(i,t) = -[(rNH3*x2(i)^(2))/2 + (YNH3s*(Mdev/A - row*D) -
rH2*Ldev/2)*x2(i)]/((Mdev*x2(i)/A) - row*D);
       if  abs(YNH3g(i,t)) > YNH3s;
           YNH3g(i,t) = 0;
       end
   YHCNg(i,t) = -[(rHCN*x2(i)^(2))/2 + (YHCNs*(Mdev/A - row*D) -
rH2*Ldev/2)*x2(i)]/((Mdev*x2(i)/A) - row*D);
       if  abs(YHCNg(i,t)) > YHCNs;
           YHCNg(i,t) = 0;
       end
            end
        end

end

%Time varience:


for t=1:time2
    for i=2:N2-1
    % CO2:
```

```
         aa2(i,t+1)=(Y1CO2g(i,t)*row/dt2) +((Mdev/A)*Y1CO2g(i,t)/dx2 );
         bb2(i,t+1)=(D*row*(Y1CO2g(i+1,t)- Y1CO2g(i,t)))/dx2 ;
        Y1CO2g(i,t+1)=(-Y1CO2g(i,t)*bb2(i,t+1))/(aa2(i,t+1))+Y1CO2g(i,t);
        if abs(Y1CO2g(i+1,t)) > Y1CO2s;
             Y1CO2g(i+1,t)=0;
        elseif abs(Y1CO2g(i,t+1))>Y1CO2s
             Y1CO2g(i,t+1)=0;
        end


%     %CO:
         aa3(i,t+1)= (Y1COg(i,t)*row/dt2)+((Mdev/A)*Y1COg(i,t)/dx2);
         bb3(i,t+1)=(D*row*(Y1COg(i+1,t)- Y1COg(i,t))/dx2) ;
        Y1COg(i,t+1)=(-Y1COg(i,t)*bb3(i,t+1))/(aa3(i,t+1))+Y1COg(i,t);
        if abs(Y1COg(i+1,t)) > Y1COs;
             Y1COg(i+1,t)=0;
              elseif abs(Y1COg(i,t+1))>Y1COs
             Y1CO2g(i,t+1)=0;
        end
    %    CH4:
         aa4(i,t+1)= (YCH4g(i,t)*row/dt2)+((Mdev/A)*YCH4g(i,t)/dx2);
         bb4(i,t+1)=(row*D*(YCH4g(i+1,t)-YCH4g(i,t))/dx2) ;
        YCH4g(i,t+1)=(-YCH4g(i,t)*bb4(i,t+1))/(aa4(i,t+1))+YCH4g(i,t);
        if abs(YCH4g(i+1,t) )> YCH4s
             YCH4g(i+1,t)=0;
        elseif abs( YCH4g(i,t+1))>YCH4s
             YCH4g(i,t+1)=0;
        end
   %     C6H6:
         aa5(i,t+1)= (YC6H6g(i,t)*row/dt2)+((Mdev/A)*YC6H6g(i,t)/dx2);
         bb5(i,t+1)=(row*D*(YC6H6g(i+1,t)-YC6H6g(i,t))/dx2) ;
        YC6H6g(i,t+1)=(-YC6H6g(i,t)*bb5(i,t+1))/(aa5(i,t+1))+YC6H6g(i,t);
        if  abs(YC6H6g(i+1,t)) > YC6H6s
             YC6H6g(i+1,t)=0;
        elseif  abs(YC6H6g(i,t+1))>YC6H6s
             YC6H6g(i,t+1)=0;
        end
      %  H2:
         aa6(i,t+1)= (YH2g(i,t)*row/dt2)+((Mdev/A)*YH2g(i,t)/dx2);
         bb6(i,t+1)=(row*D*(YH2g(i+1,t)-YH2g(i,t))/dx2) ;
        YH2g(i,t+1)=(-YH2g(i,t)*bb6(i,t+1))/(aa6(i,t+1))+YH2g(i,t);
        if  abs(YH2g(i+1,t)) > YH2s
             YH2Og(i+1,t)=0;
        elseif  abs(YH2g(i,t+1))>YH2s
             YHg(i,t+1)=0;
        end
       % N2:
         aa7(i,t+1)= (YN2g(i,t)*row/dt2)+((Mdev/A)*YN2g(i,t)/dx2);
          bb7(i,t+1)=(D*row*(YN2g(i+1,t)-YN2g(i,t))/dx2) ;
        YN2g(i,t+1)=(-YN2g(i,t)*bb7(i,t+1))/(aa7(i,t+1))+YN2g(i,t);

        if abs(YN2g(i+1,t)) > YN2s
             YH2Og(i+1,t)=0;
         elseif abs(YN2g(i,t+1))>YN2s
             YN2g(i,t+1)=0;
        end
```

```
      %NH3:
       aa8(i,t+1)=(YNH3g(i,t)*row/dt2) +((Mdev/A)*YNH3g(i,t)/dx2 );
         bb8(i,t+1)=(D*row*(YNH3g(i+1,t)- YNH3g(i,t)))/dx2 ;
        YNH3g(i,t+1)=(-YNH3g(i,t)*bb8(i,t+1))/(aa8(i,t+1))+YNH3g(i,t);
        if abs(YNH3g(i+1,t)) > YNH3s;
             YNH3g(i+1,t)=0;
        elseif abs(YNH3g(i,t+1))>YNH3s
             YNH3g(i,t+1)=0;
        end

        % HCN:
      aa9(i,t+1)=(YHCNg(i,t)*row/dt2) +((Mdev/A)*YHCNg(i,t)/dx2 );
         bb9(i,t+1)=(D*row*(YHCNg(i+1,t)- YHCNg(i,t)))/dx2 ;
        YHCNg(i,t+1)=(-YHCNg(i,t)*bb9(i,t+1))/(aa9(i,t+1))+YHCNg(i,t);
        if abs(YHCNg(i+1,t)) > YHCNs;
             YHCNg(i+1,t)=0;
        elseif abs(YHCNg(i,t+1))>YHCNs
             YHCNg(i,t+1)=0;
        end
    end
end

Y1CO2g(isnan(Y1CO2g))=0;
Y1COg(isnan(Y1COg))=0;
YCH4g(isnan(YCH4g))=0;
YC6H6g(isnan(YC6H6g))=0;
YH2g(isnan(YH2g))=0;
YN2g(isnan(YN2g))=0;
YNH3g(isnan(YNH3g))=0;
YHCNg(isnan(YHCN))=0;

indvol=find(Y1COg(:,1)==max(Y1COg(:,1)));
Lvolfinal = indvol*dx2;

for t=1
    for i=2:N2
        Y1CO2gstar(i,t) = Y1CO2g(i,t) - Y1CO2g(i-1,t);
        Y1COgstar(i,t) = Y1COg(i,t) - Y1COg(i-1,t);
        YCH4gstar(i,t) = YCH4g(i,t) - YCH4g(i-1,t);
        YC6H6gstar(i,t) = YC6H6g(i,t) - YC6H6g(i-1,t);
        YH2gstar(i,t) = YH2g(i,t) - YH2g(i-1,t);
        YN2gstra(i,t) = YN2g(i,t) - YN2g(i-1,t);
        YNH3gstar(i,t) = YNH3g(i,t) - YNH3g(i-1,t);
        YHCNgstar(i,t) = YHCNg(i,t) - YHCNg(i-1,t);
    end
end

  x2excel=x2';

for i=1:indvol
    x22(i)=dx2*i;
end

x22excel=x22';
```

```
x22excelfinal = x22excel + Levapfinal ;

%Char Combustion zone:

N3 = 500;
dx3=Lchar/N3;
dt3 = 1;
time3 = 100;
for t=1:time3;
    for i=1:N3
        x3(i)=i*dx3;
    end
end
%Initial & boundary conditiones:
for t=1
    for i=1:N3
        if i==1;
            Y2CO2g(i,t)=0;
            Y2COg(i,t)=0;
            YO2g(i,t)=0;
%         else if i==N;
%                 Y2CO2g2(i,t)=Y2CO2s;
%                 Y2COg2(i,t)=Y2COs;
%                 YO2g2(i,t)=YO2s;
            else
%
     Y2CO2g(i,t) = -[(r2CO2*x3(i)^(2))/2 + (Y2CO2s*(Mchar/A - row*D) -
r2CO2*Lchar/2)*x3(i)]/((Mchar*x3(i)/A) - row*D);
%          if abs(Y2CO2g(i+1,t)- Y2CO2g(i,t)) <0.001;
%            break;
%          end
     Y2COg(i,t) = -[(r2CO*x3(i)^(2))/2 + (Y2COs*(Mchar/A - row*D) -
r2CO*Lchar/2)*x3(i)]/((Mchar*x3(i)/A) - row*D);
%         if abs(Y2COg(i,t)- Y2COs) <0.001 ;
%            break
%         end
%      YO2g(i,t) = -[(rO2*x3(i)^(2))/2 + (YO2s*(Mchar/A - row*D) -
rO2*Lchar/2)*x3(i)]/((Mchar*x3(i)/A) - row*D);
%         if abs(YO2g(i,t)) >= YO2s;
%            break
%         end

        end
    end
end


% time variation:

for t=1:time3
    for i=2:N3-1
        %CO2
         aa10(i,t+1)= (Y2CO2g(i,t)*row/dt3)+((Mchar/A)*Y2CO2g(i,t)/dx3);
         bb10(i,t+1)=(D*row*(Y2CO2g(i+1,t) - Y2CO2g(i,t))/dx3) ;
        Y2CO2g(i,t+1)=(-Y2CO2g(i,t)*bb10(i,t+1))/(aa10(i,t+1))+Y2CO2g(i,t);
             if abs(Y2CO2g(i+1,t)) > Y2CO2s;
```

```
            Y2CO2g(i+1,t)=0;
             elseif abs(Y2CO2g(i,t+1))>Y2CO2s
            Y2CO2g(i,t+1)=0;
            end
        % CO:
          aa11(i,t+1)= (Y2COg(i,t)*row/dt3)+((Mchar/A)*Y2COg(i,t)/dx3);
          bb11(i,t+1)=(D*row*(Y2COg(i+1,t)- Y2COg(i,t))/dx3) ;
        Y2COg(i,t+1)=(-Y2COg(i,t)*bb11(i,t+1))/(aa11(i,t+1))+ Y2COg(i,t);
               if abs(Y2COg(i+1,t)) > Y2COs;
            Y2COg(i+1,t)=0;
             elseif abs(Y2COg(i,t+1))>Y2COs
            Y2COg(i,t+1)=0;
             end
        % O2:
%          aa10(i,t+1)= (YO2g(i,t)*row/dt3)+((Mchar/A)*YO2g(i,t)/dx3);
%          bb10(i,t+1)=(D*row*(YO2g(i+1,t)-YO2g(i,t))/dx3) ;
%        YO2g(i,t+1)=(-YO2g(i,t)*bb10(i,t+1))/(aa10(i,t+1))+YO2g(i,t);
%                if abs(YO2g(i+1,t)) > YO2s;
%             YO2g(i+1,t)=0;
%              elseif abs(YO2g(i,t+1))>YO2s
%             YO2g(i,t+1)=0;
              end
    end


Y2CO2g(isnan(Y2CO2g))=0;
Y2COg(isnan(Y2COg))=0;
YO2g(isnan(YO2g))=0;

indchar=find(Y2COg(:,1)==max(Y2COg(:,1)));
Lcharfinal = dx3*indchar;


for t=1
    for i=2:N3
        Y2CO2gstar(i,t) = Y2CO2g(i,t) - Y2CO2g(i-1,t);
        Y2COgstar(i,t) = Y2COg(i,t) - Y2COg(i-1,t);
    end
end

x3excel=x3';
for i=1:indchar
    x33(i) = i*dx3;
end

x33excel = x33';
x33excelfinal= x33excel + Levapfinal + Lvolfinal ;

%Energy Conservation:
% Drying Zone:
% Space Gradient:

Land = Eb/(1-Eb);
dx11 = Levapfinal/N1;
```

```
% initial conditions:
for t=1
    for i=1:indevap
        if i==1
            TgH2O(i,t) = Tsevap;
        else

     T1H2O(i,t) = Tsevap + .001*Tsevap;
    Cpf1(i,t) = YH2Og(i,t)*(32.24 + T1H2O(i,t)*0.1923*10.^(-2) +
T1H2O(i,t).^2*1.055*10.^(-5) - T1H2O(i,t).^3*3.595*10.^(-9) )*(T1H2O(i,t) -
Tsevap);
     hc1(i,t) = ((0.99 + T1H2O(i,t)*1.22*10^(-4) - T1H2O(i,t)^(-
2)*5.68*10^3)*10^3)*(T1H2O(i,t) - Tsevap);
  % TgH2O(i,t) =( Mevap*Cpf1(i,t)/(Aevap*Eb*k))*x11(i) -
x11(i)^2/(2*Eb*k)*(hc1(i,t)*Aevap*(Tsevap - T1H2O(i,t))) - x11(i)*(Tsevap -
T1H2O(i,t))/(Eb*k) + Tsevap ;
     TgH2O(i,t) = [(1/(Land*(1-
(row*Mevap*Cpf1(i,t)*x11(i)/(Land*Aevap)))))*(-hc1(i,t)*Aevap*(Tsevap -
T1H2O(i,t)) - rt*hc1(i,t))*(x11(i)^(2)/2)] + Tsevap ;
         if isnan(TgH2O(i,t))==1
             TgH2O(i,t)=0;
         end
     end
    end
end

  % time varience:
 for t=1:time1
    for i=2:indevap - 1
         aa11(i,t+1)=
(row*Cpf1(i,1)*TgH2O(i,t)/dt1)+(row*Mevap*Cpf1(i,1)*TgH2O(i,t)/(dx11*Aevap));
         bb11(i,t+1)=((TgH2O(i+1,t)-TgH2O(i,t))/dx11) ;
        TgH2O(i,t+1)=((-TgH2O(i,t)*bb11(i,t+1))/(aa11(i,t+1)))+TgH2O(i,t);
%         if isnan(TgH2O(i,t+1))==1
%             TgH2O(i,t+1)=0;
%          end
    end
 end

%figure;yyaxis left;
% Devolatilization zone:
%space varience:
Adev=Ldev*Wb;
dx22=Lvolfinal/N2;

for t=1:time2
    for i=1:N2
        x22(i)=dx22*i;
    end
end
%initial condition:
for t=1
    for i=1:indvol
        if i==1
            Tgvol(i,t) = Tsdev;
        else
```

```
          T2g(i,t) = Tsdev + 0.01*Tsdev ;
         Cpf2(i,t) = (Y1COg(i,t)*(28.16 + T2g(i,t)*0.1675*10^(-2) +
T2g(i,t)^2*0.5372*10^(-5) - T2g(i,t)^3*2.222*10^(-9)) + Y1CO2g(i,t)*(22.26 +
T2g(i,t)*5.981*10^(-2) - T2g(i,t)^2*3.501*10^(-5) + T2g(i,t)^3*7.469*10^(-9))
+ YCH4g(i,t)*(19.89 + T2g(i,t)*5.024*10^(-2) + T2g(i,t)^3*1.269*10^(-5) -
T2g(i,t)^3*11.01*10^(-9)) + YC6H6g(i,t)*(-36.22 + T2g(i,t)*48.475*10^(-2) -
T2g(i,t)^2*31.57*10^(-5) + T2g(i,t)^3*77.62*10^(-9)) + YH2g(i,t)*(29.11 -
T2g(i,t)*0.1916*10^(-2) + T2g(i,t)^2*0.4003*10^(-5) - T2g(i,t)^3*0.8704*10^(-
9)) + YN2g(i,t)*(28.90 - T2g(i,t)*0.1571*10^(-2) + T2g(i,t)^2*0.8081*10^(-5)
- T2g(i,t)^3*2.873*10^(-9)) + YNH3g(i,t)*(6.5846 + 0.34028*10^(-2)*T2g(i,t) +
0.073034*10^(-5)*T2g(i,t)^2 - 0.27402*10^(-9)*T2g(i,t)^3) +
YHCNg(i,t)*39.229)*(T2g(i,t) - Tsdev);
         hc2(i,t) = ((0.99 + T2g(i,t)*1.22*10^(-4) - T2g(i,t)^(-
2)*5.68*10^(3))*10^(3))*(T2g(i,t) - Tsdev);
         Tgvol(i,t) = ( Mdev*Cpf2(i,t)/(Adev*Eb*k))*x22(i) -
x22(i)^(2)/(2*Eb*k)*(hc2(i,t)*Adev*(Tsdev - T2g(i,t))) - x22(i)*(Tsdev -
T2g(i,t))/(Eb*k) + Tsdev ;
      %   Tgvol(i,t) = [(1/(Land*(1-
(row*Mdev*Cpf2(i,t)*x22(i)/(Land*Adev)))))*(-hc2(i,t)*Adev*(Tsdev - T2g(i,t))
- rt*hc2(i,t))*(x22(i)^(2)/2)] + Tsdev ;
         if isnan(Tgvol(i,t))==1
             Tgvol(i,t)=0;
         end
    end
    end
end
% time varience:
for t=1:time
    for i=2:indvol-1
         aa12(i,t+1)=
(row*Cpf2(i,1)*Tgvol(i,t)/dt2)+(row*Mdev*Cpf2(i,1)*Tgvol(i,t)/(dx22*Adev));
         bb12(i,t+1)=((Tgvol(i+1,t)-Tgvol(i,t))/dx22) ;
        Tgvol(i,t+1)=(-Tgvol(i,t)*bb12(i,t+1))/(aa12(i,t+1)) + Tgvol(i,t);
    end
end



% char zone:
% space varience:
Achar=Wb*Lchar;
dx33=Lcharfinal/N3;

for t=1:time3
    for i=1:N3
        x33(i)=dx33*i;
    end
end

% initial conditions:
for t=1
    for i=1:indchar
        if i==1
            Tgchar(i,t) = Tschar;
        else
        T3g(i,t) = Tschar + 0.001*Tschar;
```

```
        Cpf3(i,t) = (Y2COg(i,t)*(28.16 + T3g(i,t)*0.1675*10^(-2) +
T3g(i,t)^(2)*0.5372*10^(-5) - T3g(i,t)^(3)*2.222*10^(-9)) +
Y2CO2g(i,t)*(22.26 + T3g(i,t)*5.981*10^(-2) - T3g(i,t)^(2)*3.501*10^(-5) +
T3g(i,t)^(3)*7.469*10^(-9)) + 0.747*Mair*(28.90 - T3g(i,t)*0.1571*10^(-2) +
T3g(i,t)^2*0.8081*10^(-5) - T3g(i,t)^3*2.873*10^(-9)))*(T3g(i,t) - Tschar);
        hc3(i,t) = ((0.99 + T3g(i,t)*1.22*10^(-4) - T3g(i,t)^(-
2)*5.68*10^(3))*10^(3))*(T3g(i,t) - Tschar);
      Tgchar(i,t) = (Mchar*Cpf3(i,t)/(Eb*Achar*k))*x33(i) -
((x33(i)^(2))*(hc3(i,t)*Achar*(Tschar - T3g(i,t))  + Mair*Hair ))/(2*Eb*k) -
((Tschar - T3g(i,t))/Achar - Achar*(Mair*Hair)/((Eb*k)))*x33(i) + Tschar ;
    %    Tgchar(i,t) = [(1/(Land*(1-
(row*Mchar*Cpf3(i,t)*x33(i)/(Land*Achar)))))*(-hc3(i,t)*Achar*(Tschar -
T3g(i,t)) - rt*hc3(i,t))*(x33(i)^(2)/2)] + Tschar ;
         if isnan(Tgchar(i,t))==1
             Tgvol(i,t)=0;
         end
    end
    end
end

% time varience:

for t=1:time
    for i=2:indvol-1

         aa13(i,t+1)=
(row*Cpf3(i,1)*Tgchar(i,t)/dt3)+(row*Mchar*Cpf3(i,1)*Tgchar(i,t)/(Achar*dx33)
);
         bb13(i,t+1)=((Tgchar(i+1,t)-Tgchar(i,t))/dx33) ;
        Tgchar(i,t+1)=(-Tgchar(i,t)*bb13(i,t+1))/(aa13(i,t+1)) + Tgchar(i,t);
    end
end

 %Conversion length of the bed:

Lbnew = Levapfinal + Lcharfinal + Lvolfinal;
% Air species coming from rest of the bed:
% O2 & N2 :
YN2airs = 0.746*Mair;
Lr = Lb - Lbnew;
YO2air =YO2s;
% End of the code
```